

https://dspace.org/

Corrosion and other properties comparison of AISI 316L stainless steel surface alloyed with Ru/Ni mixtures with the parent metal and with Hastelloy© C-276

Lekala, Makgale Barclays

2016

http://hdl.handle.net/10539/22598

Lekala, Makgale Barclays (2016) Corrosion and other properties comparison of AISI 316L stainless steel surface alloyed with Ru/Ni mixtures with the parent metal and with Hastelloy© C-276, University of the Witwatersrand, <http://hdl.handle.net/10539/22598>

Downloaded from a DSpace repository. https://dspace.org/

CORROSION AND OTHER PROPERTIES COMPARISON OF AISI 316L STAINLESS STEEL SURFACE ALLOYED WITH Ru/Ni MIXTURES WITH THE PARENT METAL AND WITH HASTELLOY© C-276

LEKALA MAKGALE BARCLAYS

A dissertation submitted to

the University of the Witwatersrand

in fulfilment of the requirements for the degree of

Master of Science in Engineering

(Metallurgy & Materials)

2016

DECLARATION

This Dissertation is being submitted to the University of the Witwatersrand for the degree of Master of Science in Engineering (Metallurgy & Materials). I, LEKALA MAKGALA BARCLAYS, declare that this work is my own and has not been submitted before for any degree or examination to any other university or institution.



LEKALA MAKGALE BARCLAYS

PUBLICATIONS AND PRESENTATIONS

The following are the publications and presentation done as part of the work out of the study:

1. M.B. Lekala, J.W. van der Merwe, S. Pityane, **Laser Surface Alloying of 316L Stainless Steel with Ru and Ni Mixtures**, Vol 2012, *International Journal of Corrosion*, Hindawi Publishing Corporation, 2012.
2. M.B. Lekala, J.W. van der Merwe, S. Pityane. **Metallurgical and Surface Analysis of Ru and Ni treated steel surface**, Vol 39 (pp 50), *MSSA conference proceedings*, 2009. Durban, South Africa.

3. 1st prize: *Corrosion Institute of Southern Africa* best presented research poster. 2009

ACKNOWLEDGEMENTS

This thesis would not have been remotely possible without the guidance and support of my supervisor, Dr. Josias van Der Merwe. His mentorship allowed me to grow as a researcher and made my studies a fully enjoyable and insightful experience. I owe an indescribable amount of gratitude to my mother, Mamatebele Lekala. This is done also in memory of my late father Dinake Lekala. So much love to my sisters and brother. Junior Mohlala for the love, courage and hope you brought into my life.

ABSTRACT

The surfaces of AISI 316L stainless steel plate were laser alloyed with ruthenium powder as well as a mixture of ruthenium and nickel powders using a Nd:YAG laser set at fixed operating parameters. The microstructure, elemental composition, and corrosion characteristics of the alloyed zone were analysed using optical and scanning electron microscopy (SEM), Energy Dispersive X-ray Spectroscopy (EDS), and corrosion potential measurements. EDS analysis of the alloyed specimen showed that through the laser surface alloying, 2 mm surface layers with 12.5wt % Ru and 5.2wt% Ru were produced on an AISI 316L stainless steel.

Similar microstructures which were dendritic and columnar grains, typical of weld beads under non-equilibrium cooling conditions were observed for all samples. Hardness profile measurements showed a significant increase from 160 HV for the substrate to a maximum of 247 HV for the alloyed layer. Using an Autolab potentiostat, the corrosion behaviour and resistance of the laser alloyed layers, substrate AISI 316L, and Hastelloy© C-276 were evaluated and compared in sulphuric acid solution of different concentration and temperatures. The Hastelloy© C-276, followed by the 12.5wt% Ru presented the most noble corrosion potential (E_{corr}) and the lowest corrosion current density (i_{corr}). However, in 60wt% H_2SO_4 and 40^{o}C, the 5.22 wt% Ru alloys exhibited slightly better anticorrosive properties than 12.5wt% Ru. The observed corrosion potential, $E_{corr,}$ for untreated AISI 316L stainless steel sample in 40wt% sulphuric acid solution at 40^{o}C was -277 mV. The 5.22 wt% Ru and 12.5wt% Ru alloyed stainless steel samples presented -240 mV, and 61 mV respectively in the same solution. Besides showing comparable

performance to 5.2wt%Ru sample within specific short potential ranges, Hastelloy© C-276 was generally superior in all solutions. In addition it was found that the stability of the passive layer was improved with additions of Ru.

Based on the developed costing equation the cost of 5 mm AISI 316L stainless steel plate with surface area (A = 1 m^2) surface alloyed with 5.2wt% Ru to a depth of 2 mm using Nd: YAG laser is estimated at R15 989, and it is less than the cost of a Hastelloy© C-276 plate of similar size which is estimated at R19 900. As the material thickness increases, the cost benefit of laser surface treatment increases and vice versa. Reduction of the Ru additions to levels below 5.2wt% would improve cost competition without detracting from performance.

TABLES OF CONTENTS

DECLARATION ..... **II**

PUBLICATIONS AND PRESENTATIONS ..... **III**

ACKNOWLEDGEMENTS ..... **IV**

ABSTRACT ..... **V**

TABLES OF CONTENTS ..... **VII**

LIST OF FIGURES AND TABLES ..... **XI**

CHAPTER I : INTRODUCTION **1**

I.1 Background and Motivation 1

I.2 Problem Statement 4

I.3 Purpose and Aim 4

I.4 Objectives 5

CHAPTER II : LITERATURE REVIEW **6**

2.1 Background on Corrosion Theory 6

2.1.1 Design of Corrosion Resistant Materials *7*

2.1.2 Corrosion Resistance of Stainless Steels *9*

2.1.3 Design of Nickel Based Alloys *15*

2.1.4 Economical Consideration and Sustainability *20*

2.2 Corrosion Behaviour of Ruthenium modified Steels and Other Alloys 24

2.2.1 Background on Corrosion Modification *24*

2.2.2 Corrosion Modifying Mechanism through Ru Additions 25

2.2.3 An Overview of Postulates and Discoveries on Ru-Modified Alloys 31

2.3 LASER SURFACE ALLOYING 33

2.3.1 Background 33

2.3.2 Laser Types 37

2.4 CORROSION TESTING AND MEASUREMENTS 38

2.4.1. Background 38

2.4.2. Tafel Plots and Corrosion Rate Calculations 39

CHAPTER III : MATERIALS AND METHOD 40

3.1 METALLURGICAL INVESTIGATIONS 40

3.1.1 Laser Surface-Alloying 40

3.1.2 Determination and Analysis of the Microstructure 44

3.2 ELECTROCHEMICAL MEASUREMENTS 46

3.2.1 Solutions and Specimen Preparation 47

3.2.2 Method 48

CHAPTER IV : RESULTS 51

4.1 LASER BEAD SHAPE AND PROFILE 51

4.2 CHEMICAL COMPOSITION ANALYSIS 52

4.2.1 AISI 316L SS +12.5wt% Ru 53

4.2.2 AISI 316L SS + 5.2wt% Ru Alloy 55

4.3 MICROSTRUCTURAL ANALYSIS 58

4.3.1 AISI 316L SS +12.5wt% Ru 58

4.3.2 AISI 316L SS + 5.2wt% Ru..... 61

4.4 MICROHARDNESS 62

4.5 ELECTROCHEMICAL TESTS RESULTS 64

4.5.1 Untreated AISI 316L stainless steel 64

4.5.2 AISI 316L SS + 5.2wt% Ru..... 67

4.5.3 AISI 316L SS +12.5wt% Ru 70

4.5.4 Hastelloy© C-276 72

4.5.5 Competitive Corrosion Performance of Ru Containing Stainless Steel..... 74

CHAPTER V : DISCUSSIONS.....83

5.1. LASER BEAD CHARACTERISATION 83

5.1.1. Laser Bead Profile 83

5.1.2. Composition 84

5.1.3. Microstructure 84

5.1.4. Hardness 85

5.2. CORROSION BEHAVIOUR 86

5.2.1. Effect of Temperature..... 86

5.2.2. Effect of Acid Concentrations 87

5.2.3. Effect of Alloy Composition (i.e. Ru and Ni content)..... 88

5.3. COST ESTIMATION: ECONOMICAL FEASIBILITY 93

CHAPTER VI : CONCLUSIONS 101

6.1. CONCLUSIONS 101

6.2. SUGGESTIONS FOR FUTURE WORK 102

REFERENCES 104

List of Figures and Tables

Figure 2.1: Layer formation by diffusion of either metal ion (M^{N+}) or electrolyte species (H^+, O^{2-}) 9

Table 2.1: Roles of various alloying elements in stainless steels 12

Figure 2.2: Adiabatic saturation curve showing H_2SO_4 concentration for various temperatures [2]. 14

Table 2.2: Representative stainless steels and high nickel alloys used in sulphuric acid conditions [2]. 19

Figure 2.3: Sustainable science model [87] 21

Table 2.3: Relative cost of tanks made out of stainless steels and high nickel alloys [91] 23

Data source: Ashland Engineering internal study, June 2013 [91] 23

Table 2.4: New, improved and cost-optimised ruthenium-enhanced titanium alloys for corrosive service [28] 25

Figure 2.4: A sketch illustrating atomic clustering on a metal surface 28

Figure 2.5: Summary of the effects of alloying additions on the polarization characteristics of Fe-Cr stainless steel in sulphuric acid [6]. 31

Figure 2.6: Schematic illustration of laser surface alloying with direct injection of alloying material 34

Table 2.5: Common parameters considered in mathematical modeling of laser surface alloying processes 36

Table 2.6: Summary of influences of independent process variables on characteristics of laser surface alloyed layer 37

FIGURE 2.7: EXPERIMENTALLY MEASURED TAFEL PLOT. 39

TABLE 3.1: COMPOSITION (WT %) OF MATERIALS USED IN THE LASER ALLOYING PROCESS 41

TABLE 3.2: COMPOSITION OF THE POWDER MIXTURES PREPARED FOR SURFACE ALLOYING 41

FIGURE 3.2: MACROGRAPHS OF TWO SEPARATE LASER BEADS ON TYPE 316L STAINLESS STEEL PLATE MADE USING A 10.6 μM CO_2 LASER BEAM OF 4 KW POWER AND A TRAVERSE SPEED OF 0.8MM/S. 42

FIGURE 3.1: SCHEMATIC REPRESENTATION OF THE LASER SURFACE-ALLOYING TECHNIQUE 43

TABLE 3.3: APPLIED LASER PARAMETERS 43

TABLE 3.4: PREPARED ALLOYS IN TERMS OF USED POWDER FOR SURFACE ALLOYING 43

FIGURE 3.3: A) STRUERS MOUNTING MACHINE PRESS, AND B) ROTATING GRINDER AND POLISHER 45

FIGURE 3.4: ZEISS PPTICAL MICROSCOPE CONNECTED TO A PC 45

FIGURE 3.5: VICKERS MICRO HARDNESS TESTER 46

FIGURE 3.6: ELECTROCHEMICAL CORROSION CELL SET-UP 49

FIGURE 4.1: OPTICAL MICROGRAPHS SHOWING A), BEAD SHAPE AT THE BOTTOM, B) SPACE BETWEEN TWO ADJACENT LASER BEADS; AND SEM MICROGRAPHS SHOWING C) BEAD SHAPE AT THE BOTTOM, D) BEAD SHAPE TOWARDS THE SURFACE. 52

TABLE 4.1: (EDS) CHEMICAL COMPOSITION RESULTS 53

FIGURE 4.2: A CROSS-SECTION SEM MICROGRAPH OF THE 12.5WT% RUTHENIUM ALLOYED AISI 316L STAINLESS STEEL SURFACE SHOWING A) EVALUATED SPOTS ALONG THE DEPTH OF A LASER BEAD, B) EDS LINESCAN DIRECTION ACROSS INTERFACE 54

TABLE 4.2: EDS ELEMENTAL COMPOSITION RESULTS OF EACH POINT / SPOT SHOWN IN FIGURE 4.2 A 55

FIGURE 4.3: EDS LINES SCAN ELEMENTAL COMPOSITION PROFILE RESULTS ALONG THE DIRECTION SHOWN IN FIGURE 4.2 B 55

FIGURE 4.4: SEM MICROGRAPHS SHOWING EDS SPOTS AND LINE SCANNING IN DIFFERENT DIRECTIONS THROUGH ALLOYED AND SUBSTRATE ZONES OF A AISI 316L STAINLESS STEEL SURFACE CONTAINING 5.2WT% RUTHENIUM..... 57

FIGURE 4.5: EDS LINES SCAN ELEMENTAL COMPOSITION PROFILE RESULTS ALONG THE DIRECTION SHOWN IN FIGURE 4.4 C. 57

TABLE 4.3: EDS ELEMENTAL COMPOSITION RESULTS OF EACH POINT / SPOT SHOWN IN FIGURE 4.4 A.... 58

FIGURE 4.6: OPTICAL MICROGRAPHS SHOWING MICROSTRUCTURE OF A) AISI TYPE 316L STAINLESS STEEL, B) FUSION LINE OF 12.5 WT% RU ALLOYED ZONE, C) HIGHER MAGNIFICATION OF DENDRITES IN 12.WT% RU ALLOYED ZONE, D) LOWER MAGNIFICATION SHOWING THE INNER MOST PART OF 12.5 WT% RU ALLOYED ZONE..... 60

FIGURE 4.7: A) SEM MICROGRAPH SHOWING RU PARTICLE IN 12.5 WT% RU ALLOYED ZONE, B) EDS ELEMENTAL COMPOSITION PROFILE (WT%) CORRESPONDING TO POINT 1,2, AND 3 IN A). 60

FIGURE 4.8: OPTICAL MICROGRAPHS OF 5.2WT% RU ALLOYED STEEL SURFACE SHOWING MICROSTRUCTURE AT A) CENTRAL MOST PART OF THE ALLOYED ZONE , B) NEAR FUSION LINE ZONE OF THE ALLOYED SURFACE. 62

FIGURE 4.9: OPTICAL MICROGRAPHS SHOWING MICROHARDNESS TESTER INDENTATIONS FORMED ALONG THE WELD BEAD IN DIFFERENT DIRECTIONS 63

FIGURE 4.10: VARIATION OF HARDNESS WITH THE DISTANCE FROM THE BEAD/ SUBSTRATE INTERFACE IN AN AISI 316L STAINLESS STEEL SURFACES ALLOYED WITH RU. THE HARDNESS MEASUREMENTS SHOWED AN ERROR OF APPROXIMATELY 3%. 63

FIGURE 4.11: POTENTIODYNAMIC POLARISATION CURVES OF THE AISI 316L STAINLESS STEEL IN 40WT% SULPHURIC ACID SOLUTIONS AT VARIOUS TEMPERATURES..... 66

TABLE 4.4: ELECTROCHEMICAL RESULTS OF THE UNTREATED AISI 316L STAINLESS STEEL SAMPLE EXPOSED TO 40WT% SULPHURIC ACID SOLUTION AT VARIOUS TEMPERATURES 66

FIGURE 4.12: POTENTIODYNAMIC POLARISATION CURVES OF THE AISI 316L + 5.22WT% RU IN 40WT% SULPHURIC ACID SOLUTIONS AT DIFFERENT TEMPERATURES 69

TABLE 4.5: ELECTROCHEMICAL RESULTS OF THE UNTREATED 5.22WT% SAMPLE EXPOSED TO 40WT% SULPHURIC ACID SOLUTION AT VARIOUS TEMPERATURES 69

TABLE 4.6: ELECTROCHEMICAL RESULTS OF THE UNTREATED 12.5WT% SAMPLE EXPOSED TO 40WT% SULPHURIC ACID SOLUTION AT VARIOUS TEMPERATURES 72

FIGURE 4.13: POTENTIODYNAMIC POLARISATION CURVES OF THE AISI 316L + 12.5WT% RU IN 40WT% SULPHURIC ACID SOLUTION AT DIFFERENT TEMPERATURES 71

TABLE 4.7: ELECTROCHEMICAL RESULTS OF THE HASTELLOY© C-276 EXPOSED TO 40WT% SULPHURIC ACID SOLUTION AT VARIOUS TEMPERATURES 73

FIGURE 4.14: POTENTIODYNAMIC POLARISATION CURVES OF HASTELLOY© C-276 IN 40WT% SULPHURIC ACID SOLUTION AT DIFFERENT TEMPERATURES 73

TABLE 4.8: ELECTROCHEMICAL RESULTS OF DIFFERENT SAMPLES EXPOSED TO 40WT% SULPHURIC ACID SOLUTION AT 40^{O}C. 76

FIGURE 4.15: POTENTIODYNAMIC POLARIZATION CURVES OF VARIOUS ALLOYS IN 40WT% SULPHURIC ACID SOLUTION AT 40^{O}C 75

FIGURE 4.16: POTENTIODYNAMIC POLARIZATION CURVES OF VARIOUS ALLOYS IN 40WT% SULPHURIC ACID SOLUTION AT 60^{O}C 77

TABLE 4.9: ELECTROCHEMICAL RESULTS OF DIFFERENT SAMPLES EXPOSED TO 40WT% SULPHURIC ACID SOLUTION AT 60^{O}C 78

FIGURE 4.17: POTENTIODYNAMIC POLARIZATION CURVES OF VARIOUS ALLOYS IN 60WT% SULPHURIC ACID SOLUTION AT 40^{O}C 80

TABLE 4.10: ELECTROCHEMICAL RESULTS OF DIFFERENT SAMPLES EXPOSED TO 60WT% SULPHURIC ACID SOLUTION AT 40^{O}C 79

FIGURE 4.18: POTENTIODYNAMIC POLARIZATION CURVES OF VARIOUS ALLOYS IN 60WT% SULPHURIC ACID SOLUTION AT 60^{O}C 81

TABLE 4.11: ELECTROCHEMICAL RESULTS OF DIFFERENT SAMPLES EXPOSED TO 60WT% SULPHURIC ACID SOLUTION AT 60^{O}C 82

FIGURE 5.1: MASS OF RU USED AS A FUNCTION OF WT% RU IN THE 2MM ALLOYED LAYER ON AISI 316L STAINLESS STEEL SHEET WITH 1 M^2 SURFACE AREA. 96

FIGURE 5.2: COST, C_T, OF AISI 316L PLATE SURFACE ALLOYED WITH 5.2WT% RU AS A FUNCTION OF THE THICKNESS OF THE ALLOYED LAYER. 98

FIGURE 5.3: COST, C_T, OF AISI 316L PLATE SURFACE ALLOYED TO 2 MM DEPTH AS A FUNCTION OF THE WT% RU IN THE ALLOYED LAYER. 99

CHAPTER I : INTRODUCTION

I.1 Background and Motivation

Engineering materials find applications in virtually all industries in both the developed and the developing worlds. The field is inevitably affected by both the socio-economic and environmental challenges. Sustainable development has placed a huge responsibility on material scientists and engineers to design materials of superior and sustainable properties, both economically and environmentally reliable. Consequently, development of engineering materials can become an "atom-by-atom"; "molecule-by-molecule"; or "layer-by-layer" construction process. Engineering materials used in highly aggressive environments are particularly prone to high cost [1]. On the other hand, very few materials possess a satisfactory combination of cost and effectiveness to be regarded economically sustainable in many aggressive conditions [2]. It is therefore not surprising that, despite the high cost associated with them, nickel-based alloys continue to be the preferred materials of choice in highly corrosive environments. However, in the light of the high cost associated with these alloys, there have been ongoing efforts to design economically feasible corrosion resistant steels to replace nickel based alloys [2-7].

An approach to improving corrosion resistance of stainless steels is by minor additions of PGM's [3, 6]. In this way, corrosion resistance of certain stainless steels can be increased significantly [4]. Ruthenium, the least expensive of the PGM's, is also regarded a fairly effective cathodic modifier [7, 8]. Thus, adding Ru to stainless steel for corrosion modification purposes is an economically sound concept. Several authors [7-10] have

investigated the influence of minor Ru additions on corrosion properties of steels, and found that additions in a range of 0.1 – 0.2wt% Ru increase the corrosion resistance significantly. According to Potgieter [11], the corrosion performance of Ru-modified alloys makes them candidate alloys to compete with, or even replace, most Ni based alloys used in elevated temperature and acidic environments. However, a setback of this approach is the high cost associated with Ru. As pointed out by Higginson [5], 0.2wt% Ru in a bulk volume of steel might be regarded insignificant in terms of quantity, while by economic value it is quite a significant share. Therefore, the cost of steel is greatly increased by the addition of as little as 0.2wt% Ru. It is most probably for this reason that, well over 50 years since the cathodic modification effects on steels was first observed, there are still a limited number of a Ru-modified austenitic steel grades commercially available. On this note, it will be of great importance to corrosion engineers in particular that this method be explored, and advanced into a commercially viable corrosion limiting technique. This approach of creating new materials with superior properties and reduced overall cost is sometimes based on scientific principles, and sometimes on combinatorial materials design procedures.

In principle, designing a less expensive Ru modified steel obliges use of lower amounts of Ru per bulk volume of steel, i.e. less than 0.2wt%. This can be achieved by exploring the synergistic benefit observed by Streicher [12] and Higginson [5], when Ru and Ni were both added to stainless steels in combination. This observation presents an opportunity to explore the method for economical feasibility. Ni is much less expensive than Ru, and can be used together with Ru such that the total amount of Ru per bulk volume of steel is reduced, and the corrosion properties are still enhanced. There is no

evidence of more extensive work done on the exploitation of the synergistic effect of Ru and Ni to enhance corrosion properties of steels. A study on this subject is therefore crucial, and can ultimately lead to the development of more economically competitive Ru-modified steels.

In addition to the synergistic benefit approach, another useful technique is layering, a selective treatment of the steel surface with ruthenium and nickel, to create a surface which is rich in these two corrosion modifying elements. This technique exploits the surface phenomenology of the corrosion process, and allows the use of less expensive substrate material. As a surface phenomenon, the corrosion process can be successfully combated by simply improving corrosion properties of the surface, and avoiding alloying the substrate with expensive elements. The virtues of this method are that: a lesser amount Ru will be used viz. relative to bulk alloying, and the corrosion resistance of the surface is not compromised, but greatly enhanced by the incorporation of both Ru and Ni on the surface. Surface treatment of alloys with Ru has been recommended by Potgieter [11] and Tjong [13] as a probable way of utilizing Ru for corrosion modifications. This technique has however not received much attention, probably due to the difficulties associated with the production of high quality thin surface layers of specific compositions.

It is well known that corrosion properties of surface layers, thin films and alloys depend mainly on their bulk composition, microstructure, homogeneity and porosity [14]. While bulk composition is directly dependent on the added amounts of the alloying element, the microstructure, homogeneity and porosity depend mainly on the chemistry of the

alloying elements as well as the solidification process. Furthermore, the physical and mechanical characteristics of surface layers are heavily dependent on the technique used to form them. There are various techniques which are commercially available to do surface alloying on different engineering components. Laser surface-alloying technology is regarded as versatile, and is used commercially to produce high quality modified surfaces. This technique has therefore been chosen for this study, and was used to treat AISI 316L steel substrate with ruthenium and nickel mixtures of varying composition such that experimental alloys of varying Ni and Ru contents are obtained.

I.2 Problem Statement

As constituents of the bulk steel alloys, Ru and Ni have undoubtedly shown dramatic improvements on the corrosion resistance of many steel alloys. Literature survey shows little published work on the incorporation of both these two elements onto the surface of a relatively less corrosion resistant substrate i.e. AISI 316L, by means of laser alloying. An effort was made to understand the nature of Ni and Ru containing laser applied layers such that their effects on corrosion, microstructure and mechanical properties will be evaluated and discussed. According to Toyserkani et al. [14], the formation of high quality surface layers using laser alloying technology is not always possible. It depends on the chemistry of the major constituents and the thickness of the layer.

I.3 Purpose and Aim

The purpose of the study was to produce a ruthenium containing corrosion resistant surface layer on AISI 316L stainless steel substrate, to investigate its corrosion behaviour, physical and mechanical properties with the intent of comparing, particularly

the corrosion performance, to Hastelloy© C-276. It was within the purpose of this study to evaluate the influence of Ru content on the corrosion rate and compare the findings, to the results from previous studies where Ru was used as a minor constituent of the bulk alloy.

I.4 Objectives

1. The intention of the study was to explore the limitations of using the laser surface-alloying technique to create thin Ru and Ni containing surfaces of superior corrosion and mechanical properties through electrochemical tests, microstructure investigations, composition analysis, and hardness testing.

2. The second objective was to run electrochemical tests in sulphuric acid solutions of different concentrations at varying temperatures and compare the corrosion rate of the laser alloyed surfaces to that of Hastelloy© C-276, and quantify their capability of competing with them under similar conditions.

3. Third objective was to evaluate the value for money of the surface alloying technique. The estimated cost of the experimental alloy, their corrosion performance, in comparison to the investigated Hastelloy© C-276, and the characteristics of the surfaces were considered collectively in order to determine the economical feasibility of using the laser-surface alloying technique.

CHAPTER II : LITERATURE REVIEW

2.1 Background on Corrosion Theory

It is a well-established fact that mainly, corrosion process is a chemical reaction of electrochemical nature [1, 15]. The two governing half-cell reactions completing a corrosion reaction can be represented by the following two general forms:

Anodic reaction: $Mn \longrightarrow Mn^{n+} + ne^-$ ……[1]

Cathodic reaction: $X^{n+} + ne^- \longrightarrow X$ ……[2]

Where M = Metal elemental form/ symbol

M^{n+} = Metal ion

X = Electrolyte species such as H, O

X = Ionic form of electrolyte species such as H^+, H_3O^+

The two reactions take place on the metal surface. The surface is the interface between environment and the metal substrate. The Gibbs free energy of the system (metal-environment combination) is well-established driving force behind occurrence of corrosion [15, 16]. Corrosion under favourable conditions occurs as to minimize the Gibbs free energy of the system i.e. to form more stable corrosion products. In an active corrosion process it is expected that corrosion products will always be stable if the conditions of the environment remains the same throughout the entire process. However, the stability of the corrosion products is also dependent on its physical and mechanical properties. The kinetics of corrosion processes determines the rate at which the process occurs, and can be very useful in controlling and managing corrosion [15, 16]. The

common parameters having a considerable effect on the rate of corrosion are temperature, concentration, type of metal/alloy, and the nature of the corrosion product.

2.1.1 Design of Corrosion Resistant Materials

Based on the fact that corrosion phenomena are extrinsic in nature, it can be said that the term, corrosion-resistant alloy, is purely relative. For instance, an alloy with certain electrochemical properties will exhibit different corrosion behaviour in environments of varying aggressiveness [1, 15, 16]. Thus, corrosion resistance of any specific alloy is generally a limited property. Corrosion resistant alloys are designed by looking at possible means of enhancing the resistance to electrochemical attack in a given environment.

According to Tomashov [3], there are four mechanisms through which corrosion-resistant alloys can be produced and the resistance to electrochemical attack increased, namely:

i. An increase in degree of thermodynamic stability;
ii. Retardation of the kinetics of the cathodic process;
iii. Retardation of the kinetics of the anodic process;
iv. Production of a stable passive oxide layer.

A common and effective method of enhancing corrosion properties of engineering materials is through the addition of major and / or minor alloying elements to the bulk material. Through alloying, either one or more mechanisms of protection can be induced. However, this is dependent upon the chemical nature of the alloying elements.

According to various researchers [5, 6, 15, 16], the increased thermodynamic stability of the alloy, mechanism (i), and the retardation of the anodic process, (iii), which are achieved through minor additions of noble elements such as the PGM's or gold to the alloy. The virtues of noble metals for this purpose are that they inherently require high potentials for oxidation to occur. Thus incorporation of these metals onto the alloy induces thermodynamic stability, and also reduces the rate of anodic dissolution. Other studies [10, 15, 17] have shown that mechanisms (i) and (iii) are also achievable even through additions of less noble elements such as Ni, Mn, and Cr. The influence of these alloying elements on (i) and (iii) is attributed to their remarkable modification of the microstructure. These elements stabilise certain phases of the alloys thereby causing it to only start decomposing at higher potentials.

Also induced through alloying, and undoubtedly the most popular characteristic of corrosion resisting alloys is the formation of a thin passive oxide layer on the surface, (iv) (see Figure 2.1), when the alloy is exposed to a corrosive atmosphere. Stainless steels are well known for this in oxidizing atmosphere. Due to their high Cr content, more than 11wt%, Figure 2.1 illustrates the formation of an oxide layer on the metal substrate due to corrosion, also shown is the diffusion of the metal cations and other anions through the layer. Depending on porosity of the oxide layer, adherence on the metal, and the solubility in the electrolyte, the diffusion rate of the ions can be the rate determining step.

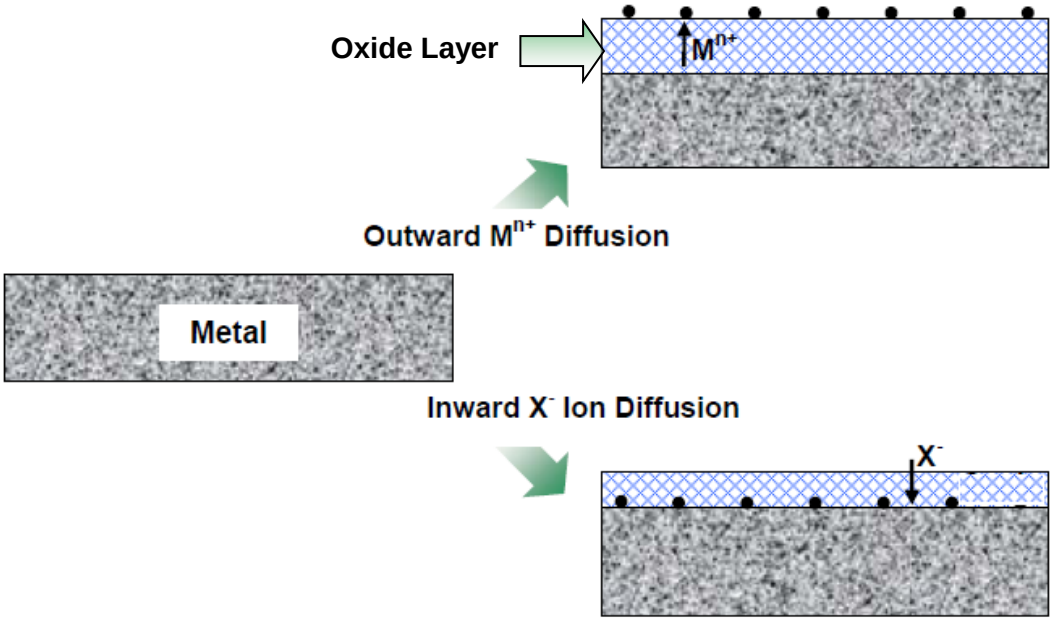


Figure 2.1: Layer formation by diffusion of either metal ion (Mn^{n+}) or electrolyte species (H^+, O^{2-})

2.1.2 Corrosion Resistance of Stainless Steels

2.1.2.1 Design and Performance

A breakthrough of metallic alloying for corrosion purposes came over a century ago when Monnartz [17] observed that additions of Cr to iron based alloy resulted in increased corrosion resistance and almost no tarnish under atmospheric conditions.. It was further established that when the chromium is in excess of 10.5% in iron based alloy, the corrosion product barrier changes from an active film to a passive film. This was due to the formation on an oxide layer on the surface of steel. This passive layer is extremely thin, in the order of 10 to 100 atoms thick, and is composed mainly of chromium oxide. The chromium oxide prevents further diffusion of oxygen into the base metal. This discovery let to the development of the class of steels known as stainless steel, and hence

thereof by definition, stainless steel must contain a minimum of 50% iron, and at least 10.5% chromium. The dramatic corrosion resistance of the chromium oxide layer is attributed to a strong bond between Cr and O, their dense and non-porous structure, and the complete adherence to the substrate/ un-corroded part of the alloy [17, 18].

However, the corrosion resistance of conventional stainless steels is greatly reduced in highly corrosive environments. For instance, in chloride ion containing medium, the chromium in the chromium oxide layer combines with the chloride ions to form a soluble chromium chloride thereby destroying the passive film. Also, investigations into the corrosion resistance of various stainless steels in acidic environments at elevated temperatures show that the resistance is far less than in atmospheric conditions [2]. Development of corrosion resistant steels involves alloying with suitable elements, which individually brings specific properties to the alloy. Through alloying and heat-treatment various classes of stainless steel are manufactured. Based on the phases of their microstructure, stainless steels are divided into four main groups: ferritic, austenitic, martensitic and austeno_ ferritic. According to a technical product handbook published by Columbus Stainless Steels Corporation [19], there are over 100 commercially available corrosion-resistant stainless steel grades designed for specific corrosive environments.

It is well established that even in minor quantities, additions of some elements greatly change both the microstructure and properties of stainless steels. For instance, as pointed out by Lai [80] the austenitic molybdenum-containing AISI type 316 stainless steel has been widely used within the power-generating industry. It has higher creep strength than

the unstabilized molybdenum-free AISI type 304 steel and better resistance to heat-affected zone cracking during welding than the niobium- and titanium-stabilized grades, *i.e.* AISI types 347and 321. However the effectiveness of each alloying element on corrosion resistance of stainless steels is not always linear i.e. higher content is does not always give better corrosion properties. For instance, although additions of Mo to stainless steel is known to improve corrosion resistance, one study [83] has shown that increasing Mo in not always beneficial. Pardo et al. [83] investigated the effect of Mo and Mn additions on the corrosion resistance of two austenitic stainless steels, AISI 304 and 316, in 30wt.% H_2SO_4 an found that the corrosion current density was one order of magnitude lower than for stainless steels with low molybdenum content. This observation shows that the positive effects of alloying elements on corrosion properties of stainless steel are limited to some amount added for each type. Above or below certain level (amount), the effectiveness of adding alloying elements either dimishes or shows no added benefit to the properties, or becomes detrimental to the properties. Design of corrosion resistant stainless steels and other alloys involved optimisation of all important alloying element such Cr and Mo contents in order to achieve this resistance to corrosion. It is therefore a common practice that there are specified allowable amount of each element for all stainless steel grade [15]. Roles of various elements on stainless steels are presented in Table 2.1 in the next page.

Table 2.1: Roles of various alloying elements in stainless steels

Element	Modifying Mechanism or Effects
Chromium (Cr)	- greater affinity to oxygen than Fe - Hence, form a strong non-porous oxide on the surface
Nickel (Ni)	- Less readily oxidized than Cr and Fe - Austenite former - Increases resistance to mineral acids Produces tightly adhering high temperature oxides
Manganese (Mn)	- Austenite former - Combines with sulfur - Increase solubility of N and Mo
Molybdenum (Mo)	- Form complex oxides that stabiles the passive layer
Titanium	- Stabilizes carbides to prevent formation of chromium carbide Precipitation hardener
Tungsten (W)	- Form complex oxides that stabiles the passive layer
Nitrogen (N)	- Reduce the dissolution rate of iron
Carbon (C)	- Carbide former and strengthener
Sulfur (S)	- Austenite former - Improves resistance to chlorides - Improves weldability of certain austenitic stainless steels Improves the machinability of certain austenitic stainless steels
Niobium	- Carbide stabilizer - Precipitation hardener
Aluminum	- Deoxidizer - Precipitation hardener

Furthermore, passive layers forming on different stainless steel differ in both composition and characteristics. The actual chemical composition of the passive layer that forms on stainless steel varies greatly with each type. In acidic solutions, austenitic stainless steels form a passive layer consisting of three layers of varying compositions [17]. The first layer is at film/metal interface and is enriched in nickel, while the second layer is mainly chromium oxide (Cr_2O_3). The outer layer is consisting of a hydroxide film. The high concentration of nickel at the film/metal interface is attributed to the selective oxidation of Cr and Fe that takes place during polarization

Eventhough stainless steels show great corrosion performance in many industrial environments, their corrosion resistance is not adequate in highly aggressive environments such as highly acidic conditions at elevated temperatures. This is because when the stainless steel is exposed to an oxidizing atmosphere and high temperatures, the chromium diffusion to the oxide layer will create a chromium depleted region under the oxide and this will weaken the stainless steels resistance to corrosion particularly when the oxide layer is destroyed. Exposure at elevated temperatures also results in changes in microstructures such as the formation of carbides and intermetallic phases [80]. This in turn affects the corrosion behaviour of stainless steels, which often leads to reduced resistance to corrosion. A study that compared the effect of temperature and concentration on the corrosion rates of some of the certain nickel based and some steels was carried out [2] and the results are shown in Figure 2.2. Figure 2.2 shows that high nickel alloys perform much better than steels particularly at elevated temperatures.

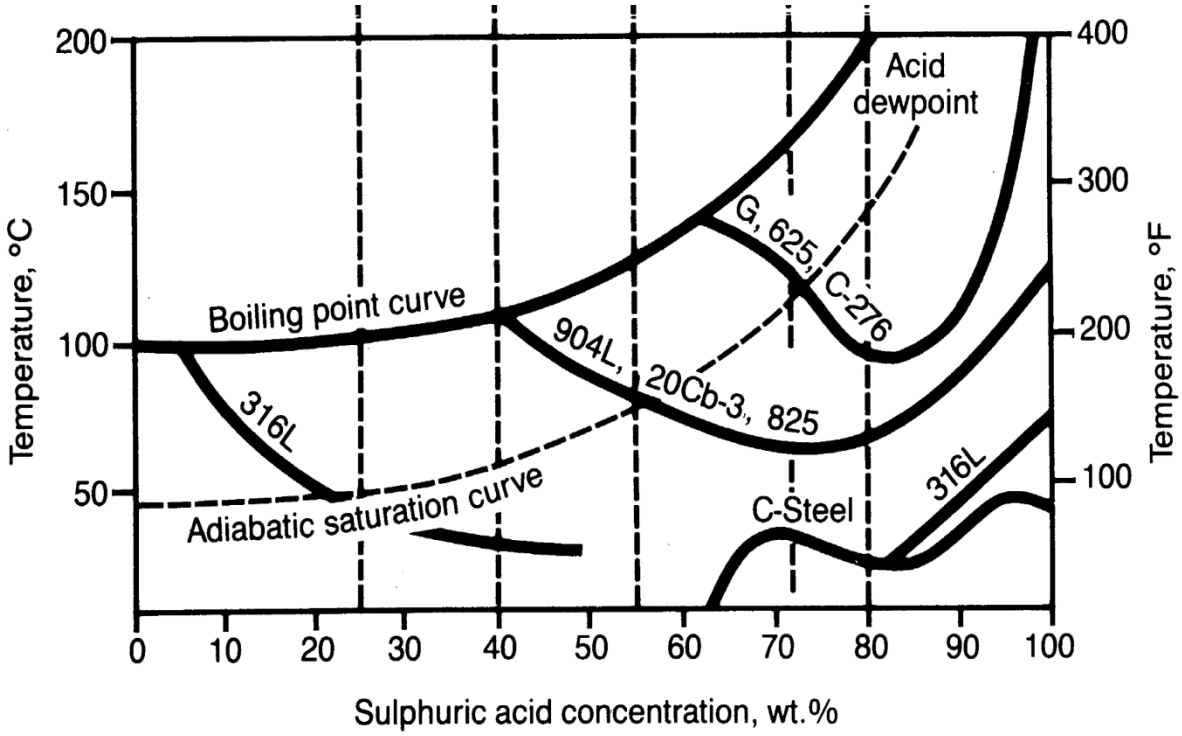


Figure 2.2: Adiabatic saturation curve showing H_2SO_4 concentration for various temperatures [2].

2.1.2.2 Effects of Contaminants

According to Jessen [76], the formation of passivating chromium oxides on stainless steels requires a certain oxidising effect, and, up to a certain limit, stainless steel thus performs better in oxidising acids than in non-oxidising acids i.e. sulphuric acid. Therefore, presence of oxidizing contaminants / agents such as dissolved oxygen, sulphur dioxide, nitrate ions, ferric ions, chromates, etc in sulphuric acid helps in inhibiting corrosion of stainless steels. To the contrary, reducing contaminants such as halides, hydrogen sulphides and compounds of arsenic have adverse effects on corrosion performance of stainless steels and other passivating alloys. In sulphuric acid, small variations in these impurities or temperature can greatly affect service corrosion rates and hence potential durability of stainless steels. There are various modes by which specific

electrolyte species interacts with the stainless steel at the metal/electrolyte interface to reduce the stainless steels ability to resist corrosion. As pointed out by Olsson and Landolt [81], in case of chloride and suplhate ions, three different models are suggested: adsorption leading to local film dissolution, penetration of anions in the film leading to weakening of the oxide bonds, and film break down at defects such as cracks and dislocations.

2.1.3 Design of Nickel Based Alloys

Nickel based alloys have been developed to cope with intermediate sulphuric acid concentrations i.e. 20 to 70 wt% sulphuric acid, in conditions beyond the capability of AISI 316L stainless steel [2]. The virtue of nickel based alloys is their high nickel content as compared to stainless steels. Investigations concerning electrochemical behaviour and importance of nickel as a major constituent of high corrosion resistant material are divided into passivity and dissolution behaviour [2, 77]. Inherently nickel is electrochemically more stable than iron, and therefore show lower dissolution rates than iron in most acidic environments. According to Deo et al. [78], the lower efficiency of nickel dissolution in dilute sulphuric acid is apparently the consequence of the formation of insoluble passive oxide films during the electrochemical evolution of oxygen in the positive half cycle. The nature of the passive film on nickel is reported to vary with the electrolyte but is mainly nickel oxide. Passive films species observed and reported in literature include NiO, Ni_2O_3 and NiOOH [77].

Nickel 200 alloy is commercially pure (99.6% Nickel), and is best at resisting corrosion in reducing environment. It can withstand sulphuric acid at low and moderate temperature, anhydrous hydrofluoric acid at elevated temperatures, organic acids of all concentrations, and many other conditions [79]. With increase in concentration of sulphuric acid, the passivating effect of nickel diminishes and therefore dissolution efficiency increases. The following grades of pure nickel are commercially available:

- Nickel 200 (99.6% Ni, 0.04% C)
- Nickel 201 (99.6% Ni, 0.02% C maximum)
- Nickel 205 (99.6% Ni, 0.04% C, 0.04% Mg)
- Nickel 270 (99.97% Ni)

Addition of alloying elements onto nickel has led to development of corrosion resistant material wherein each alloying element plays a specific role in prohibiting corrosion rate of high nickel alloys. Alloying nickel with different elements at varying concentrations has led to the development of various types of nickel based alloys. Owing to their high resistance to localized attack in chloride media, Ni-Cr-Mo alloys are considered to be the most corrosion resistant of the Ni base super alloys [77-79, 82]. The roles of the major alloying elements used to promote corrosion resistance in nickel-base alloys are summarised below.

Copper:

Copper is a main constituent of nickel-copper alloys such Monel® 400 and Monel® K-500. It improves corrosion resistance of nickel-base alloys to non-oxidising acids while also providing toughness over a wide temperature range.

Chromium:

The addition of Cr to Ni changes the electrochemical behavior of the alloy by lowering both the passivation potential and the passive dissolution current. When added to nickel chromium produces an adherent protective scale containing Cr_2O_3 on the surface of the material when heated in an oxidising environment [2, 79, 83]. Thus it improves corrosion resistance of nickel-base alloys to oxidising media such as nitric (HNO_3), chromic acids (H_2CrO_4) as well as hot phosphoric acid (H_3PO_4). It also improves resistance to high temperature oxidation. According to Sim and Hagel [83], optimum oxidation resistance in nickel-chromium alloys is obtained with chromium content in the range 15 to 30%.

Molybdenum:

Substantially improves resistance to non-oxidizing acids as well as oxidizing acids [79]. Molybdenum also markedly improves the pitting and crevice corrosion resistance of nickel-base alloys. There are postulates attempting to discuss mechanisms through which Mo actually achieves its corrosion modifying effects. Most common suggesting is that molybdenum preferentially locates at the defects sites in the passive layer thereby by blocking less noble elements such as Fe, and Ni from freely movement [83].

Tungsten:

Similar effects as molybdenum although its high atomic weight is a disadvantage.

Cobalt:

Like iron, cobalt increases the solubility of carbon in nickel-base alloys, and this increases resistance to carburization.

Silicon:

Silicon is typically present only in minor amounts in most nickel-base alloys as addition to promote high temperature oxidation resistance.

Although nickel-base alloys are generally superior to stainless steels, there are several speciality stainless steel grade that give comparable corrosion performance to nickel based alloys in highly aggressive sulphuric acid conditions inspite of lower nickel content [2]. Chemical compositions of iron and nickel based alloys used in aggressive sulphuric acid conditions are given in Table 2.2.

Table 2.2: Representative stainless steels and high nickel alloys used in sulphuric acid conditions [2].

	Stainless steels								High-nickel alloys			
Generic designation	304L	316L	317LM	2205	904	904hMo	28	20	825	G-3	C276	625
UNS designation	S 30403	S 31603	S 31725	S 31803	N 08904	N 08925	N 08028	N 08020	N 08825	N 06985	N 10276	N 06625
Nominal analysis	%	%	%	%	%	%	%	%	%	%	%	%
C max	0.03	0.03	0.03	0.03	0.02	0.02	0.02	0.03	0.025	0.015	0.015	0.1
Cr	18	17.5	18	22	20.5	20.5	27	20	21	22	16	21.5
Ni	10	13.5	13	3	25	25	31	37.5	42	41	57	51
Mo		2.5	4.5	3	4.7	6	3.5	2.5	3	7	16	9
Cu					1.5	1	1	3.5	2.5	2		
N			0.14	0.15		0.12						
Cb orTa								0.3		0.3		3.65
Others								Cb	Al,Ti	Co,W	Ti	AI,Ti.Co
Fe	Bal.	Bal.	Bal.	Bal.	Bal.	Bal.	Bal.	Bal.	Bal.	Bal.	Bal.	Bal.

2.1.4 Economical Consideration and Sustainability

It is reported [15, 73] that the cost of corrosion is in the range of 3.0 to 5.0% of GNP in many developed and developing countries. A research study carried out South Africa in 2004 showed that South Africa's corrosion related losses were at 5.2% of GNP [15]. This study was done based on steel that is sold to replace corroded material, and was found to be about half of all produced steel.

When following a holistic approach however, the consequences of corrosion are far more pronounced than just economical. In the last two decades, a more societal perspective of studying and controlling corrosion phenomenon emerged, probably due to increased awareness of environmental degradation, and the legislative developments thereof. Considering that corrosion degrades material properties and thereby depleting natural resources, and more importantly lead to the contamination of resources e.g. water by forming poisonous soluble products, it can be seen that indeed corrosion will lead to adverse economical, ecological and health conditions. With this all round impact of corrosion, corrosion control and practices needed a much more comprehensive review. As a result, many non-profit NGO's corrosion based international organisations, such as: Southern African Institute of Corrosion (SAIC), National Association of Corrosion Engineers International (NACE), European Federation of Corrosion (EFC), the World Corrosion Organisation (WCO), etc. have steered their vision towards promoting education and best practices in corrosion control for the socio-economic benefit of the society, preservation of resources, and protection of the environment. Their vision can be summarised by the concept of sustainable science, Figure 2.3, which aims to govern and guide the modern scientific solutions or designs.



Figure 2.3: Sustainable science model [87]

It is widely suggested that a definition of the costs of corrosion must contain elements of cost that are measurable and amenable to studies. The cost of corrosion is essentially the total cost that is incurred because corrosion exists, at least theoretically. The main elements in the cost of corrosion are postulated as follows [1, 2]:

- Increased capital cost
- Increased operating cost
- Increased business cost
- Increases in fixed cost
- Production losses

Problems in corrosion design generally demand a synthesis of corrosion theory, training, cost consciousness, common sense, and experience. In all these considerations, it is easy

to acknowledge that alloy cost is the obvious factor. In any sensible approach, the aim should always be to use the less expensive materials commensurate with the specifications. While the capital cost of the material is an important indicator, properties such as shape, weight to mass ratio (density) of the engineering component are critical in evaluating the actual corrosion cost of the material for a particular service. For instance, services which require thick steel plates for a specific surface area are most likely to have higher capital cost than services that require steel plates with lesser thickness. However under similar corrosion conditions, the thick component will have shorter life span than the thin plates, and consideration should therefore be taken in determining which of the component is actually less cost effective. Corrosion is a surface phenomenon, and its well known that corrosion resistant alloys are inherently expensive. It is therefore not necessary for the bulk of the material to have high corrosion resistance, for as long the bulk material satisfies other engineering requirements such as strength, toughness, creep, etc. Surface alloying and surface treatments appear more economically sound and relevant for corrosion protection of thick component where less expensive material can be used on the bulk of the material.

By virtue of specifications, materials used in highly aggressive environments generally are also relatively more expensive. A survey [2] was carried out to compare cost of various steels and high nickel alloys used in acidic conditions. The data in Table 2.3 shows that cost of alloys used in highly aggressive conditions are twice the price of standard plain carbon steel. Based on the data in the Table 2.3, there is an opportunity to design steels of comparable performance to alloy C-276 but which would be less expensive. The present study seeks to modify SS 316L surface such that its corrosion

properties can be enhanced, and overall cost remain lower than the cost of these more corrosion resistant alloys. This can be done by using the effects of ruthenium as postulated by several authors, who investigated the impact of Ru on corrosion properties of stainless steels.

Table 2.3: Relative cost of tanks made out of stainless steels and high nickel alloys [91]

Generic designation	Carbon Steel	316L	2205	Hastelloy© C-22	Hastelloy© C-276
Tank	1.0	1.8	2.7	6.0	6.8

Data source: Ashland Engineering internal study, June 2013 [91]

2.2 Corrosion Behaviour of Ruthenium modified Steels and Other Alloys

2.2.1 Background on Corrosion Modification

Minor additions of ruthenium to the bulk of steel, chromium, and titanium based alloys improve their corrosion properties significantly [3]. This method of enhancing corrosion properties through minor additions of noble metals was developed by Tomashov [3, 20] in the late 1940's, and is known as cathodic modification. There has been a considerable contribution from several other authors [5, 6, 12, 21, 22] on the subject. Most of the work was done prior to the early 1990's, and findings thereof have been comprehensively reviewed by Potgieter and co-workers [6, 23]. It would seem that these early studies on cathodic modifications were characterized by comparing the effects of various PGMs on the corrosion behaviour of certain alloys. Ruthenium additions showed overall better corrosion properties than both platinum and palladium additions in many non-oxidizing fairly aggressive environments. Some of early comprehensive studies on the influence of various PGM additions on corrosion include on the following alloys i.e. chromium based alloys by Green et al [21] and Tomashov [4], titanium based alloys by Stern and Wissenburg [22], and ferritic stainless steels by Streicher [12] and Higginson [5].

However, the commercial viability of Ru-modified alloys was heavily discouraged by its high cost at the time. In the last twenty years though, Ru became the least expensive element of the PGM's, and its price has been relatively stable. As a result, several authors [7-10, 24-27] have investigated the corrosion behaviour of several alloys cathodically-modified with ruthenium with the aim to commercialise. The revitalisation of research on

ruthenium modified alloys has led to commercial breakthroughs of lower cost corrosion resistant ruthenium modified titanium alloys [28]. Apart from enhanced corrosion in acids, ruthenium additions to titanium also effectively inhibit crevice corrosion in hot aqueous halide and sulphate environments [28]. Table 2.4 gives some commercial ruthenium modified titanium alloys.

Table 2.4: New, improved and cost-optimised ruthenium-enhanced titanium alloys for corrosive service [28]

Traditional Alloy		**Improved Alloy**		**Motivation for New Alloy**
Alloy (UNS Number)	**ASTM Grade**	**Alloy**	**ASTM Grade**	
Ti-0.15Pd (R52400)	7	Ti-0.1Ru	26	Lower cost
Ti-0.15Pd (R52250)	11	Ti-0.1Ru	27	Lower cost
Ti-3Al-2.5V (R56320)	9	Ti-3Al-2.5V-0.1Ru	28	Enhanced crevice corrosion and reducing acid resistance
Ti-6Al-4V (R56400)	5	Ti-6Al-4V-0.1Ru	29	Enhanced crevice corrosion , reducing acid, and SCC resistance
Ti-3Al-8V-6Cr-4Zr-4Mo	19	Ti-38644-0.1Ru	-	Enhanced crevice corrosion, reducing acid

2.2.2 Corrosion Modifying Mechanism through Ru Additions

It is not entirely clear how alloys containing minor quantities of ruthenium achieve their improved corrosion properties [3]. However, several corrosion studies [4, 5, 7-10, 12, 20–22, 24-28] have shown that alloys containing lower levels of Ru (0.1- 0.5wt %) exhibit enhanced passivity as compared to alloys containing no Ru, and a remarkably reduced rate of anodic reaction. According to Schutz [28], the basic mechanism of ruthenium addition to titanium is considered to be very similar to that of palladium and

other platinum group metals, and results from alloy ennoblement. Essentially, elements making up an alloy have different electrochemical characteristics. According to Potgieter et al. [6] these elements are conceived to maintain their electrochemical properties. Thus, due to its noble nature, ruthenium rich particles on the corroding surface provide cathodic sites of low hydrogen overvoltage, and accelerated hydrogen ion (H_3O^+) reduction [6]. This phenomenon produces a substantial shift in the corrosion potential of the alloy in acid towards the noble value. In addition to its nobility, Ru might be improving corrosion properties through microstructural modification of the alloy, which in turn influences how the alloy behaves during corrosion [6]. It is a well-known fact that corrosion behaviour changes with a change in microstructure of same alloy [6, 8]. Olubambi et al. [8] observed that addition of as little as 0.2wt% Ru to superferritic stainless steel resulted in highly refined grains and the formation Cr-rich phases. They then reported that the enhanced corrosion behaviour of the Ru-modified superferritic steels might be partly due to the refinement of the grains, and the presence of Cr-rich phases.

An active area of research has been in the understanding of the mechanism by which alloying with Ru achieves these improved effects. These can be partly achieved by separately analysing the impact of Ru additions on the anodic dissolution rate, and the passivation behaviour of the Ru-modified alloys.

2.2.2.1 ANODIC DISSOLUTION OF RU-MODIFIED ALLOYS

It was shown that alloys in aqueous media corrode by a process of anodic dissolution, whereby the alloying elements on the surface dissolves into the electrolyte or form various corrosion products [16], which can deposit on the surface. The extent and rate of dissolution varies for every alloy-electrolyte combination. Essentially, alloying elements possess different electrochemical characteristics and, as already mentioned, according to Potgieter [6] these elements are perceived to maintain their electrochemical properties at atomic level. On the basis of this statement, it is expected therefore that during anodic dissolution of a multicomponent alloy, various alloying elements will dissociates at different rates and/or modes.

Varga et al. [10] carried out a comparative study investigating the dissolution rates of the main alloying components (Fe, Cr, Ni, Mn and Mo) during open-circuit corrosion of austenitic stainless steel type AISI 316L + 0.5%Ru in H_2SO_4 acid solution. In accordance with the findings by Olefjord et al. [29] the results of the study showed substantial dissolution rates of the less noble alloying components (Fe and Cr) as compared to those of Ni, Mo and Ru. Furthermore, Varga et al. [10] found that no Ru was detected in the solutions. This suggests that the dissolution rate of ruthenium was very low. While these selective dissolution tendencies and their various rates are well explained on the basis of the difference in electrochemical characteristics of the alloying elements, the reports made in separate studies by Higginson [5] and Biefer [30] that cathodically-modified alloy undergoing a stable active dissolution is simultaneously undergoing structural changes at atomic level have prompted much interest and debate.

Investigations [20, 21] of the Cr-Ru alloys by electron microscopy after active corrosion has taken place showed that ruthenium accumulated on the surface, and formed separate islets rather than a homogeneous layer. Similar results were found by Higginson [5] who performed Auger analysis on the corroded Fe-40Cr-0.1%Ru, and found that ruthenium existed as separate round nano particles on a spontaneously passive surface. It is well known that in cathodically modified stainless steels and chromium based alloys, ruthenium atoms exist in solid solution and are bonded to the atoms of the less noble elements such as iron and chromium respectively.

As pointed out by Potgieter [23], cathodically modified alloys of titanium, stainless steel and chromium based alloys, there is enrichment of PGM atoms on the onset of passivation, and this can be explained as being due to a diffusion mechanism. The figure below illustrates the clustering phenomenon on the surface during corrosion.

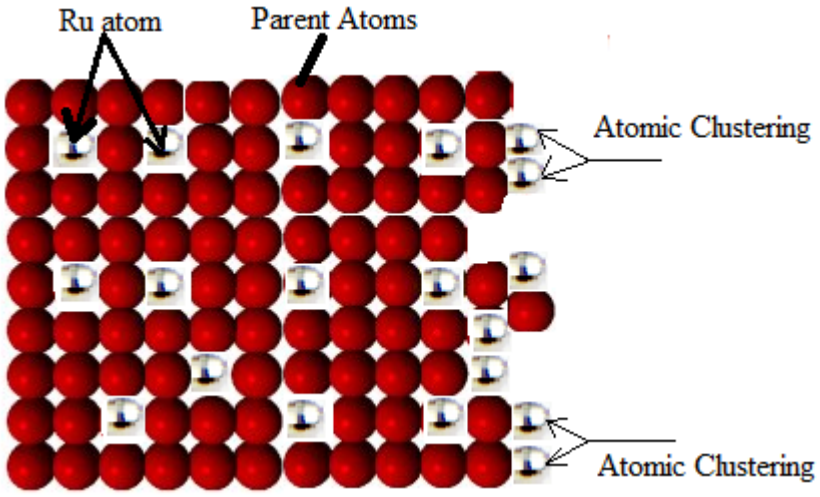


Figure 2.4: A sketch illustrating atomic clustering on a metal surface

In principle, an increase in ruthenium atoms on the corroding surface leads to an increase in the area of the exposed surface which is shielded by ruthenium. Consequently, owing to the electrochemical nobility of ruthenium in non-oxidizing media, the rate of the

dissolution of the surface will be reduced, since it requires higher potentials to dissociate Ru. Critical current density of the alloy was lowered by addition of ruthenium [23]. These reductions were found to increase with the increase in ruthenium content of the alloy [6, 23].

2.2.2.2 PASSIVATION BEHAVIOUR OF RU-MODIFIED ALLOYS

Tomashov *et al.*[33] determined that an Fe- 25%Cr alloy to which ruthenium is added passivated easier in 5% to 50% H_2SO_4, and 1% to 5% HC1 at 50°C to 100°C than did unmodified Fe- 5%Cr. This tendency to self-passivate of alloys containing lower % of chromium has been observed by several authors in separate studies [5, 7-9, 14, 22]. In an attempt to understand the role of Ru on passivation a number of authors [5,7-9,14 22] investigated the morphology, composition and thickness of the passive layer of Ru modified alloys, Higginson *et al.* [5] studied the nature of spontaneously formed passive films of Fe-40%Cr containing 0.1wt% and 0.2wt% Ru in both 0.5M HCL and 1M H_2SO_4 and found that the morphology of the passive film exhibited a loosely-adherent layer for 0.1wt% Ru alloy, and a solid planar layer for the 0.2wt% Ru alloy. Similar observations were made by Tjong [14] in a similar but separate study. The difference in the morphology was ascribed to the dissolution dynamics which prevailed during the initial stages of the anodic dissolution. It is said that due to lower amount of Ru in 0.1% Ru alloy, faster dissolution of less noble metals such as Cr, Fe, etc. occured initially thereby giving rise to a highly porous surface on which the passive layer formed [14]. On the contrary, Higginson [5] found that 0.2% Ru alloys underwent lesser dissolution before

passivation, hence a solid planar passive layer formed. Although of varying morphologies, all the alloys exhibited enhanced passivation.

The changes that took place on the surface of Ru-modified alloys varied with the composition of the alloy, and the corrosive media [5]. As it has already been discussed in the previous section, there was evidence that ruthenium accumulated on the surface during initial stages of anodic dissolution.

The distribution of various elements on the surface during dissolution had a principal effect on the passivity. A passive film analyses has shown that ruthenium was incorporated in the passive film [10, 11] during the passivation process. Though Tomashov [33] never ruled it out as a possibility in other alloys, he indicated that this was a characteristic of Cr containing steels. No extensive work on the nature of the passive film of other alloys (i.e. containing no chromium) alloyed with ruthenium was found in literature. It is well known that the presence of a PGM in an alloy promotes the hydrogen-evolution reaction and causes a shift in the corrosion potential to more noble values [6] as shown in Figure 2.5 in the next page.

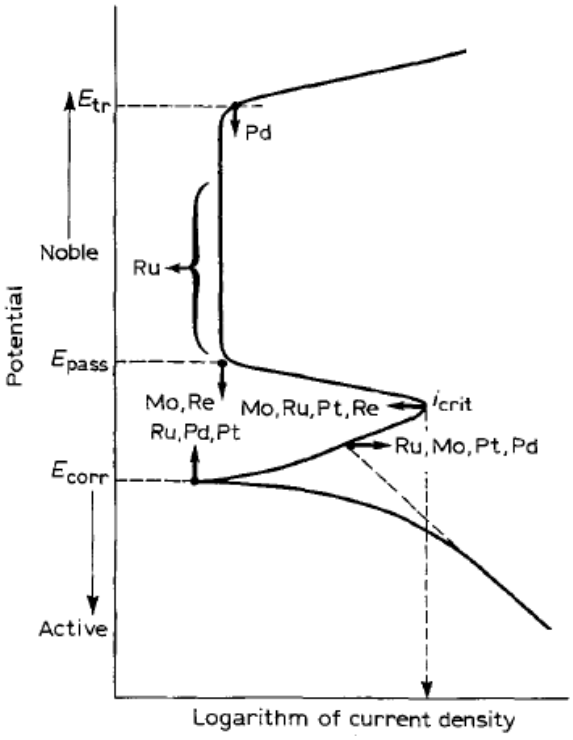


Figure 2.5: Summary of the effects of alloying additions on the polarization characteristics of Fe-Cr stainless steel in sulphuric acid [6].

2.2.3 An Overview of Postulates and Discoveries on Ru-Modified Alloys

From the work of Potgieter [6, 11, 23] there are important postulates and/or observations made regarding ruthenium-modified steels and alloys. These can be summarised as follows:

Ideal conditions for effective cathodic modifications:

1. Ru was regarded as a more effective cathodic modifier in reducing acids than even palladium or platinum.
2. The effect of the ruthenium on corrosion inhibition of austenitic stainless steels was not as dramatic as for ferritic stainless steels.

3. Ruthenium additions to steels for corrosion purposes is well suited for reducing conditions.
4. Effect of Ru addition on pitting corrosion was insignificant.
5. Synergistic benefit were observed when Ru is added together with nickel at content of 0.1wt% each.
6. Ru additions were more effective in steels containing higher chromium contents
7. Ruthenium reduced the overvoltage of cathodic hydrogen generation more effectively thereby increasing the efficiency of the cathodic process.
8. Ruthenium reduced the rate of anodic dissolution by reducing the critical current density required for passivation, especially in media containing chloride ions.
9. Ruthenium additions to alloys changed the microstructure which in turn influences the behaviour of the alloy to electrochemical attack.

2.3 Laser Surface Alloying

2.3.1 Background

Owing to a number of special features, laser treatment has emerged as a popular technique in surface modification. According to Kwak et al. [60] it drives its attractiveness in engineering applications mainly from:

1. The formation of a small heat affected zone, thus leaving the bulk properties unchanged and introducing minimal distortion.
2. Refinement and homogenization of microstructure, leading to enhanced mechanical properties and corrosion resistance.
3. The possibility of forming novel surface alloys unattainable by other methods because of the equilibrium nature of the process.

The process of laser surface alloying is accomplished through selective melting of metal surface and extraneous addition of the alloying element to the melt pool. There are two main ways of introducing the alloying element into the melt pool. These include direct injection of powder into the melt pool at the time of laser treatment, and the pre-placement of the alloying material/powder on the substrate surface prior to laser surface melting [14, 85]. In the former, the powder particles are injected in trajectory such that they exposed to laser beam as it strikes the surface. Schematic illustration of laser surface alloying with direct injection of alloying material is shown in Figure 2.6.

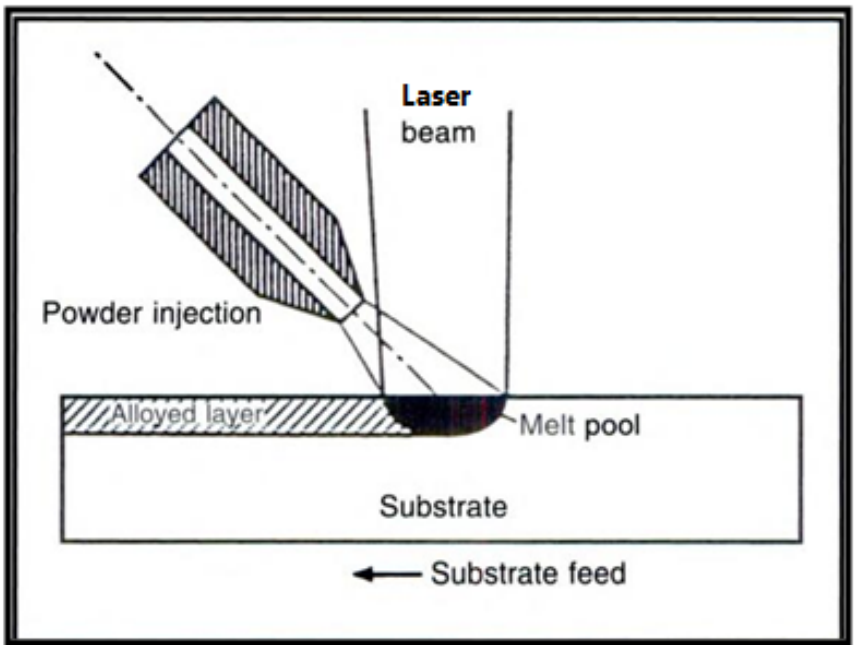


Figure 2.6: Schematic illustration of laser surface alloying with direct injection of alloying material

Laser surface alloying technique has been investigated on ferritic [61, 62], and austenitic [60, 63] stainless steels. The technique is used to enhance properties such as corrosion resistance, wear, and hardness. Tjong [13, 64] used the technique to modify steel surfaces with Ru and observed improved corrosion and mechanical properties. The success of laser surface alloying applications is dependent on a number of factors including technology, operator's skills and experience, laser operational parameters, chemistry of the alloying elements, and alloy type [14]. Any specific combinations of these factors yield different results. By employing appropriate laser processing parameters, a homogeneous alloyed layer of a required thickness can be achieved. Empirical experimentation is often used to optimize laser surface alloying of specific materials.

Khalfallah et al. [71] has successfully modified AISI 316 stainless steel surface by laser melting using laser powers of 2 and 4 Kw, and scanning speed ranging from 300 to 1500

mm/min. However, empirical experimentation with laser surface heat treatments can be costly and time-consuming [14, 84]. In order to avoid this costly exercise, numerical models that correlate and hence predicts the effects of laser process parameters on surface melt depth, cooling rates, homogenization, and surface rippling during laser surface melting have been constructed. The models are useful in selecting parameters to use for most common laser treatment processes such stainless steel laser melting. According to Fedotov et al [84], mathematical model for the surface heat treatment process will allow a significant decrease in costs, and reduce the time required for optimization. It would therefore be advantageous to use an applicable model to predict the desired treatment time, power, and temperature gradient for the required phase transformation. For instance, during laser welding a simple mathematical model that correlates dependence of processing rates, V, to laser power, q, and the material thickness, d, is given as:

$$V = k \times q \times d^{-j} \quad \ldots\ldots\ldots\ldots\ldots\ldots\ldots\ldots \quad (A)$$

Where k and j are constants

Also, the effect of the laser power, transverse scan speed, beam diameter, amount alloying element added and laser beam focal position (focus, positive and negative defocus) on the coating geometry and the properties of the cladding or alloying have been investigated [14]. These parameters are regarded as the independent variables in laser surface alloying process, and have shown to have major influences on the final product i.e. alloyed surface layer. The following is the list of common parameters which are considered during modeling of laser surface process.

Table 2.5: Common parameters considered in mathematical modeling of laser surface alloying processes

• Heat transfer coefficient
• Thermal diffusivity constant
• Radiation adsorption coefficient of metal surface
• Defocused laser beam spot
• Laser power, P
• Distance of treatment of sample surface
• Distance to middle of laser spot from sample sides
• Treated surface thickness
• Laser travelling speed, S
• Beam Diameter, D

While the effects of the laser parameters on the characteristics of laser alloyed layer varies greatly with different substrate and alloying material, there is recognition that some of the independent process variables such as laser power generally show consistent influences regardless of material type. For instance, characteristics of the laser alloyed surface layer such as the depth of alloying are directly proportional to the laser power i.e. higher laser power leads to deeper penetration of the substrate by the laser beam power [14]. There are well established influences of other parameters on characteristics of laser surface layers. Table 2.6 show some of general influences of independent process variables on characteristics of laser surface alloyed layer.

Table 2.6: Summary of influences of independent process variables on characteristics of laser surface alloyed layer

LAZ Characteristics	Prominent Influencing Process Variable	Comments
Width	Increases as P increases, Decreases as S increases	No interaction between variables
Depth	Increases as P increases Decreases as S increases Decreases as D increases	S and D interact Change in absorption mechanism
Alloying Element Content	Decreases as P increases Increases as S increases Increases as D increases	P and D interact Related to the melt volume
Average Composition Flactuation	Increases as S increases Increases as D increases	

P = Power, S = Tranverse Speed, D = Beam Diameter

2.3.2 Laser Types

Material laser processing applications are currently dominated by two types of laser sources namely: CO_2 lasers and Nd: YAG lasers [14]. One of the main advantage of the Nd: YAG laser source is that the wavelength of the laser light (1.06μm) allows the beam to be delivered via an optical fiber with relatively small energy losses. However, high-power diode lasers (HPDL) are making inroads into industrial applications, as they are compact, easy to cool, permit to yield power efficiency beyond 50%, about five times higher than any either kind of laser, and their cost is becoming increasingly attractive [85]. Using HPDL for cladding, it is possible to assert that the degree of absorption at the diode laser wavelength exceeds that of the CO_2 wavelength by a factor of at least 2.5 and are available with power outputs up to 6 kW and rectangular beam profiles that are much larger than those of CO_2 and Nd:YAG lasers.

2.4 Corrosion Testing and Measurements

2.4.1. Background

Although non-aqueous corrosion is not an unknown phenomenon to corrosion scientists and engineers, it has been generally accepted that corrosion phenomenon is largely an electrochemical process [15]. Thus, owing to this electrochemical nature, the progress of corrosion phenomenon on a metal surface may be satisfactory studied by measuring changes in metal potential with time or with applied current. The thermodynamics and kinetics principles are essential to qualitatively and quantitatively study corrosion process. Although thermodynamic principles can explain corrosion in terms of the possibility of reactions associated with corrosion processes under specific conditions, they cannot be used to predict corrosion current or corrosion rate [15].

Electrochemical methods provide an alternative to traditional methods used to determine the rate of corrosion. Direct and quantitative determination of corrosion rates can be determined from simple electrochemical measurement like a linear sweep voltammetry (LSV). Potentiodynamic anodic polarization is the characterization of a metal specimen by its current-potential relationship. A potentiodynamic polarization plot can yield important information such as the following:

[1] The ability of the material to spontaneously passivate in the particular medium

[2] The potential region over which the specimen remains passive; and

[3] The corrosion rate in the passive region as well as in the active region

2.4.2. *Tafel Plots and Corrosion Rate Calculations*

When reaction mechanisms for the corrosion reaction are known, the corrosion currents can be calculated using Tafel Slope Analysis. It is over a century since the first two articles [89, 90] on Tafel equation were first published. As explained in Princeton Applied Research instrumentation manual [88], the corrosion current, i_{corr}, is obtained from a Tafel plot by extrapolating the linear portion of the curve to E_{corr}, as shown in Figure 2.7. The corrosion rate in mil per year (mpy) can then be calculated from i_{corr} by using equation the following equation [14, 88]:

$$Corrosion\ Rate\ (mpy) = \frac{0.13 i_{corr}(E.W)}{d}$$

E.W.(g) = equivalent weight of the corroding species; d = density of the corroding species, g/cm^2; i_{corr} = corrosion current density, µA/cm^2.

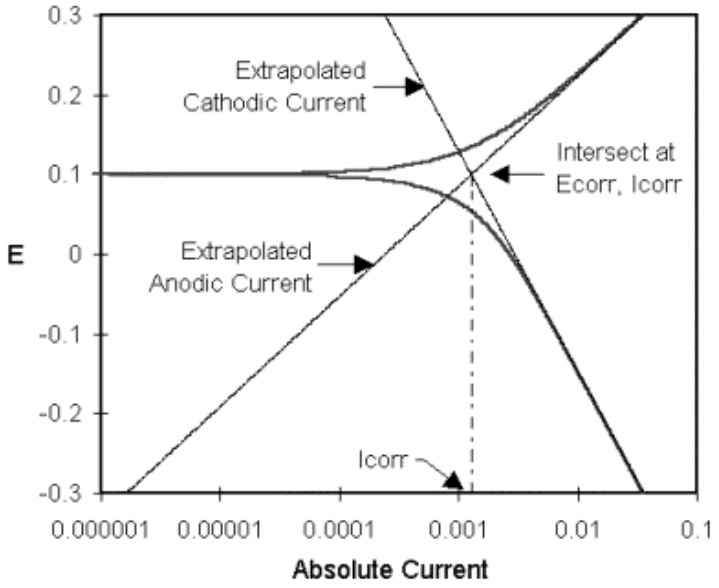


Figure 2.7: Experimentally measured Tafel plot.

CHAPTER III : MATERIALS AND METHOD

3.1 Metallurgical Investigations

The specimen and sample preparation for metallurgical investigations included laser surface alloying, cutting, and mounting. To perform metallurgical investigation, relevant processes were followed and precautions taken wherein specific equipment, material and techniques were used. The process description as well as material and equipment used are given in the following sections.

3.1.1 Laser Surface-Alloying

Laser surface alloying can be done in a variety of ways. The materials, equipment and process followed in this study are given in the section below.

3.1.1.1 ALLOYS AND MATERIAL PREPARATION

AISI 316L stainless steel was used as a substrate material for this surface alloying application. Annealed AISI 316L stainless steel sheet of commercial quality was obtained from a local stainless steel manufacturer. Nickel powder and sponge ruthenium, also of commercial quality, were used as sources of nickel and ruthenium respectively. The compositions of the AISI 316L steel sample, nickel powder and sponge ruthenium are listed in Table 3.1. It is important to note that no further heat treatment was carried out on the steel samples prior to laser treatment. The surfaces of the steel samples were cleaned using acetone to remove grease and dirt.

Nickel powder and sponge ruthenium were proportionally mixed, and blended using an automatic mixer operated for two hours. Two powder mixtures with different compositions were prepared in this manner. Two rectangular steel samples of dimensions 100 mm x 50 mm and thickness 5 mm were cut from the main sheet. These samples were subjected to laser alloying using the prepared powder mixtures. The compositions of the prepared powder mixtures are given in Table 3.2.

Table 3.1: Composition (wt %) of materials used in the laser alloying process

Element	AISI 316L Sample	Nickel Powder	Sponge Ruthenium
Fe	Balance	-	-
Cr	18.03	-	-
Ni	9.8	99.9	-
Mo	2.24	-	-
Ru	0	-	99.9
Mn	1.59	-	-
Cu	0.005	-	-
Al	0.43	-	-
Si	0.46	-	-
S	1.02	0.008	-
C	0.005	-	-
P	0.22	-	-

Table 3.2: Composition of the powder mixtures prepared for surface alloying

Mixture no	Ru powder content (wt. %)	Ni powder content (wt. %)
1	~100	0
2	~50	~50

3.1.1.2 PROCESS DESCRIPTION AND PROCEDURE

Each of the two steel samples was placed on the laser table, and separately coated with the differently prepared powder compositions. The mixed powders were preplaced on the steel surface using a chemical binder. The thickness of the preplaced powder coatings could be controlled to approximately 1 mm. The coated surfaces were then subjected to laser surface treatment using an Nd:YAG laser, equipped with a fiber optics beam delivery system in an argon atmosphere. This resulted in the powder and a small portion of the substrate melting. A 10.6 µm CO_2 laser beam of 4 kW power and a traverse speed of 0.8 m/s were used for all samples. The laser was operated in a continuous beam mode and parallel tracks with no overlapping were laid with the laser beam focused 10 mm above the coated surface. A weld bead of 4 mm width formed on the surface. Each sample was treated separately, then left to cool in ambient temperature conditions. Figure 3.1 below illustrates the laser alloying operation. Laser beads were formed by using a preplaced ruthenium powder on a AISI 316L stainless steel substrate. Micrographs presented in figure 3.2 shows images of the laser beads after cooling down under room temperature conditions. As can be seen from figure 3.2, the beads have the same length and width.

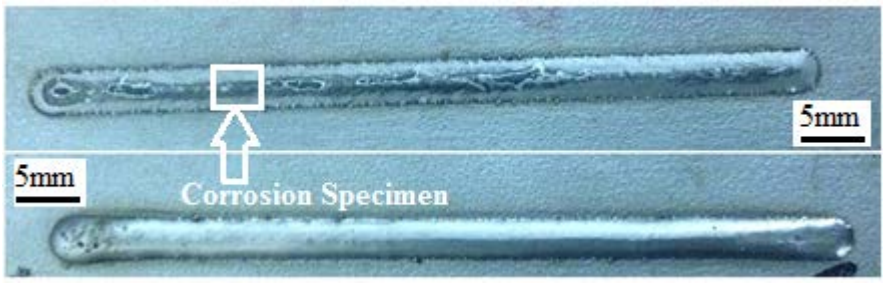


Figure 3.2: Macrographs of two separate laser beads on Type 316L stainless steel plate made using a 10.6 µm CO_2 laser beam of 4 kW power and a traverse speed of 0.8mm/s.

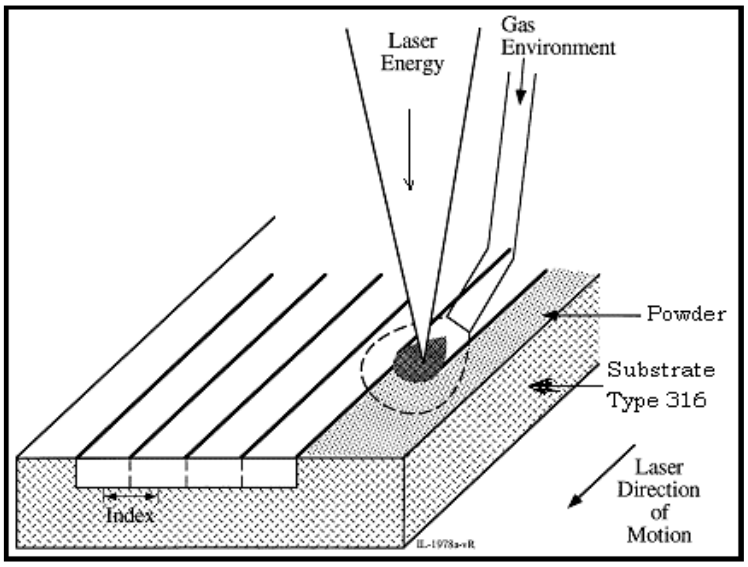


Figure 3.1: Schematic representation of the laser surface-alloying technique

The actual laser parameters used in the experiment were essentially obtained with the help and guidance from technicians and scientists who are experienced in daily activities of using the laser on material similar to the ones used in this study. Laser parameters used in this study are given in Table 3.3. Table 3.4 classifies samples, as alloys in terms of the mixture used for alloying.

Table 3.3: Applied laser parameters

Laser Source	Laser Power (kW)	Wavelength(um)	Scan Speed ($mm.s^{-1}$)	Overlapping (mm)
CO_2	4	10.6	0.8	0

Table 3.4: Prepared alloys in terms of used powder for surface alloying

Alloy no	Mixture used
1	1
2	2

3.1.1.3 SAFETY PRECAUTIONS

1. Safety glasses, closed leather shoes and a suitable laboratory coat were worn throughout the surface alloying.
2. Safety gloves were used to hold the sample before and after the operation.

3.1.2 Determination and Analysis of the Microstructure

3.1.2.1 METALLOGRAPHIC SPECIMEN PREPARATION

Samples of approximately 25 mm x 4 mm were cut from the laser alloyed plate. The samples were sectioned transversally across the weld bead, and were hot-mounted in a Bakelite and Lucite powder using a mounting press (Figure. 3.3a). The specimens were then wet ground to 1200 µm grit using progressively finer SiC grinding papers stuck onto a rotating grinder(Figure.3.3b), wet-polished to 1 µm alumina solution on a rotating polishing machine, cleaned with water and acetone before air drying.. Due to resistance of the weld bead to Marble's solution etchant, an electrolytic oxalic acid solution etchant was applied for 2 min to the weld bead after the rest of the specimen was etched for 2 min in Marble's solution. Specimens for Scanning Electron Microscopy (SEM) microanalysis were left un-etched.

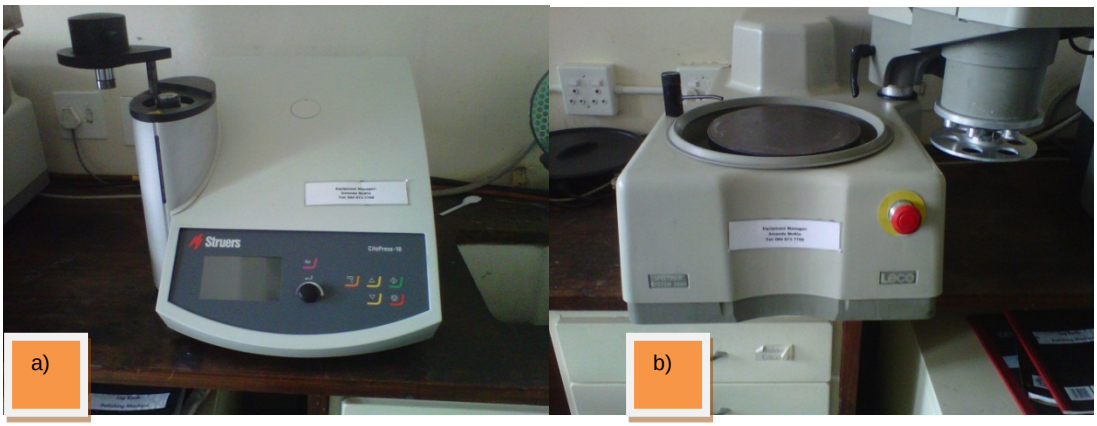


Figure 3.3: a) Struers mounting machine press, and b) Rotating grinder and polisher

3.1.2.2 OPTICAL MICROSCOPY

A Zeiss Axiotech 25 HD optical microscope (Figure 3.4) was used for imaging and the photomicrographs were taken at 50x, 100x, 500x and 1000x magnification.



Figure 3.4: Zeiss pptical microscope connected to a PC

3.1.2.3 SCANNING ELECTRON MICROSCOPY

JSM 5800 LV SEM with X-ray microanalysis that employs the Energy Dispersive X-ray Spectroscopy (EDS) technique was used to evaluate the elemental composition profile along the depth of the weld bead. Both qualitative and quantitative EDS analyses were performed on the same system.

3.1.2.4 HARDNESS MEASUREMENTS

The hardness values of the laser-alloyed were evaluated using a Vickers Micro-Hardness Tester (Figure 3.5). A load of 1 kgf was applied for all specimens and the mean diagonal of the resulting indentation was calculated and used to obtain the corresponding Vickers hardness value.



Figure 3.5: Vickers Micro hardness tester

3.2 Electrochemical Measurements

Specific procedures were followed to prepare specimens for electrochemical analysis. Samples of approximately 4 mm x 4 mm were cut as shown in Figure 3.2 using a wheel feed abrasive saw. The specimens were prepared such that as only the alloyed surface is exposed to the corrosion medium. Electrochemical measurements require careful specimen and solution preparation and adoption of precautionary measures. Solution and specimen preparations procedures are given in this section.

3.2.1 Solutions and Specimen Preparation

The following is a list of raw material used in preparation of sulphuric acid solutions and corrosion specimens.

Chemicals

1. 98.8wt% sulphuric acid
2. Distilled water
3. Polyester resin

Samples

4. AISI 316L stainless steel samples
5. As-laser-alloyed type AISI 316L stainless steel samples
6. Alloy Hastelloy© C-276
7. Insulated copper wires

40wt% and 60wt% sulphuric acid solutions were prepared by mixing proportional amounts of 98wt% H_2SO_4 and distilled water in a 1l glass flask. As a necessary precaution the acid was gradually and slowly added into the water containing flask to avoid eruptions.

The samples for electrochemical analysis were prepared by attaching an insulated copper wire to one face of the sample using an aluminium conducting tape, and cold mounted in resin. The specimen were prepared such that only the alloyed face is exposed for testing, The samples were then left for the resin to dry at room temperature conditions. Before measurements, these working electrodes were polished successively with metallographic

emery paper of increasing fineness of up to 1000 grit. The electrodes were then washed with distilled water, degreased with acetone, washed using distilled water again and finally dried with tissue paper. In order to prevent the possibility of crevice corrosion during measurement, the interface between sample and resin was coated with Bostik Quickset, a polyacrelate resin. The total exposed area of the working electrodes was $0.16cm^2$ as shown in Figure 3.2.

3.2.2 Method

An Eco-Chemie designed corrosion test cell was used to simulate the corroding system for the purpose of the present corrosion study. Figure 3.6 shows a picture of the cell showing all important components. A 4 m long tubing system was designed such that it was possible to purge nitrogen through the acidic solution in order to reduce the levels of the dissolved oxygen. The nitrogen gas was purged for 30 minutes per 200 mm of the solution. Purging was performed before each run, and was continued for the whole duration of the tests. Presumably the dissolved oxygen level was kept very low in this manner.

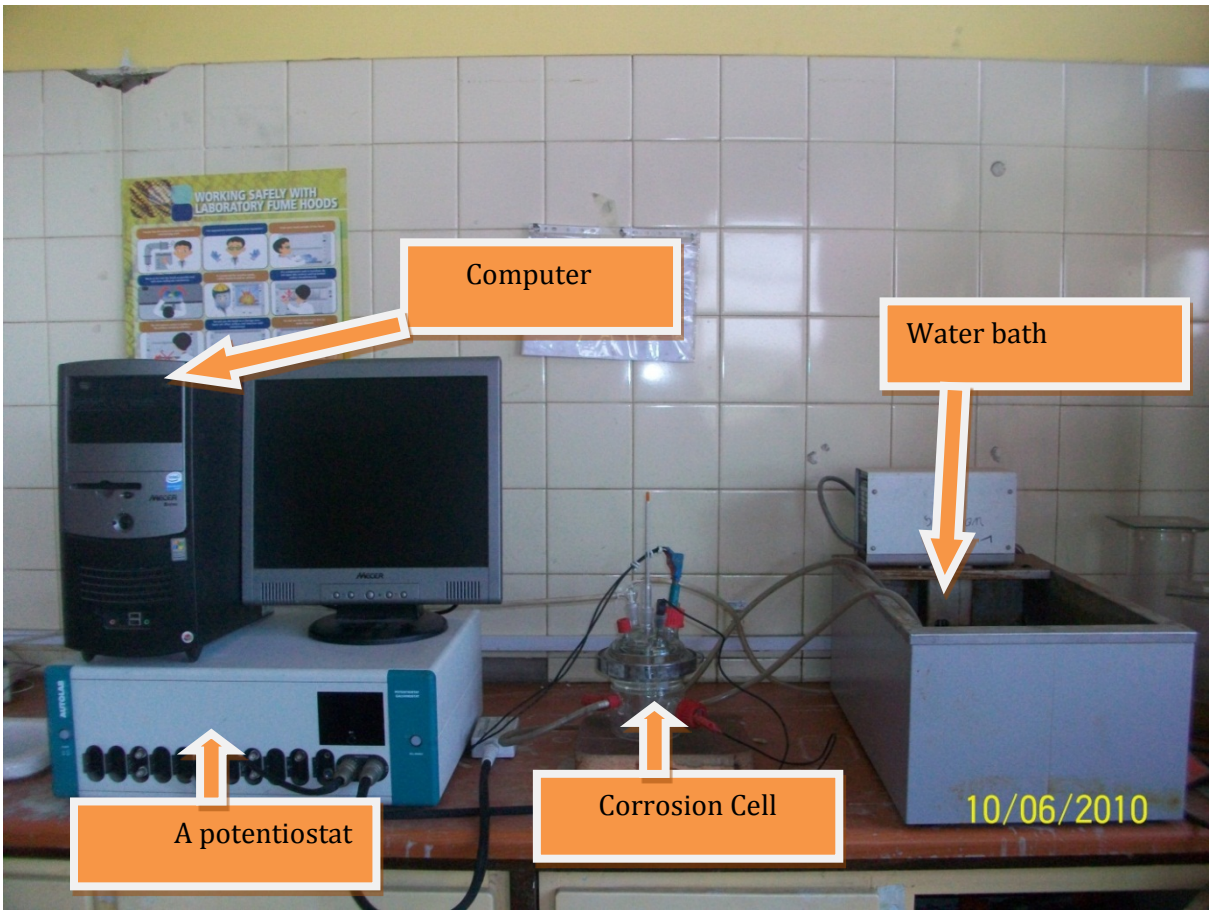


Figure 3.6: Electrochemical corrosion cell set-up

The corrosion behaviour of the alloys was evaluated by means of electrochemical polarisation measurements in the prepared sulphuric acid solutions using Autolab potentiostat. The potentiostat utilises platinum as the counter electrode and a saturated silver-silver chloride electrode as the reference electrode. Polarisation measurements were carried out according to ASTM standard G5-87 and G59-78. The potentiodynamic measurements were conducted using a scanning rate of 0.1 mV/s. Potentiodynamic polarization curves were separately obtained for each alloy-solution combination. The tests were conducted in 40wt% and 60wt% sulphuric acid solutions, kept at 25^{o}C, 40^{o}C and 60^{o}C. The temperature was controlled by use of a water bath, and was constant to

$\pm 1^{o}C$ from the set temperature. The polarization resistance technique was used to derive corrosion rates from polarization data to establish the effect of nickel and ruthenium concentrations on corrosion rates. A General Purpose Electrochemical System (GPES) software program was used for the calculation of various electrochemical parameters from the potentiodynamic responses. The corrosion parameters obtained included the corrosion potential, E_{corr}, corrosion current, I_{corr} and corrosion current density (i_{corr}). After each polarization scan the electrolytes were replaced and the samples were polished and rinsed in water to remove the products that might form on the surface which could affect measurements.

CHAPTER IV: RESULTS

This chapter presents the results obtained from the various investigations performed on the laser alloyed samples. These results include the weld bead characterisation through microscopic, compositional analysis and hardness tests, as well as corrosion properties through electrochemical characterisation by evaluating potentiodynamic polarization curves.

4.1 Laser Bead Shape and Profile

The weld bead interface with the base plate as obtained during the laser surface alloying experiments is shown in figure 4.1 (a – b). At the interface, the laser bead exhibited a near perfect semi-circular shape as shown in the optical and SEM micrographs showed in figures 4.1 a) and c) respectively. Near the surface, the width of bead gradually widened as shown in figure 4.1 d).

From the micrographs, it appears that under the applied laser parameters, the laser beam was able to penetrate and thus melt the substrate to a depth of approximately 2 mm. The depth was measured using an Axio-vision image processing software that allows parameters such as size of microstructural phases to be interactively determined. The depth of penetration was virtually the same for all investigated alloys, under the same operating parameters. This observation shows that the difference in composition of the pre-coating powders has an insignificant influence on the beam power to melt the substrate.

4.2 Chemical Composition Analysis

The average chemical compositions (by wt %) of the laser alloyed layers were obtained from the energy dispersive spectroscopy (EDS) results and the values are given in Table 4.1. Results in Figure 4.1 were measured from the transverse cross-section view, and therefore represent the average composition within the alloyed layer. The elemental composition profile along the cross-section of the alloyed surface was evaluated using JSM 5800 LV SEM with energy dispersive X-ray spectroscopy (EDS).

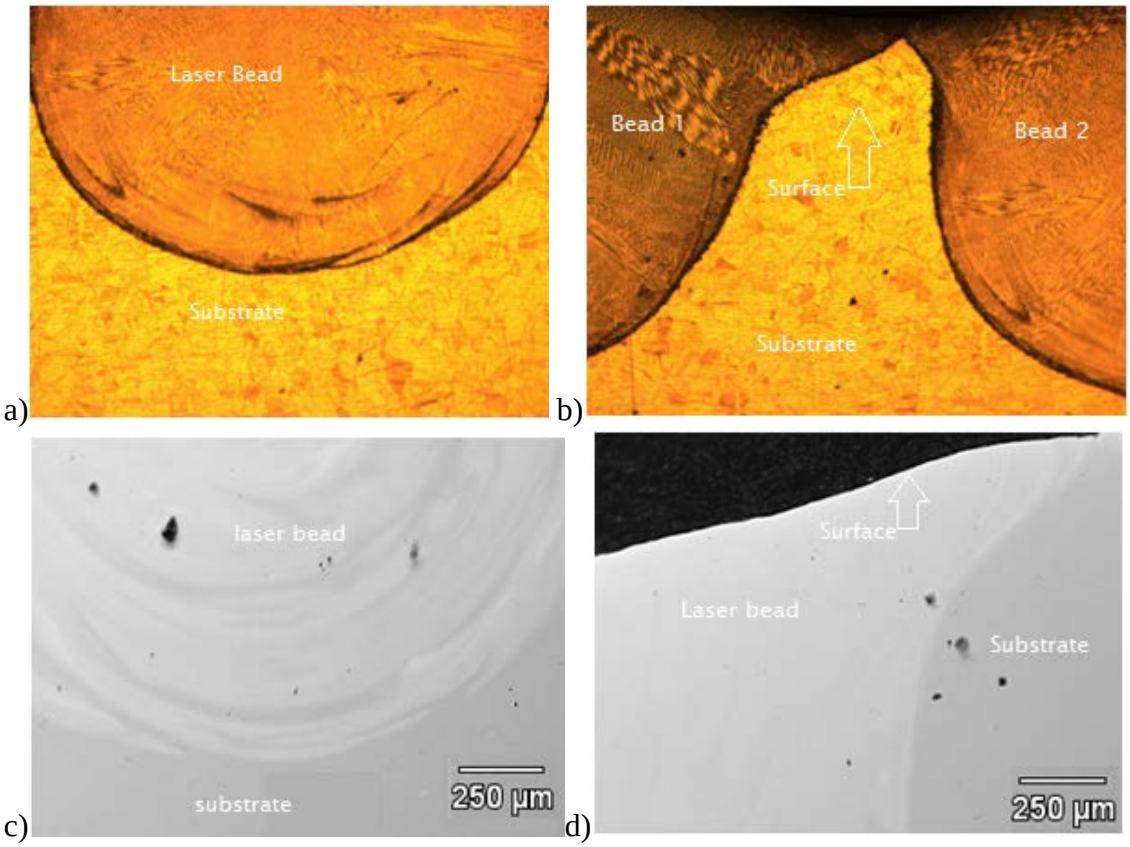


Figure 4.1: Optical micrographs showing a), bead shape at the bottom, b) space between two adjacent laser beads; and SEM micrographs showing c) bead shape at the bottom, d) bead shape towards the surface.

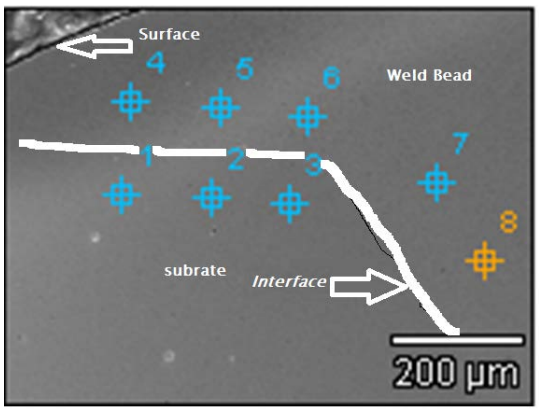
Table 4.1: (EDS) chemical composition results

Alloy	*Si-K*	*Cr-K*	*Mn-K*	*Fe-K*	*Ni-K*	*Cu-K*	*Mo-L*	*Ru-L*
AISI 316L	0.46	18.03	1.59	66.2	9.8	0.005	2.24	0.00
Alloy 1	0.41	17.07	1.84	63.67	9.45	0.31	1.85	5.22
Alloy 2	0.866	14.794	1.272	52.636	16.422	0	1.07	12.48

The elemental analysis was done in two ways i.e. single spot analysis and line scans. In single spot analysis, the electron beam was kept at a single spot/area within the alloyed layer to produce localized elemental information. A number of spots/areas located at various positions on the cross-section of the laser bead were evaluated.

4.2.1 AISI 316L SS +12.5wt% Ru

A cross-section SEM micrograph of the ruthenium alloyed AISI 316L stainless steel surface showing evaluated spots along the depth of a weld bead is shown in Figure 4.2. The specimen in Figure 4.2 was obtained from treating the substrate with 50 wt% Ru-50wt% Ni powder. The corresponding elemental composition of each spot shown in Figure 4.2 is shown in Table 4.2. It can be seen from the results that spots 1, 2 and 3 were in the untreated/unaffected substrate portion of the sample, and had a composition corresponding to AISI 316L stainless steel with no ruthenium. This shows that there was no ruthenium diffusion from the alloyed zone to spots 1, 2 and 3. In contrast, spots 4, 5, 6, 7 and 8 which were within the laser bead had higher ruthenium and nickel content. This is showing effective alloying of the bead zone with ruthenium and nickel mixtures.

a) 

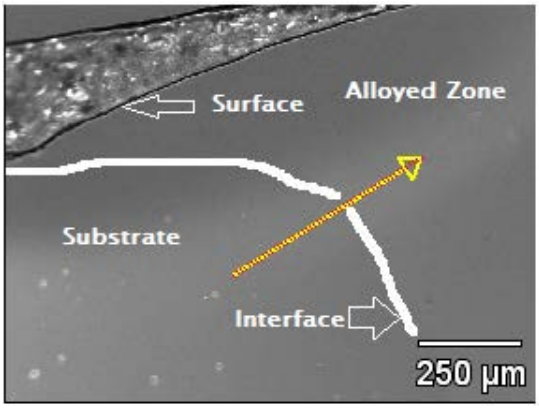
b) 

Figure 4.2: A cross-section SEM micrograph of the 12.5wt% ruthenium alloyed AISI 316L stainless steel surface showing a) evaluated spots along the depth of a laser bead, b) EDS linescan direction across interface

Despite the fact that spot 4 lies closer to the surface and spot 8 deeper towards the bottom of the laser bead, they recorded a comparable amount of ruthenium content at 12.75 wt% and 12.9 wt% respectively. Nickel content for spot 4 and 8 were 16.97 wt% and 15.86 wt% respectively. These observations suggest that ruthenium and nickel particles were able to diffuse relatively homogenously into the melt pool that formed during the laser surface alloying. This observation is further supported by the EDS elemental composition profile results (Figure 4.3) obtained through running of EDS lines scans taken along the weld beads In this manner the actual gradient of particularly nickel and ruthenium elements were evaluated and the results are as shown in Figure 4.3. Figure 4.3 show results corresponding to linescan shown in Figure 4.2.a). It can be seen from the obtained EDS lines scans that the ruthenium composition profile across the weld bead as shown in Figure 4.3 is relatively uniform.

Table 4.2: EDS Elemental composition results of each point / spot shown in Figure 4.2 a

	Al-K	*Si-K*	*Cr-K*	*Mn-K*	*Fe-K*	*Ni-K*	*Mo-L*	*Ru-L*
pt1	0.41	0.58	18.11	1.68	67.11	9.87	2.24	0.00
pt2	0.45	0.44	18.03	1.57	67.14	10.28	2.07	0.00
pt3	0.40	0.45	17.97	1.78	67.23	9.80	2.37	0.00
pt4	0.38	0.93	14.84	1.20	51.92	16.97	1.02	12.75
pt5	0.46	0.89	14.91	1.46	52.98	17.00	1.12	11.06
pt6	0.52	0.91	14.84	1.54	51.67	16.97	1.11	12.44
pt7	0.40	0.73	14.63	1.00	53.57	15.31	1.08	13.27
pt8	0.40	0.87	14.75	1.16	53.04	15.86	1.02	12.90

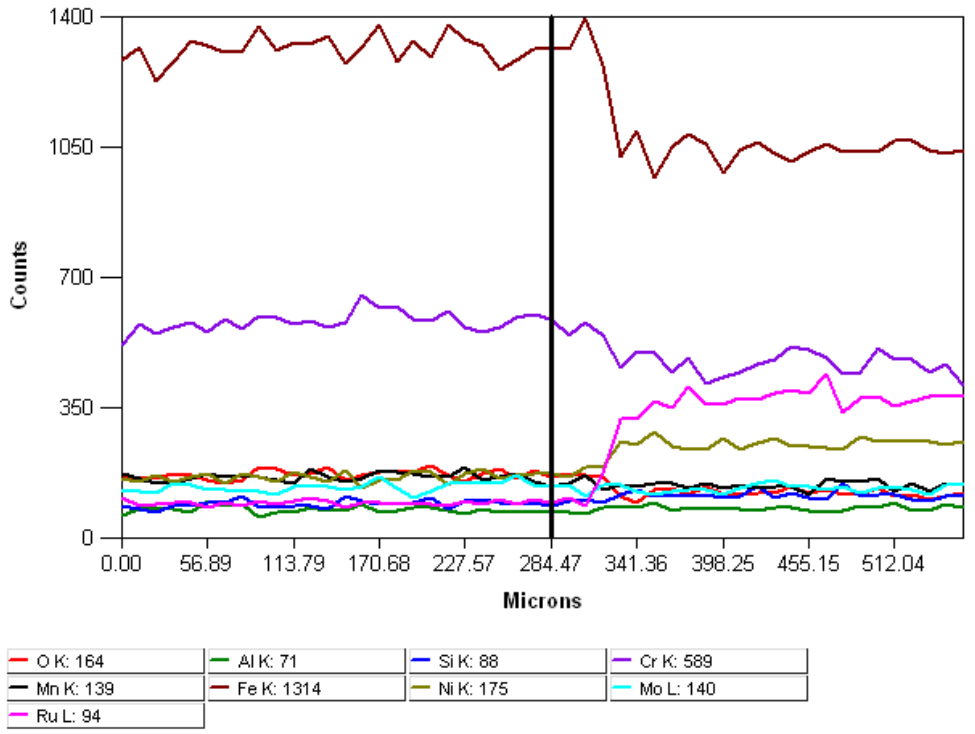


Figure 4.3: EDS lines scan elemental composition profile results along the direction shown in Figure 4.2 b

4.2.2 AISI 316L SS + 5.2wt% Ru Alloy

Treating the AISI 316L stainless steel substrate with ruthenium powder of commercial purity (i.e. 99.9%) has resulted in a surface containing 5.2wt% Ru. A cross-section SEM micrograph of the 5.2wt% Ru steel surface showing evaluated spots on the weld bead is

shown in Figure 4.4a. The chemical composition results corresponding to the evaluated spots in Figure 4.4a are given in Table 4.3. Despite their different locations within the bead, point 1 and point 7 have recorded comparable ruthenium composition of 4.43wt% Ru and 4.29wt% Ru respectively. Although all the other evaluated points that are situated in between point 1 and 7 have varying ruthenium content, their variations are not significantly high. The highest recorded value is 6.11wt% Ru at point 3, and the lowest is 4.29wt% Ru at point 7. This observation is an indication that the AISI 316L stainless steel surface was successfully alloyed with ruthenium using ruthenium powder.

EDS linescan results taken in different direction along the bead are given in Figure 4.4 (b - d). The linescan profiles on Figure 4.4 (b, d) show a relatively uniform distribution of ruthenium along the bead in different directions. Figure 4.5 show results corresponding to linescan shown in Figure 4.4.c). Figure 4.5 also shows that ruthenium and nickel elements were distributed relatively uniform along the bead, again showing that the laser technology was able to melt and alloy the AISI 316L stainless steel substrate with ruthenium.

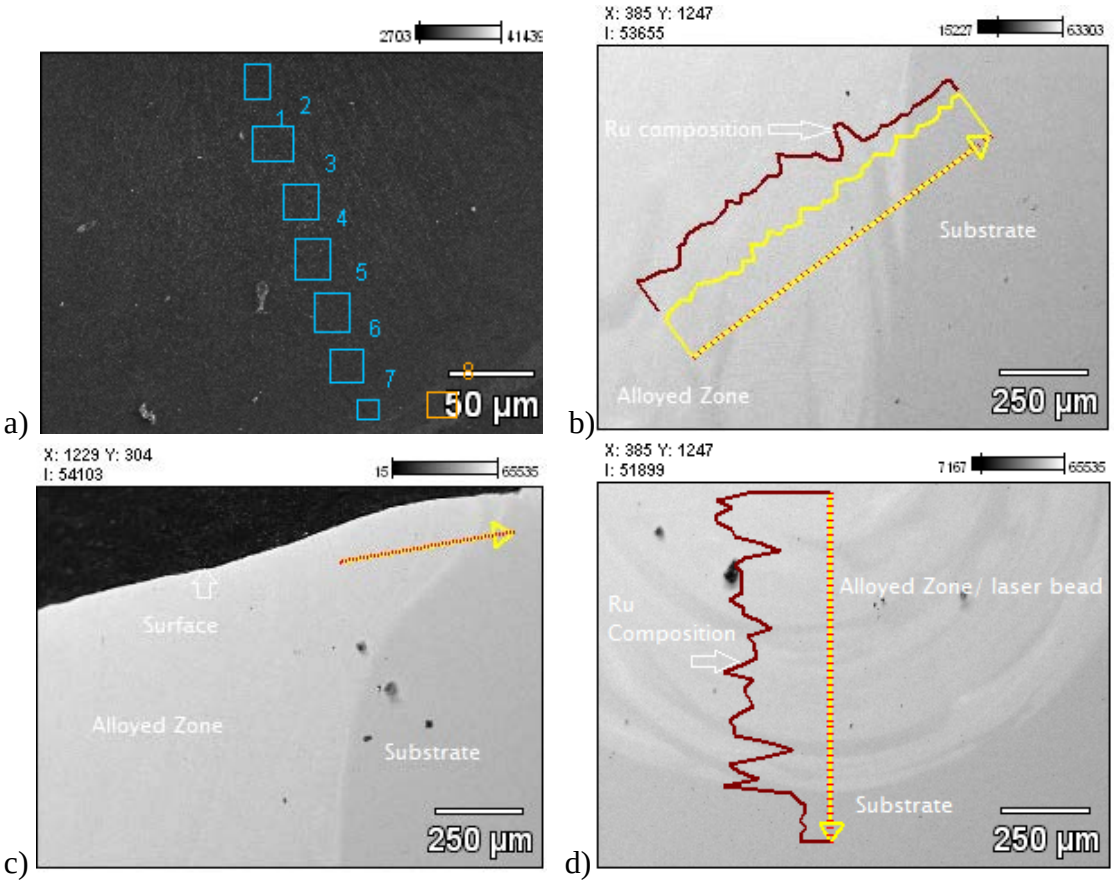


Figure 4.4: SEM micrographs showing EDS spots and line scanning in different directions through alloyed and substrate zones of a AISI 316L stainless steel surface containing 5.2wt% ruthenium.

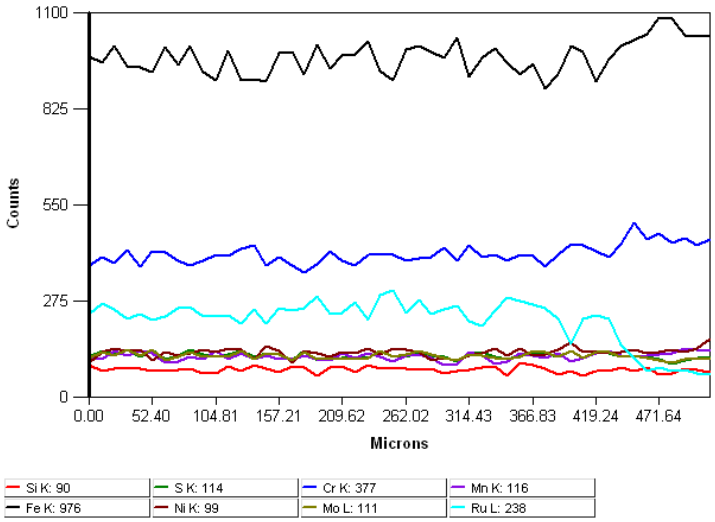


Figure 4.5: EDS lines scan elemental composition profile results along the direction shown in Figure 4.4 c.

Table 4.3: EDS Elemental composition results of each point / spot shown in Figure 4.4 a

	Si-K	*P-K*	*Cr-K*	*Mn-K*	*Fe-K*	*Ni-K*	*Cu-K*	*Mo-L*	*Ru-L*
100 Ru 2(2)_pt1	0.47		17.20	1.50	64.72	9.72	0.08	1.88	4.43
100 Ru 2(2)_pt2	0.52		17.07	1.97	64.05	9.41	0.00	1.74	5.25
100 Ru 2(2)_pt3	0.35		16.74	1.34	63.56	9.41	0.32	2.15	6.11
100 Ru 2(2)_pt4	0.36		17.12	1.70	64.49	9.08	0.00	1.92	5.34
100 Ru 2(2)_pt5	0.41		16.77	1.92	63.28	10.34	0.74	1.87	4.66
100 Ru 2(2)_pt6	0.42		17.45	2.05	63.50	8.94	0.00	2.09	5.58
100 Ru 2(2)_pt7	0.25		17.79	1.75	64.75	9.32	0.36	1.58	4.29
100 Ru 2(2)_pt8	0.54	0.22	17.34	1.71	66.86	9.72	0.38	1.44	0.02

4.3 Microstructural Analysis

Optical microscopic investigations were carried out on both the laser-alloyed region and the AISI 316L stainless steel substrate. Figure 4.6 (a) shows an optical micrograph of untreated AISI 316L stainless steel substrate.

4.3.1 AISI 316L SS +12.5wt% Ru

Applying laser surface alloying using 50wt% Ru-50wt% Ni powder mixture has yielded a steel surface containing 12.5wt% Ru, and a fine microstructure consisting of mainly Columnar - Equiaxed - Transition (CET) dendrites of various sizes and shapes, and few dendritic columnar grains as shown in a optical micrographs given in Figure 4.6 (b, c, d).

In order to evaluate the microstructure holistically, a lower magnification optical micrograph showing a larger central part of the alloyed zone area was taken, and is presented in Figure 4.6 (d). Figure 4.6 (d) shows clearly that there are more acicular and Columnar - Equiaxed - Transition (CET) grains than columnar grains in larger parts of

the alloyed zone. At the substrate-laser bead interface region of the alloyed zone, the observation is the similar as shown in Figure 4.6 (b) i.e. more Columnar - Equiaxed - Transition (CET) dendrites than columnar grains. Dendrites shown in Figure 4.6 (b) can be seen in details through higher magnification view shown in Figure 4.6 (c). Also noted is that grain growth at the fusion line zone was not completely epitaxial i.e. there is no apparent long columnar grains growth from the fusion line. This observation shows that during solidification of the melt pool at the region near the fusion line there were more nuclei for grain growth initiation other than the partly melted substrate.

The higher magnification SEM micrograph (Figure 4.7) reveals a secondary phase within the matrix in the alloyed zone of the 12.5 wt% Ru alloyed sample. The EDS analysis results showed that a 99 wt% ruthenium phase (points 1 and 2 in Figure 4.7 (a)). The presence of partially melted ruthenium particle within the melted zone suggests that there was insufficient energy in the melt pool to dissolve all particles. EDS analysis at the edge (point 3, Figure 4.7 (a)) gives ruthenium content of 45wt% Ru giving evidence that the particle was actually dissolving at some point. The ability of a pure ruthenium particle to be retained within the laser melt pool is governed by the initial size of the particles, the thermal cycle that the particles experience, the thermodynamic stability of the particles within the molten pool, and the rate at which dilution may occur.

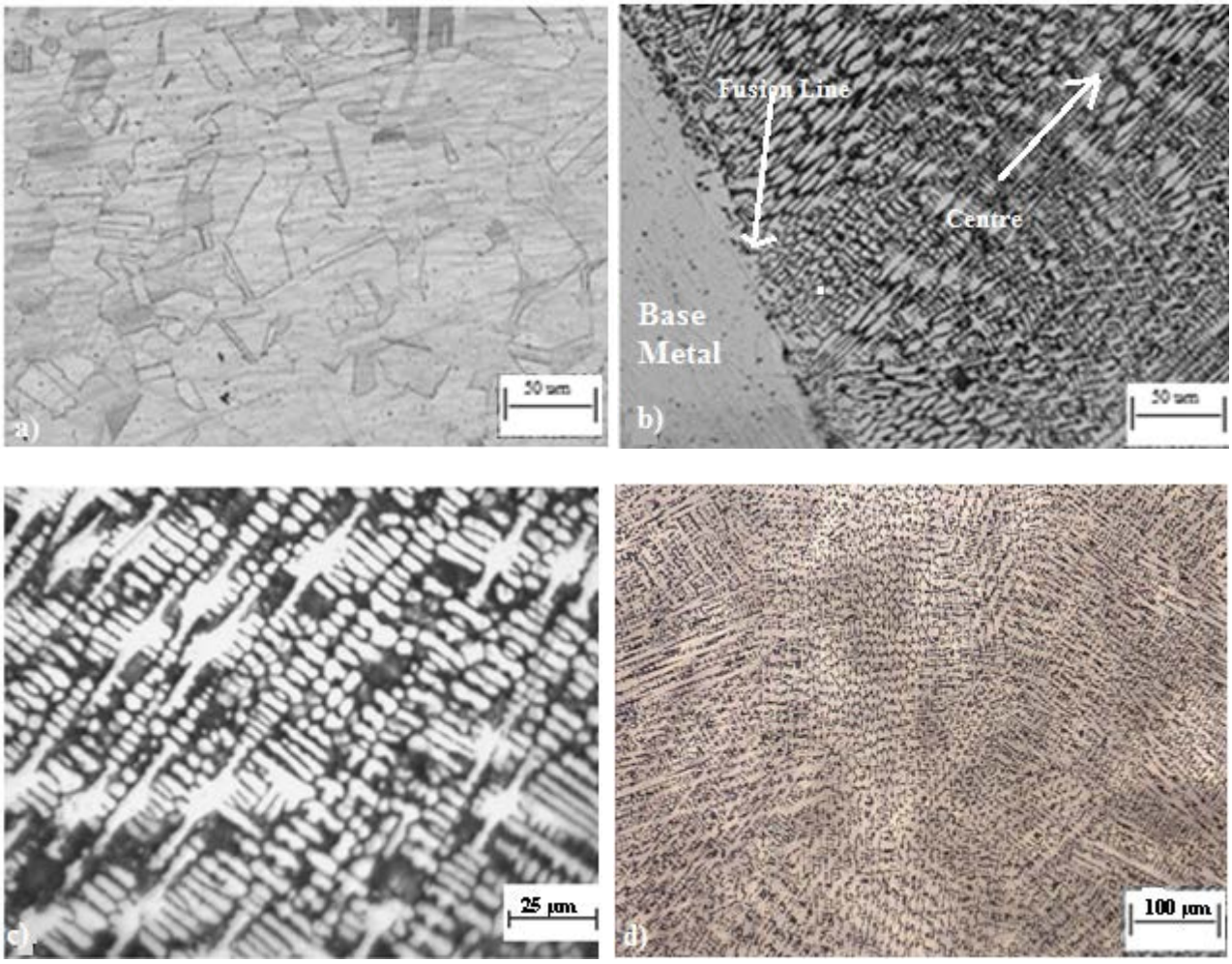
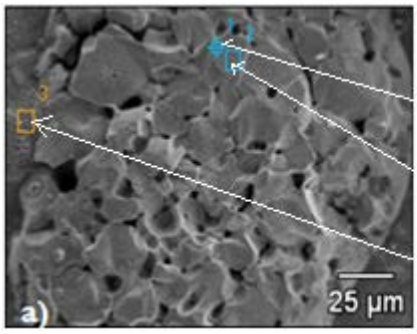


Figure 4.6: Optical micrographs showing microstructure of a) AISI Type 316L Stainless Steel, b) Fusion line of 12.5 wt% Ru alloyed zone, c) Higher magnification of dendrites in 12.wt% Ru alloyed zone, d) Lower magnification showing the inner most part of 12.5 wt% Ru alloyed zone



	Si-K	Cr-K	Mn-K	Fe-K	Ni-K	Cu-K	Mo-L	Ru-L
pt1	0.02	0.00	0.09	0.55	0.00	0.15	0.00	99.01
pt2	0.02	0.05	0.10	0.01	0.32	0.00	0.00	99.50
pt3	0.22	10.72	1.08	36.88	4.23	0.55	1.14	45.18

b)

Figure 4.7: a) SEM micrograph showing Ru particle in 12.5 wt% Ru alloyed zone, b) EDS elemental composition profile (wt%) corresponding to point 1,2, and 3 in a).

4.3.2 AISI 316L SS + 5.2wt% Ru

In contrary to 12.5 wt% Ru alloyed surface, the 5.2wt % Ru alloyed surface showed a microstructure consisting of mainly long dendritic columnar grains, and fewer acicular/Columnar - Equiaxed - Transition (CET) grains as shown in figure 4.8(a). There is evidence of significant epitaxial grain growth at the fusion line for 5.2wt% Ru alloyed surface as shown in Figure 4.8 (b). The distinctive feature of the microstructure of the 5.2wt% Ru alloyed surface as compared to 12.5wt% Ru alloyed surface is that the columnar grains grows much longer.

It can be seen from the micrograph of 5.2wt% Ru surfaces that grains of different sizes and shapes are obtained through laser treatment. The microstructures in Figure 4.6 and 4.8 are typical of weld beads which cooled under non-equilibrium conditions [14].There is neither apparent porosity nor cracks observed within the microstructure. It is mentioned [68] that, since solidification of the weld metal proceeds spontaneously by epitaxial growth of the partially melted grains in the base metal. Without additional nucleation, this will promote a columnar grain structure [14, 68].

Essentially, the microstructures of both 5.2 wt% Ru and 12.5 wt% alloyed surfaces are not homogeneous and consist of grains of various shapes and sizes at different zones. The other observation that is similar in both is that grains grow mainly on specific direction towards the centre of the laser bead.

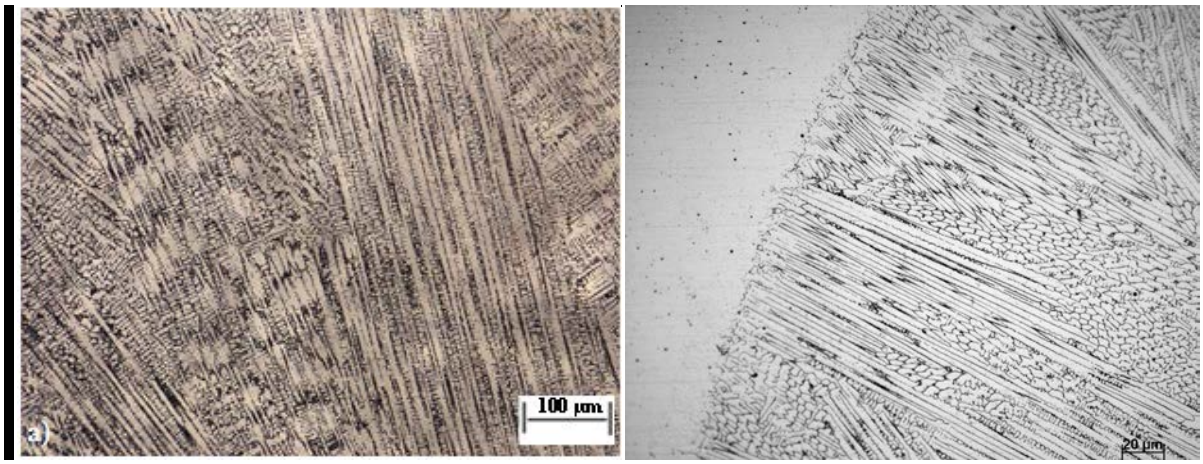


Figure 4.8: Optical micrographs of 5.2wt% Ru alloyed steel surface showing microstructure at a) central most part of the alloyed zone , b) near fusion line zone of the alloyed surface.

4.4 Microhardness

Indentations made by the micro hardness tester on the specimens during the hardness testing show relatively similar shapes and sizes for a given specimen as shown in Figure 4.9. Figure 4.9 also shows straight line arrays formed by successive indentations with sufficient equal spacing in between to produce hardness profiles. The profiles along the centre of the laser bead (longitudinal), along the near surface region and through the middle (transversally across) starting from the substrate were all determined.

Micro-hardness measurements across the bead-substrate interface revealed a significant increase in hardness, varying from 158HV for the AISI 316L substrate to 247HV for the laser alloyed bead, containing 12.5 wt% Ru, as shown in Figure 4.10. The increased hardness value in samples alloyed with ruthenium and nickel can be attributed to the microstructural changes due to rapid cooling following laser heating. The hardening effect of both ruthenium and nickel on alloys is well-known [40]. However, despite the observed fairly uniform concentration of both ruthenium and nickel within the alloyed

zone, there is a slight drop in hardness from the interface region towards the centre of the laser weld bead as shown in Figure 4.10. The drop is more pronounced for 12.5 wt% Ru alloyed surface. The structural heterogeneities observed in the alloyed zone region are the reasons for the large fluctuations in the value of micro-hardness across the surface alloy.

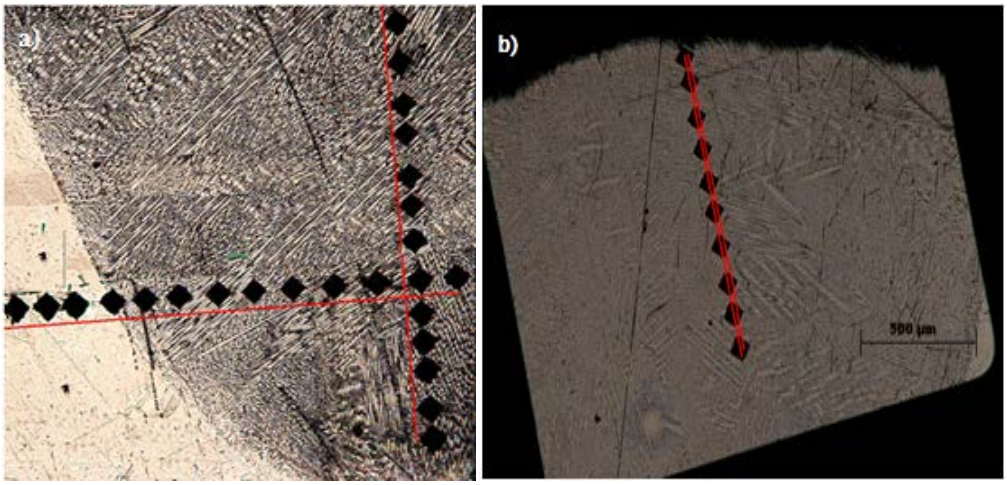


Figure 4.9: Optical micrographs showing microhardness tester indentations formed along the weld bead in different directions

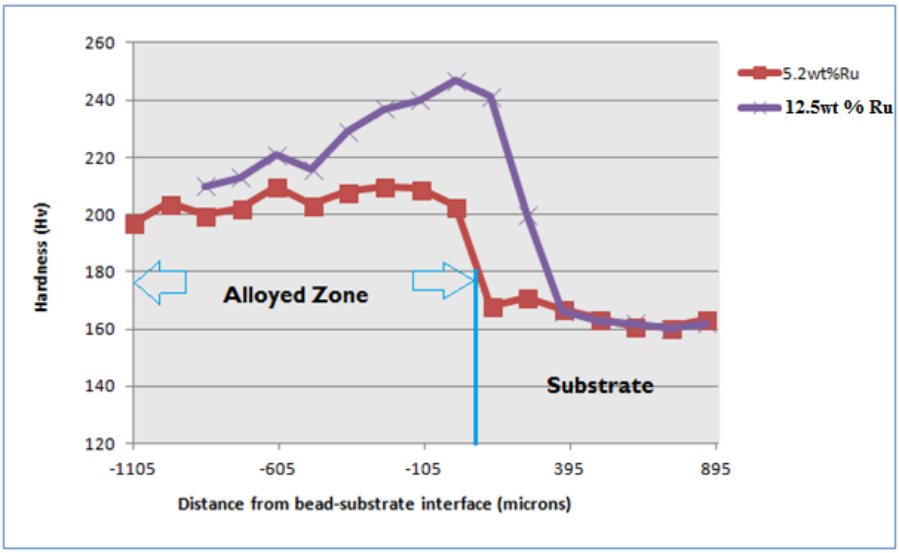


Figure 4.10: Variation of hardness with the distance from the bead/ substrate interface in an AISI 316L stainless steel surfaces alloyed with Ru. The hardness measurements showed an error of approximately 3%.

4.5 Electrochemical Tests Results

Potentiodynamic polarisation tests were conducted on control alloys (stainless steel AISI 316L and Hastelloy© C-276), and on all two laser surface alloyed stainless steel samples in various sulphuric acid solutions. The areas of the specimen were kept the same at $0.16cm^2$.

4.5.1 Untreated AISI 316L stainless steel

Potentiodynamic polarisation curves showing passivation behaviour of untreated AISI Type 316L stainless steel samples in 40wt% sulphuric acid solution at 25^oC, 40^oC and 60^oC were obtained, and are presented in Figure 4.11. Results shown in Figure 4.11 and Table 4.4 were obtained after the samples were polarised in respective solutions, and the potential scanned from -0.6 V to 1.4 V at a scan rate of 0.1 mV/s. The measured corrosion potentials, E_{corr}, in 40wt% sulphuric acid solution were: -297 mV, -277 mV and -217 mV at 25^oC, 40^oC and 60^oC temperatures respectively. The corresponding I_{corr} values in 40wt% sulphuric acid solution at 25^oC, 40^oC and 60^oC were: 7.3×10^{-5} A/cm^2, 49×10^{-5} A/cm^2 and 90.8×10^{-5} A/cm^2 respectively. It can be observed that there is an increase in current density with increasing solution temperature.

It appears from these results that the E_{corr} value increased towards nobler values with increasing solution temperature. Above the E_{corr}, the AISI 316L sample underwent active corrosion shown by a steady increase in current density with a slight increase in corrosion potential until the critical potential, E_{crit}, and critical current density, i_{crit}, were reached. This phenomenon was observed in all solutions although the actual values

differed. The i_{crit} values were virtually comparable at 25^{o}C and 60^{o}C, while it was higher at 40^{o}C as shown in Figure 4.11.

Beyond the E_{crit}, there was a steep decrease in current density for a slight increase in corroding potential. This indirect proportionality gradually phases out with an increase in potential until there is virtually no increase in current density as the corroding potential increases. This is a typical passivation phenomenon and was observed in all solutions although the measured passive current density, i_{pass} differed in each solution. The i_{pass} values are presented in Table 4.4.

Raising the solution temperature from 25^{o}C to higher temperature (i.e. 40^{o}C and 60^{o}C) led to a decrease in the extent of the passive potential range within which the sample passivated, and an increase i_{pass} values. It can further be deduced from these results that the passive region was extended through increasing solution temperature, although the level of instability associated with passive layer formation at higher temperatures was also raised. In the 40wt% sulphuric acid solution at 40^{o}C, between 900 mV and 1075 mV a drastic change in current density for a slight change in corroding potential was observed, suggesting the point of pit initiation. Above 1075 mV there was a stable increase in current density.

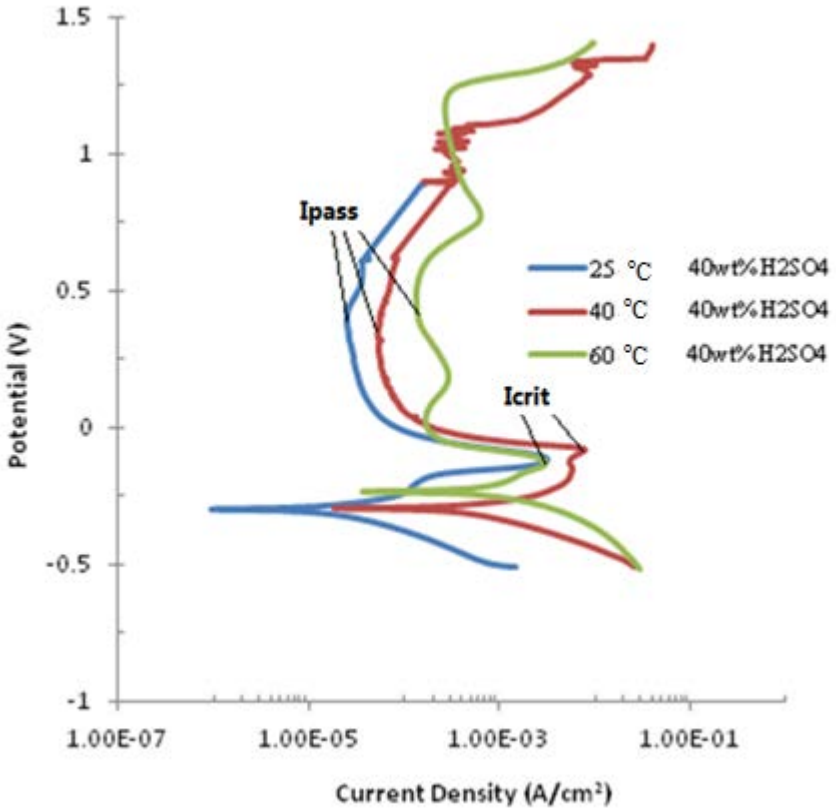


Figure 4.11: Potentiodynamic polarisation curves of the AISI 316L stainless steel in 40wt% sulphuric acid solutions at various temperatures

Table 4.4: Electrochemical results of the untreated AISI 316L stainless steel sample exposed to 40wt% sulphuric acid solution at various temperatures

Temp (^{o}C)	$i_{corr,}$ (A/cm^2)	$E_{corr,}$ (mV)	i_{crit} (A/cm^2)	E_{crit}(mV)	i_{pass} (A/cm^2)
25	7.3 x 10^{-5}	-297	1000 x 10^{-5}	-143	2.6 x 10^{-5}
40	49 x 10^{-5}	-277	280 x 10^{-5}	-81	5.2 x 10^{-5}
60	90 x 10^{-5}	-217	261 x 10^{-5}	-149	20.5 x 10^{-5}

4.5.2 AISI 316L SS + 5.2wt% Ru

Potentiodynamic polarisation curves of the laser alloyed 5.2wt% Ru + AISI 316L stainless steel specimen in 40 wt% sulphuric acid solutions at 25^{o}C, 40^{o}C and 60^{o}C are shown in Figure 4.12.

In 40wt% sulphuric acid at 25^{o}C, 40^{o}C and 60^{o}C, the specimen recorded different values on each parameter such as corrosion current density, corrosion potential, critical current density, passive current density, etc. The values are given in Table 4.5. The specimen had the lowest i_{corr} in the 25^{o}C solution, while the E_{corr} values were comparable in all three solutions. This indicates that at an elevated solution temperature, the corrosion resistance of the alloy was reduced. Based on chemical reaction kinetics, the effect of temperature on corrosion is well established.

When polarised in a 40wt% sulphuric acid at 25^{o}C, the specimen recorded a corrosion potential (E_{corr}) and corrosion current density (i_{corr}) values of approximately –239 mV and 4.5 x 10^{-5} A/cm^2 respectively. During scanning, the specimen experienced active corrosion in this medium until a critical current density, i_{crit}, of approximately 11.5 x 10^{-5} A/cm^2 and a corresponding, E_{crit} value, of -151 mV were reached. Beyond this point, the current density decreased significantly with a slight increase in potential until a potential of -34 mV was reached. At this point it appears that the specimen experienced the first passive stage with a passive current density of 7.6 x 10^{-5} A/cm^2. Although this showed passivation characteristics, it occurred for a very short potential range, and is not as significant as the more extensive passive region at higher potentials.

It can further be observed on the polarization curve obtained when the specimen was polarised in a 40wt% sulphuric acid at 25^{o}C that between 110 mV and 400 mV the specimen was passivating i.e. a slight decrease or no change in current density for any increase in corrosion potential. The passive current density for this passive region was measured to be approximately 2.7 x 10^{-5} A/cm^{2}. Within the potential range, 400 mV to 500 mV, the specimen underwent active corrosion until re-passivation occurs at potentials beyond 500 mV. In this second passive region, the passive current density, i_{pass}, was recorded to be approximately 3.4 x 10^{-5} A/cm^{2}. Above 950 mV, the transpassive region is observed as characterised by the unprecedented increases in current density for a slight change in corroding potential.

In 40wt% sulphuric acid at 40^{o}C, the 5.2wt% Ru sample showed two passive regions. The first passive region was between −160 and 390 mV, while the second passive region occurred at potential range between 547 mV and 1039 mV. The passive current density for the first passive range was measured to be approximately 7.1 x 10^{-5} A/cm^{2}, and approximately 17.0 x 10^{-5} A/cm^{2} for the second passive range. The transpassive region is observed at potentials greater than 950 mV. In 40wt% sulphuric acid at 40^{o}C, the specimen recorded a corrosion potential (E_{corr}) and corrosion current density (i_{corr}) values of approximately -240 mV and 20.7 x 10^{-5} A/cm^{2} respectively. The critical current density in this medium was approximately 110.0 x 10^{-5} A/cm^{2}.

The phenomenon of re-passivation was also observed when the temperature of the solution was increased to 60^{o}C. The second passive region occurred between 560 mV

and 1040 mV potentials (i.e. E_{pass} range = 480 mV). The potential range was between 34 mV and 340 mV for the first passive region (i.e. E_{pass} range = 300 mV). In 40wt% sulphuric acid at 60°C, the specimen recorded a corrosion potential (E_{corr}) and corrosion current density (i_{corr}) values of approximately -243 mV and 34.0 x 10^{-5} A/cm^2 respectively. The critical current density was recorded as 162.0 x 10^{-5} at a potential of-82 mV.

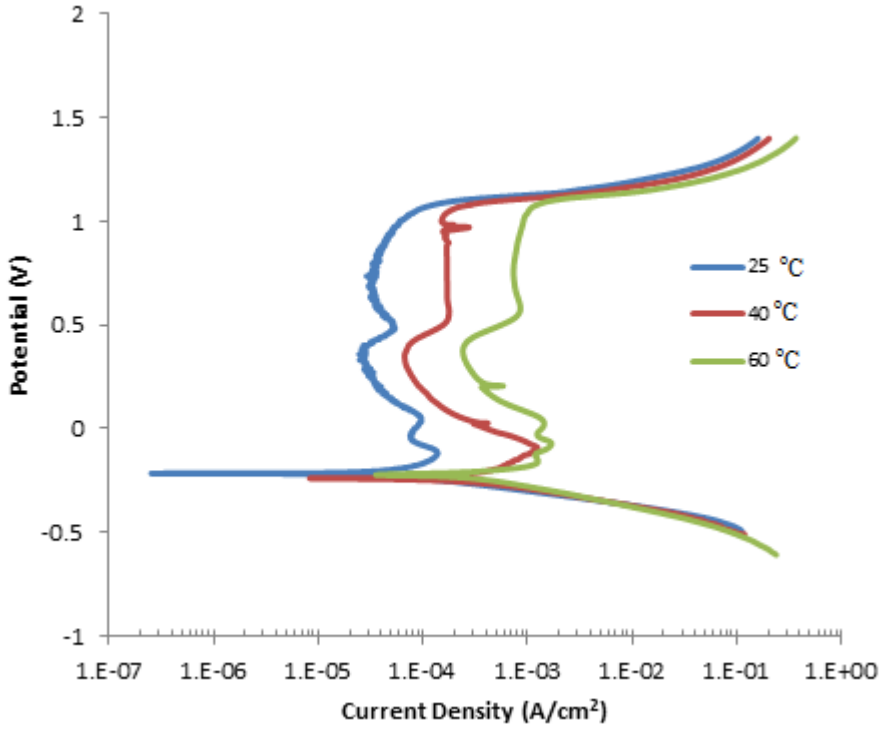


Figure 4.12: Potentiodynamic polarisation curves of the AISI 316L + 5.22wt% Ru in 40wt% sulphuric acid solutions at different temperatures

Table 4.5: Electrochemical results of the untreated 5.22wt% sample exposed to 40wt% sulphuric acid solution at various temperatures

Temp (°C)	$i_{corr,}$ (A/cm^2)	$E_{corr,}$ (mV)	i_{crit}(A/cm^2)	E_{crit}(mV)	$i_{pass\ 1}$(A/cm^2)	$i_{pass\ 2}$(A/cm^2)
25	4.5 x 10^{-5}	-239	11.5 x 10^{-5}	-151	2.7 x 10^{-5}	3.4 x 10^{-5}
40	20.7 x 10^{-5}	-240	110.0x 10^{-5}	-77	7.1 x 10^{-5}	17.0 x 10^{-5}
60	34.0 x 10^{-5}	-243	162.0 x 10^{-5}	-82	24.3 x 10^{-5}	78.7 x 10^{-5}

4.5.3 AISI 316L SS +12.5wt% Ru

In 40 wt% sulphuric acid solution at 25^{o}C, the 12.5wt% Ru alloyed stainless steel specimen had a corrosion potential, E_{corr}, and the corresponding corrosion current density, i_{corr}, of -260 mV and 5.0 x10^{-5} A/cm^2 respectively. In this medium, the specimen underwent active corrosion whereby the current density increased gradually with increasing potential until a critical current density, i_{crit}, of 36.0 x 10^{-5} A/cm^2 was reached at a critical potential, E_{crit}, of -97 mV. Passive current density, i_{pass}, was found to be approximately 4.5 x 10^{-5} A/cm^2, with a passive potential region lying between 150 mV and 930 mV, and therefore a passive potential range, E_{pass}, of 790 mV. It can however be seen from the curve that within this potential range (150 mV to 930 mV), the specimen experience active corrosion between 364 mV and 464 mV before passivation was restored. This observation suggests that the passive layer showed some instability within this potential range.

At a higher solution temperature of 40^{o}C, the specimen recorded E_{corr} value of approximately 59 mV and a corrosion current density value of approximately 0.6 x 10^{-5} A/cm^2. At the critical corrosion potential of 339 mV, a critical current density was recorded to be approximately 47.0 x 10^{-5} A/cm^2. The i_{pass} value in this medium was recorded as 6.2 x 10^{-5} A/cm^2, and a passive region range was between 410 mV and 1000 mV i.e. E_{pass} = 590 mV.

In 40 wt% sulphuric acid solution at 60^{o}C, the 12.5wt% Ru alloyed recorded an E_{corr} value of -239 mV, and a corrosion current density value of 39 x 10^{-5} A/cm^2. Passive

current density, i_{pass}, was found to be approximately 39 x 10^{-5} A/cm^2 at a passive region between 250 mV and 390 mV. Above 390 mV, the specimen experienced active corrosion until a potential of value 522 mV was reached. Beyond 522 mV, re-passivation started, and a second passive corrosion state was reached at a passive current, $i_{pass\ 2}$ of value 89.0 x 10^{-5} A/cm^2. This second passive region at higher potential occurred between 532 mV and 990 mV (E_{pass} = 458 mV). The critical current density at 60 ^{o}C was recorded as 503 x 10^{-5} A/cm^2.

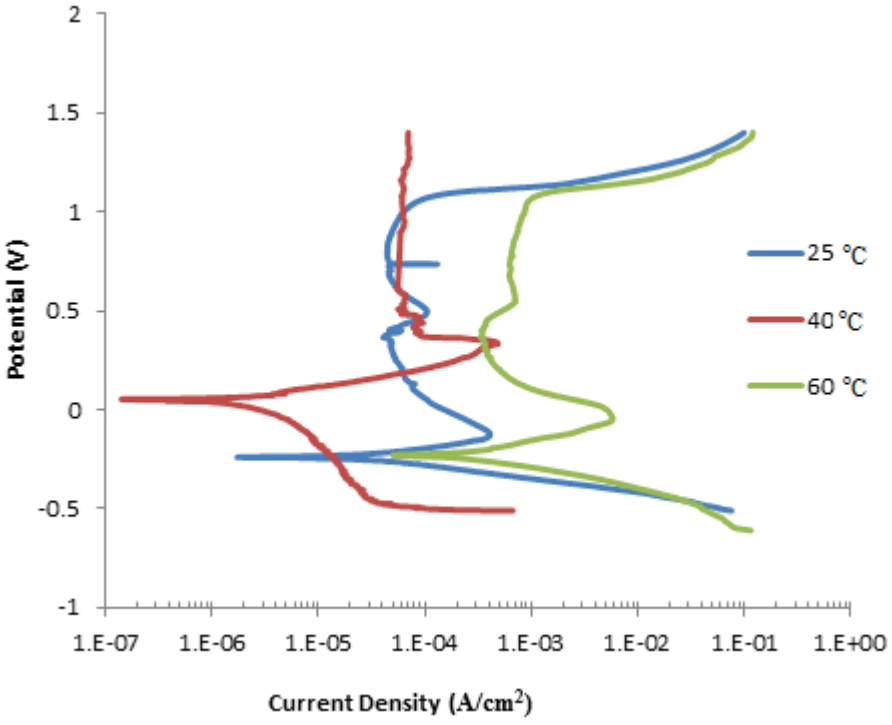


Figure 4.13: Potentiodynamic polarisation curves of the AISI 316L + 12.5wt% Ru in 40wt% sulphuric acid solution at different temperatures

Table 4.6: Electrochemical results of the untreated 12.5wt% sample exposed to 40wt% sulphuric acid solution at various temperatures

Temp (^oC)	$i_{corr,}$ (A/cm^2)	$E_{corr,}$ (mV)	i_{crit}(A/cm^2)	E_{crit}(mV)	$i_{pass\ 1}$(A/cm^2)	$i_{pass\ 2}$(A/cm^2)
25	5.0×10^{-5}	-229	36×10^{-5}	-97	4.2×10^{-5}	4.5×10^{-5}
40	0.6×10^{-5}	59	47×10^{-5}	339	6.2×10^{-5}	-
60	39.0×10^{-5}	-239	503×10^{-5}	-68	39.2×10^{-5}	89.0×10^{-5}

4.5.4 Hastelloy© C-276

In 40wt% sulphuric acid solution at 25^{o}C, Hastelloy© C-276 recorded i_{corr} value of approximately 0.4 x 10-5 A/cm^2 at a potential value of -110 mV. Upon increasing the scanning potential the sample corroded actively until a critical current density of approximately 1 x 10^{-5} A/cm^2 was reached at a potential value of -20 mV. Above -20 mV the sample started passivating until a passive current density, i_{pass}, was reached at approximately 0.7 x 10^{-5} A/cm^2. This i_{pass} value was sustained until a potential of a value approximately 900 mV was reached. Beyond 900 mV, the sample started to gradually corrode actively again thus indicating that a trans-passive stage was reached.

At a higher solution temperature of 40^{o}C, the specimen recorded an E_{corr} value of approximately -153 mV and a corrosion current density value of approximately 0.8 x 10^{-5} A/cm^2. At the critical corrosion potential of -55 mV, a critical current density was recorded to be approximately 6.0 x 10^{-5} A/cm^2. The i_{pass} value in this medium was recorded as 1.2 x 10^{-5} A/cm^2, and a passive region range was between -55 mV and 1100 mV.

Increasing the temperature of the solution to 60°C resulted in increased i_{corr}, i_{crit}, and i_{pass} values, recorded as 8.2 x 10^{-5} A/cm^2, 40.2 x 10^{-5} A/cm^2 and 10.0 x 10^{-5} A/cm^2 respectively. The E_{corr} value was recorded to be -125 mV while the E_{crit} was 180 mV. The passive potential range in this medium was between 200 mV and 1000 mV i.e. E_{pass} = 800 mV. The results are shown in Figure 4.14 and Table 4.7.

Table 4.7: Electrochemical results of the Hastelloy© C-276 exposed to 40wt% sulphuric acid solution at various temperatures

Temp (°C)	i_{corr} (A/cm^2)	E_{corr} (mV)	i_{crit}(A/cm^2)	E_{crit}(mV)	i_{pass} (A/cm^2)
25	0.4 x 10^{-5}	-110	1.0 x 10^{-5}	-20	0.7 x 10^{-5}
40	0.8 x 10^{-5}	-153	6.0 x 10^{-5}	-55	1.2 x 10^{-5}
60	8.2 x 10^{-5}	-125	40.2 x 10^{-5}	180	10.0 x 10^{-5}

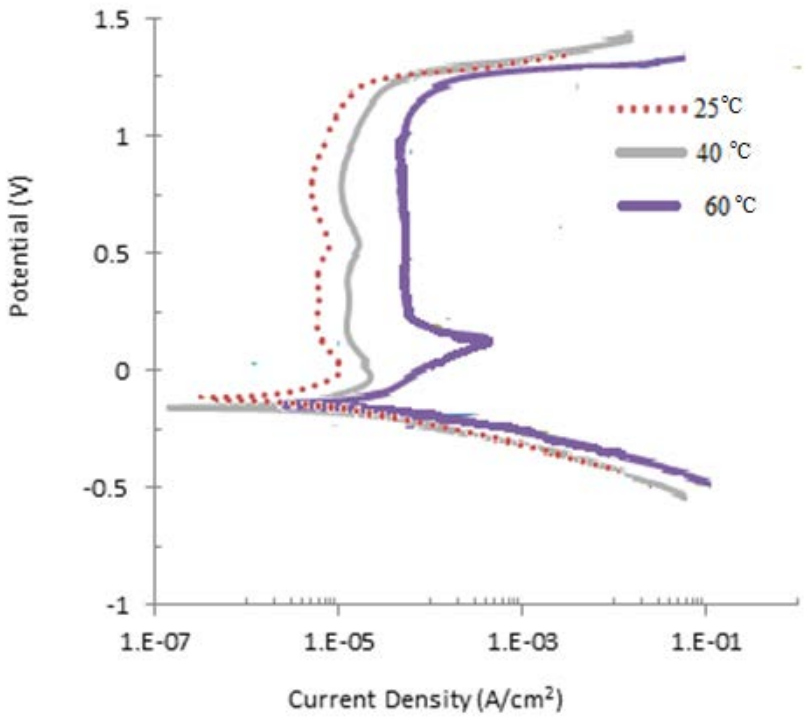


Figure 4.14: Potentiodynamic polarisation curves of Hastelloy© C-276 in 40wt% sulphuric acid solution at different temperatures

4.5.5 Competitive Corrosion Performance of Ru Containing Stainless Steel

In order to arrive at conclusive results on the possibility of Ru alloyed AISI Type 316L stainless steel to replace or compete with Hastelloy© C-276 in acidic environments, their corrosion performance in various sulphuric acids solutions at different temperatures were evaluated and compared. Appropriate acidic environments for this purpose were considered to be 40wt% and 60wt% sulphuric acid at 40^{o}C and 60^{o}C. Hastelloy© C-276 was considered ideal for the comparison since it is widely used in the acidic environments proposed above. The potentiodynamic polarisation curves for 12.5 wt% Ru alloyed stainless steel, 5.2wt% Ru alloyed stainless steel sample, Hastelloy© C-276, and untreated AISI 316L stainless steel were obtained in each solution. The corrosion performance results in each of these test media are presented separately in the following sections.

It should be noted that the polarization curves obtained when the samples were exposed to 40wt% sulphuric acid at 40 ^{o}C and 60 ^{o}C are the same results already presented above except that they are plotted on the same set of axis with Hastelloy© C-276 sample results for comparison. In addition, electrochemical results obtained when samples were exposed to 60wt% sulphuric acid at 40 ^{o}C and 60 ^{o}C are presented also plotted on the same axis with Hastelloy© C-276 results.

4.5.5.1 40WT% SULPHURIC ACID SOLUTION AT 40°C

Plotted on the same graph, the potentiodynamic polarisation curves of 12.5wt% Ru alloyed stainless steel, 5.2wt% Ru alloyed stainless steel, Hastelloy© C-276, and untreated AISI 316L stainless steel in 40wt% sulphuric acid at 40°C are shown in Figure 4.15. The 12.5wt% Ru sample shows the lowest corrosion current density, i_{corr} at an approximate value of 0.6 x 10^{-5}A/cm^2 with the most noble corrosion potential, E_{corr} at a value of 59 mV as given in Table 4.8. Hastelloy© C-276 gave the second lowest and comparable corrosion current density at a value of 0.8 x 10^{-5}A/cm^2 although its corrosion potential value was relatively lower at -159 mV.

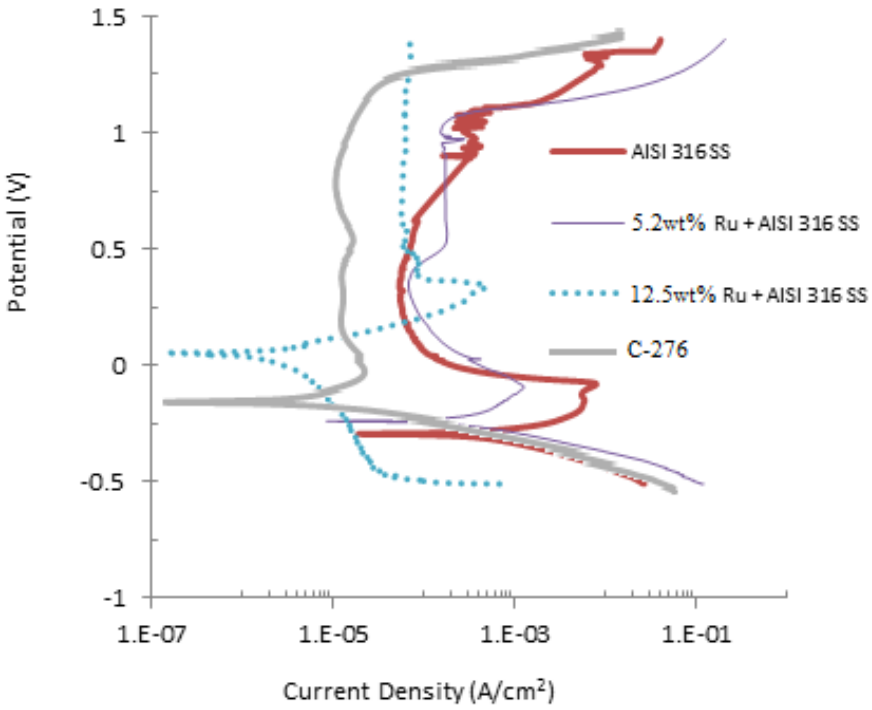


Figure 4.15: Potentiodynamic polarization curves of various alloys in 40wt% sulphuric acid solution at 40°C

Table 4.8: Electrochemical results of different samples exposed to 40wt% sulphuric acid solution at 40°C.

ALLOY	$i_{corr,}$ (A/cm^2)	$E_{corr,}$ (mV)	i_{crit}(A/cm^2)	E_{crit}(mV)	i_{pass} (A/cm^2)
Untreated AISI 316L SS	49.4×10^{-5}	-278	280.1×10^{-5}	-81	5.2×10^{-5}
5.2wt% Ru + AISI 316LSS	20.7×10^{-5}	-240	110.0×10^{-5}	-77	7.1×10^{-5}
12.5wt% Ru + AISI 316L SS	0.6×10^{-5}	59	47.0×10^{-5}	339	6.2×10^{-5}
C-276	0.8×10^{-5}	-153	6.0×10^{-5}	-55	1.2×10^{-5}

As shown in Figure 4.15, all alloys passivated when polarised in 40wt% sulphuric acid at 40°C. The passive potential range was the widest on the Hastelloy© C-276 sample, and the most constricted was observed on untreated AISI 316L stainless steel sample. It can also be seen from the graphs in Figure 4.15 that within their passive regions, Hastelloy© C-276 and 12.5 wt% Ru samples gave more stable passive films. This observation is a sign of stable passive layer during passive corrosion stages. Of all samples at their passive corrosion stage, Hastelloy© C-276sample gave the lowest passive corrosion, i_{pass}, thus showing that the passive layer which formed had superior corrosion resistance to the other samples. Furthermore, the Ru containing specimens showed the most noble passive potential range as well as the most stable passive layer as compared to untreated AISI 316L stainless steel. However, it should be noted that the passive layer on AISI 316L stainless steel sample recorded a lower passive current density, i_{pass} than the 5.2wt% Ru sample at potentials lower than 750 mV. Therefore, the passive layer on AISI 316L was more resistant and stable than the passive layer on the 5.2wt% Ru alloy at potentials less than 750 mV. Therefore, based on i_{pass} values obtained, the effect of ruthenium on passive current density is non-linear.

The amount of ruthenium added to AISI 316L stainless steel is also seen to affect the critical current density, i_{crit}, as can be deduced from Figure 4.15. The 12.5wt% Ru sample had the lowest i_{crit} value and untreated AISI 316L stainless the highest value. This observation suggests an inverse proportionality correlation between the amount of ruthenium in the AISI 316L stainless steel sample and the critical current density i.e. as the amount of ruthenium in the sample increased the i_{crit} value was reduced.

4.5.5.2 40WT% SULPHURIC ACID SOLUTION AT 60°C

Presented in Figure 4.16 are potentiodynamic polarisation curves obtained when various alloys were polarised in 40wt% sulphuric acid at 60°C.

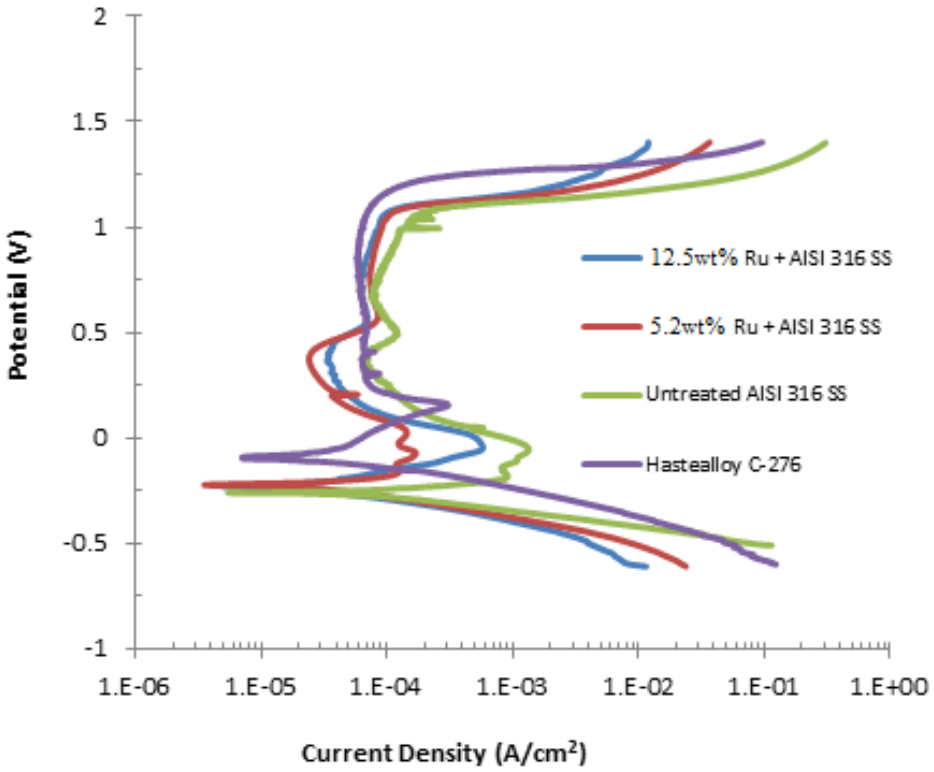


Figure 4.16: Potentiodynamic polarization curves of various alloys in 40wt% sulphuric acid solution at 60°C

It can be seen from Figure 4.16, potentiodynamic polarisation curves for 5.6wt% Ru and 12.5wt% Ru samples show evidence of similar shapes, and are lying very close to each other within the greater part of the scanned corrosion potential range.

As already seen in Figure 4.12.and 4.13, each of the 5.6wt% Ru and 12.5wt% Ru samples exhibited two distinct passive regions with the passive region occurring at the higher corrosion potential having a higher passive current density, i_{pass} value. Although the untreated AISI 316L stainless steel sample also exhibited two passive regions with the i_{pass} values for these regions virtually equal. Table 4.9 presents measured values for current density, corroding potential, critical current density, passive current density, and critical potential for all samples.

Table 4.9: Electrochemical results of different samples exposed to 40wt% sulphuric acid solution at 60°C

ALLOY	Current density, $i_{corr.}$ (A/cm^2)	Corroding potential, $E_{corr.}$ (mV)	Critical current density, i_{crit}(A/cm^2)	E_{crit}(mV)
Untreated AISI 316L SS	90.2×10^{-5}	-217	261.2×10^{-5}	-149
5.2wt% Ru + AISI 316LSS	34.0×10^{-5}	-243	162.0×10^{-5}	-82
12.5wt% Ru + AISI 316L SS	39.0×10^{-5}	-239	503×10^{-5}	-68
C-276	8.2×10^{-5}	-125	40.2×10^{-5}	180

The addition of ruthenium to the AISI 316L stainless steel enhanced the corrosion properties. From 40 mV to 470 mV, the ruthenium containing steel samples corroded at lower current density than the Hastelloy© C-276sample thus showing superior corrosion resistance in this range. However, the Hastelloy© C-276 sample showed the most stable passive layer demonstrated by the verticality of the curve within passive region.

Furthermore, the C-276 samples gave the most noble corrosion potential than all other samples in this solution.

4.5.5.3 60WT% SULPHURIC ACID SOLUTION AT 40°C

In 60wt% sulphuric acid solution at 40°C, the 5.2wt% Ru sample showed superior properties to both 12.5wt% Ru sample and the untreated AISI 316L stainless steel sample as shown by potentiodynamic polarization curves in Figure 4.17. The corrosion potential, E_{corr} was slightly higher, and the passive current density, i_{pass} lower for 5.2wt% Ru sample as compared to 12.5wt% Ru sample. This observation suggests that the higher ruthenium content of the sample does not always result in better corrosion properties. However, alloy Hastelloy© C-276 showed superior properties in these conditions. Notable also from Figure 4.17 is the instability of the passive layer of the untreated AISI 316L stainless steel sample as shown the unevenness of the curve in the passive region. It can thus be said that addition of ruthenium to the AISI 316L stainless has stabilized the passive layer in this medium.

Table 4.10: Electrochemical results of different samples exposed to 60wt% sulphuric acid solution at 40°C

ALLOY	Current density, $i_{corr,}$ (A/cm^2)	Corroding potential, $E_{corr,}$ (mV)	Critical current density, i_{crit}(A/cm^2)	E_{crit}(mV)
Untreated AISI 316L SS	1000.0×10^{-5}	-150	1165.0×10^{-5}	-55
5.2wt% Ru + AISI 316LSS	50.3×10^{-5}	-105	105.2×10^{-5}	90
12.5wt% Ru + AISI 316L SS	90.3×10^{-5}	-80	108.4×10^{-5}	198
C-276	2.0×10^{-5}	-65	80.2×10^{-5}	250

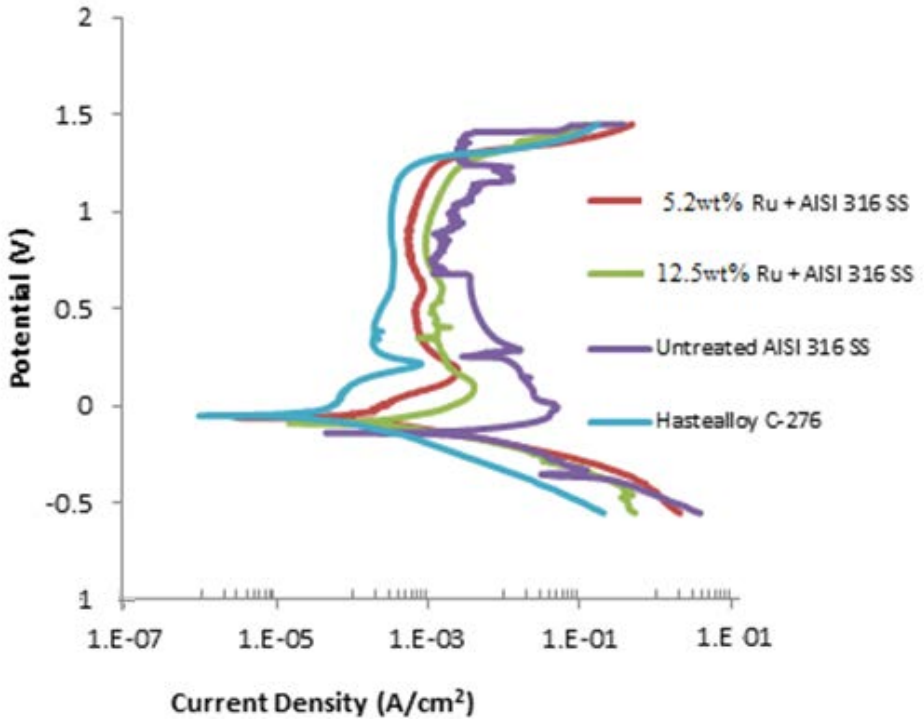


Figure 4.17: Potentiodynamic polarization curves of various alloys in 60wt% sulphuric acid solution at 40°C

4.5.5.4 60WT% SULPHURIC ACID SOLUTION AT 60°C

Potentiodynamic polarisation curves in Figure 4.18 show the corrosion behaviour of various alloy samples when exposed to 60wt% sulphuric acid solution at 60°C. Table 4.9 shows values of current density, corroding potential, critical current density, and critical potential of the different samples.

In comparison with other samples, the untreated AISI 316L stainless steel sample had the highest i_{corr} and lowest E_{corr} values recorded as 1000 x 10^{-5} A/cm^2 and -150 mV respectively. This observation shows that addition of ruthenium on the AISI 316L stainless steel improved its corrosion properties in 60wt% sulphuric acid solution at 60°C. The effects of ruthenium additions were much more pronounced on the critical

current density which was reduced greatly from 1165 x 10^{-5}A/cm^2 for untreated AISI 316 L stainless sample to 106.2 x 10^{-5} A/cm^2 for 5.2wt% Ru sample.

Although higher in ruthenium content, the 12.5 wt% Ru steel sample exhibited slightly inferior corrosion properties to 5.2 wt% sample in 60wt% sulphuric acid solution at 60^{o}C. However, it can also be noted from figure 4.17 that, above 250 mV potential, both untreated AISI 316L and 12.5wt% Ru samples passivate at lower corrosion current density than 5.2wt% Ru sample although the passive layers are unstable. Hastelloy C-276 gave a more noble corrosion potential, E_{corr}. Also observed is the more stable passivation layer exhibited by Hastelloy© C-276.

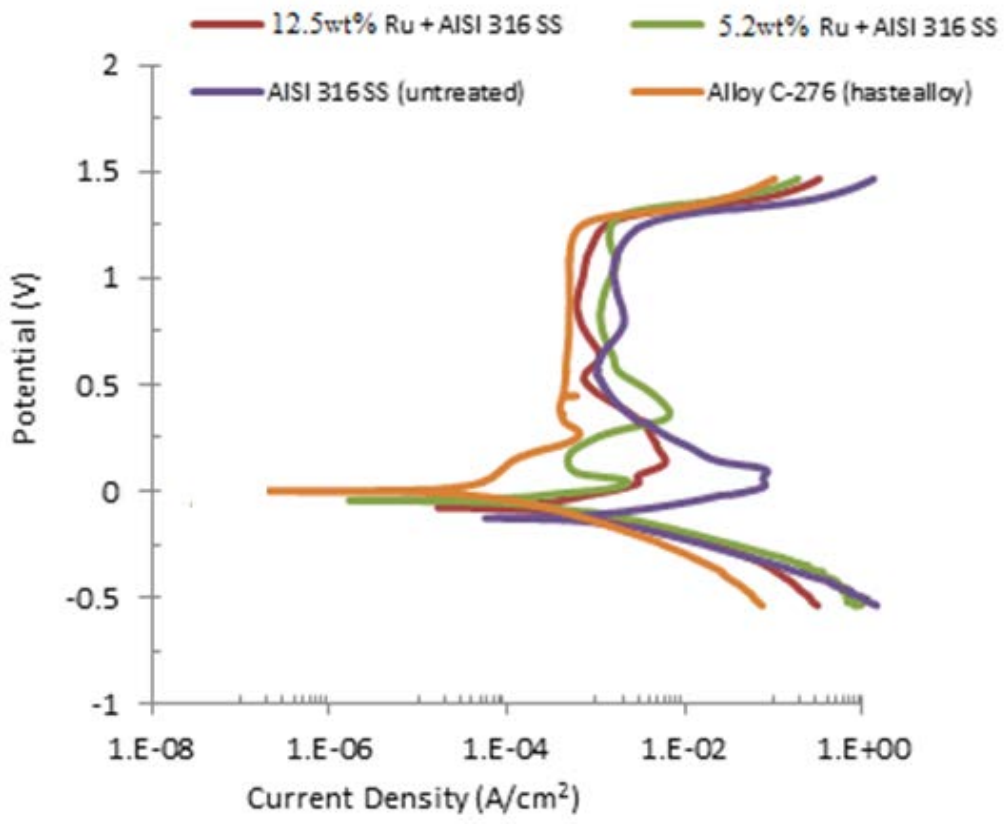


Figure 4.18: Potentiodynamic polarization curves of various alloys in 60wt% sulphuric acid solution at 60^{o}C

Table 4.11: Electrochemical results of different samples exposed to 60wt% sulphuric acid solution at 60^{o}C

ALLOY	Current density, $i_{corr,}$ (A/cm^2)	Corroding potential, $E_{corr,}$ (mV)	Critical current density, i_{crit}(A/cm^2)	E_{crit}(mV)
Untreated AISI 316L SS	110.3 x10^{-5}	-236	9981.1 x 10^{-5}	-70
5.2wt% Ru + AISI 316LSS	11.3 x 10^{-5}	-168	998.2 x 10^{-5}	-50
12.5wt% Ru + AISI 316L SS	11.5 x 10^{-5}	-193	206.0 x 10^{-5}	30
C-276	5.1 x 10^{-5}	-95	100.0 x 10^{-5}	159

CHAPTER V : DISCUSSIONS

5.1. Laser Bead Characterisation

5.1.1. Laser Bead Profile

The laser bead profile depends on various parameters such as beam power (BP), travel speed (TS) and focal position (FP) of the laser spot [14, 66, 68]. These parameters were selected suitably to obtain the desirable output. The laser surface alloying technique employed in this study through the pre-placed ruthenium powder on an AISI 316L stainless steel substrate has resulted in a relatively uniform alloying of the surface with ruthenium to a depth of about 2 mm. The depth of penetration was virtually the same for all the laser treated alloys. This observation shows that the difference in composition of the pre-coating powders has a insignificant influence on the penetration depth of the substrate. According to Toyserkani et al. [14], only a very small fraction of the laser power which is transferred to the pre-coating powders. According to other studies [14, 66, 68], penetration depth of the alloyed layer increases with the laser beam power. Fractional substrate melting was possible because the chosen laser parameters were able to melt the surface, resulting in a molten pool in which the powder particles dissolved evenly [14]. The observed oval shape or profile of the laser bead as viewed on the cross-section micrograph is according to Katayama [68], a result of the applied laser parameters. The laser beam power is in particular related to the shaping of remelting bottom and convexity of remelting face that are influenced by strong convection motions within the molten metal [66]. According to Katayama [68], analysis of the heat

conduction in the laser weld pool and convection phenomena has allowed prediction of the pool geometry based on the laser welding parameters. It can thus be said that the laser bead profile as seen on the laser alloyed AISI 316L stainless steel samples in this study is a result of the chosen parameters, and is likely to change with changing laser parameters.

5.1.2. Composition

A relatively even distribution of alloying elements (ruthenium and nickel) was observed in all laser alloyed samples. This shows the surface of the substrate (AISI 316L stainless steel) which was melted and the powder which was able to dissolve into the formed melt pool during laser heating. According to Popoola et al. [69] and other authors [14, 68] even elemental distribution within the melt pool during laser welding is made possible by the convection flow that accompanies laser melting of the substrate.

5.1.3. Microstructure

It was observed that the microstructure of the molten zone consisted mainly of fine Columnar - Equiaxed - Transition (CET) dendrites and long dendritic columnar grains. Most metal alloys solidify in Columnar - Equiaxed - Transition (CET) or columnar dendritic mode [14, 68]. According to Brytan et al. [66] Columnar - Equiaxed - Transition (CET) and columnar growth modes are produced when the growth of crystal structures occurs without formation of any secondary dendrite arms. If additional dendrite arms form, the solidification mode shifts to dendritic. Columnar and dendritic solidification depends on several factors, including cooling rate, alloy content, and

undercooling [14]. The cooling rate in the laser melt pool ranges from $10^5 K^{S-l}$ for continuous wave carbon dioxide lasers to 1010 K^{S-l} with pulsed lasers [64, 65].

Unlike the 12.5 wt% Ru alloyed surface, the 5.2wt % Ru alloyed surface showed a microstructure consisting of mainly long dendritic columnar grains, and fewer equiaxed dendritic grains. It was the opposite for the 12.5wt% Ru alloyed sample. It is known [70] that solidification of the weld pool proceeds spontaneously by epitaxial growth of the partially melted grains in the base metal. Without additional nucleation, this will promote a columnar grain structure [70]. Addition of powder to the melt pool results in many solute powder particles acting as heterogeneous nuclei site, thus promoting equiaxed grain growth and suppressing columnar grain growth. Since more powder particles were added in 12.5wt% Ru alloyed sample, under similar laser alloying conditions, it is expected for the microstructure to have shorter and fewer columnar grains than the 5.2wt% Ru alloyed sample. The grain growth occurred in specific directions, from the fusion line mainly towards the centre of the laser bead. The orientation is controlled by temperature gradient and the cooling rate [14, 66, 68, 69, 70]. The fine and dendritic microstructures observed are typical of weld beads which cooled rapidly under non-equilibrium conditions [14, 66].

5.1.4. Hardness

A hardness profile of the laser surface treated AISI 316L was shown in Figure 4.10. The surface alloyed layer exhibits higher hardness values than the base alloy, as expected. The higher surface hardness is the result of the fine dendritic microstructure and solid

solution strengthening by ruthenium. The grain refining ability of the Ru has been reported by Rhys [40] and several other authors [41, 44]. Ruthenium is used to refine and improve mechanical properties of gold and silver castings in dentistry [41, 44]. It has been observed that there is generally increased hardness with increasing Ru concentration of the specimen. As shown in Figure 4.10, AISI 316L recorded hardness value of 158HV, 210HV for 5.2wt% Ru sample and 12.5 wt% Ru sample recorded a maximum of 247HV.

5.2. Corrosion Behaviour

5.2.1. Effect of Temperature

As can be seen in Figure 4.12, increasing the temperature of the 40wt% sulphuric acid solution, shifted the polarization curve of untreated AISI 316L stainless steel sample towards the right, and therefore increased corrosion current density, passive current density, and critical current density with increasing solution temperature. This direct linear correlation was also observed for 5.2wt% Ru sample in similar conditions. Similar observations were made by Potgieter et al. [6] when investigating corrosion behaviour of steels containing lower content of ruthenium. This tendency of alloys to corrode faster at elevated temperatures is a well-known phenomenon [15], and is explained according to laws of kinetics governing chemical reactions.

However, in 40wt% sulphuric acid solution at higher temperatures of 40^{o}C and 60^{o}C, the 12.5wt% Ru specimen recorded E_{corr} values of approximately 59 mV and -239 mV respectively. There was no linear correlation between the three solution temperatures and

the recorded corroding potentials. Notably though, at 40°C a significant shift in the polarization curve towards nobler potentials was seen resulting in a positive E_{corr} value. Critical current density increased with increasing temperature as can be seen in Figure 4.13 and Table 4.6.

The corrosion results of the study showed that an increase in temperature of the solution resulted in reduced corrosion resistance of the alloys. The observed results in this study are in agreement with the well-established hypothesis on the effect of temperature on the corrosion resistance of ruthenium containing stainless steels.

The recorded passive current density in the first passivation region was the lowest at 25°C, and the highest at 60°C. This trend was also observed at the second passive potential region. At the second passive region the potential range is between 547 mV and 1039 mV (i.e. E_{pass} range = 492 mV) at 40°C, and between 560 mV and 1040 mV (i.e. E_{pass} range = 480 mV) at 60°C. Moreover at potentials above 563 mV, the specimen exhibited a more stable passive layer at 40°C.

5.2.2. *Effect of Acid Concentrations*

The corrosion resistance of all samples was negatively affected by increasing sulphuric acid concentration in the solutions i.e. the current density was increased when the concentration of the acid was increased. However, the loss in corrosion resistance due to increased concentration of sulphuric acid in the solution was more pronounced on the 12.5wt% Ru sample and less on the C-276 Hastelloy© sample. Trepanier et al. [67]

found that the general corrosion resistance of stainless steels was negatively affected by a decrease in pH.

5.2.3. *Effect of Alloy Composition (i.e. Ru and Ni content)*

In 40wt% sulphuric acid solution at 40^{o}C, the untreated AISI 316L stainless steel, 5.2wt% Ru and 12.5 wt% Ru specimens have E_{corr} values of -278 mV, -240 mV, and 59 mV respectively thus showing that addition of Ru shifted the potentiodynamic polarisation curve towards a nobler corrosion potential. In 40wt% sulphuric acid solution at 60^{o}C, the ruthenium containing samples also had slightly nobler corroding potentials and lower corroding current densities, i_{corr}, as compared to the untreated AISI 316L stainless steel sample. Similar trends were observed when the samples were exposed to 60wt% sulphuric acid at 40^{o}C and 60^{o}C. This phenomenon has been observed in many other studies [6, 7] when PGM's are added to austenitic steels in minor quantities.

The obtained i_{corr} values for the 5.2wt% Ru, 12.5wt% Ru samples and untreated AISI 316L stainless steel samples as given in Table 4.7 show that, there is no linear correlation between the amount of Ru in the alloy and the current density i.e. there was a decrease in current density value from 49.4 x 10^{-5} A/cm^2 for 0% Ru sample (untreated AISI 316L) to 20.7 x 10^{-5} A/cm^2 for 5.2wt% Ru sample, however doubling the amount of Ru in the sample to 12.5wt% Ru resulted in a slight increase in the i_{corr} value to 24.0 x 10^{-5} A/cm^2.

The observed lower passive current density, i_{pass}, exhibited by 12.5wt% Ru and 5.2wt% Ru as compared to the untreated AISI 316L stainless steel sample, is similar to the

observation made by Potgieter [6,7, 11, 22] and other authors [8-10, 24] of a shift towards a lower passive current density, i_{pass}, in the ruthenium containing stainless steel when investigating the effect of minor additions of ruthenium. The ability of the material to passivate and the stability of the passive layer are enhanced through additions of ruthenium [10, 11, 22-29]. This is an indication that the surface becomes more corrosion resistant with an increase in the Ru content. It has been suggested [5, 9-11] that the incorporation of Ru in the passive layer that form during corrosion of ruthenium containing stainless steels is one way of enhancing passivation behaviour since Ru retains its noble electrochemical properties [6, 11]. The sample containing 12.5wt% Ru gave a more stable passive layer than the untreated and 5.2wt% Ru sample. Other than higher Ru content, 12.5wt% Ru sample contained higher Ni content than 5.2wt% Ru sample, and according to observations made by Steicher [12] and Higginson [5] higher Ni content in steels tend to positively influence the effect of Ru on passivation. It should be noted though that Steicher [12] and Higginson [5], observed the synergistic effect on steels with lower concentrations of around 0.5wt% Ru. It is not well understood how the synergistic effect of using nickel and ruthenium together in steels is achieved. However, as mentioned earlier, these two elements are known to have lower dissolution rates compared to the main elements in stainless steels i.e. Cr and Fe, and have also been observed [11, 10] to be incorporated into the passive layer during corrosion.

The substrate (AISI 316L stainless steel) showed the lowest E_{corr} in all solutions and the highest i_{corr}, which suggested that the Ru containing steels, exhibited the best corrosion resistance. E_{corr} values were more positive for ruthenium containing steel sample i.e. 12.5wt% Ru and 5.2wt% Ru samples than the untreated sample. This observation on

electrochemical measurements which revealed an increase in the corrosion potential towards more positive values with an increase in the Ru concentration was also made in other studies [6–11, 13], although in some cases the investigations were performed on a different type of stainless steel.

According to Potgieter et al. [7, 10,11 and refs. therein], generally the dissolution rate of the main elements in the stainless steel, i.e. Fe and Cr, is higher than that of the alloying elements such as Ni, Mo and Ru thus the presence of these elements on the surface will accordingly inhibit the dissolution rate of the surface during active corrosion. This analogy can be used to understand how both 12.5wt% Ru and 5.2wt% Ru samples showed improved corrosion resistance compared to the untreated stainless steel sample. However, the analogy runs short of explaining why the 12.5wt% Ru sample with higher Ni and Ru contents exhibited slightly less or comparable corrosion resistance than the 5.2wt% Ru sample. The corrosion potential, E_{corr} was slightly higher, and the passive current density, i_{pass} lower for 5.2wt% Ru sample as compared to 12.5wt% Ru sample in 60wt% sulphuric acid at 40^{o}C. This observation suggests that a higher ruthenium content of the sample does not necessary result in better corrosion properties. In addition, on the basis of the Ru and Ni dissolution rate as a means of inhibiting corrosion in stainless steel, it is expected that the surface with higher Ni and Ru content to be more corrosion resistant, which was not entirely the case in this study as already mentioned. Thus, there has to be another way of explaining how the 5.2wt% Ru sample exhibited better corrosion properties than the 12.5wt% Ru sample. The better corrosion properties of the 5.22wt% Ru in certain instances can be attributed to better alloying. On the other hand, although insignificant in number (only two were observed), the presence of undissolved

Ru particles in 12.5wt% was a sign of insufficient alloying and most likely led to poor corrosion properties.

According to Olubambi et al. [8] in addition to other mechanisms such as its noble electrochemical properties ruthenium also achieves corrosion enhancing effect on stainless steel through modification of their microstructure. Grain refinement is one effect that was pointed [8] out as a way minor Ru additions modify stainless steel microstructure for better corrosion properties. Khalfallah et al. [71] investigated the surface modification of AISI 316L stainless steel by laser melting without adding any other metals, and found that the corrosion resistance was increased. The results were attributed to the fine dendritic microstructure that resulted from the laser treatment. It can thus be deduced that the better corrosion properties observed on the AISI 316L stainless steel laser treated with 5.2wt% Ru and 12.5wt% Ru were partly due to the fine dendritic structure observed. The microstructure of the 12.5wt% Ru sample consisted of mainly dendritic Columnar - Equiaxed - Transition (CET) grains, while that of 5.2wt% Ru sample consisted of mainly long dendritic columnar grains. Although not much published work on the effect of columnar and an equiaxed grains on the corrosion of stainless steel is available in literature, Mendez al. [71] have shown that columnar grains in AISI 316L stainless steel tend to yield higher general corrosion resistance than CET grains in 3% NaCl solution. This observation is in line with the results of the study in 60wt% sulphuric acid solution at 40^{o}C, where corrosion resistance of 5.2wt% Ru sample (mainly columnar grains) showed slightly better corrosion properties than 12.5wt% sample (mainly CET grains). Therefore, three possible methods through which ruthenium

additions to the surface through laser alloying of AISI 316L stainless steel modified corrosion properties were discussed, to explain the observed results.

In all test solutions used in this study it was observed that untreated AISI 316L and ruthenium containing AISI 316 stainless steel sample were short of outperforming alloy C-276, particularly on the passive current density, i_{pass}, and stability of passive layer. It is known [73] that at particularly lower concentrations, i.e. below 60wt% sulphuric acid, alloy C-276 show significantly higher resistance than AISI 316L. Thus, to compete C-276, the corrosion resistance of AISI 316 will need to be greatly improved through additions of 12.5wt% Ru and 5.2wt% Ru. Although 12.5wt% Ru and 5.2wt% Ru samples had improved corrosion resistance of AISI 316L, the improvements were not significant enough. In addition, the results of the study have shown laser surface alloying AISI 316 stainless steel with ruthenium for corrosion enhancement purposes, does not necessarily need a higher Ru content than 5.2wt%, since the 5.2wt% sample outperformed or was comparable to 12.5wt% in many instances. Many studies have limited Ru additions to steels [3-13], and other alloys [23, 25-27] to values around 0.5wt%. To a greater extent, the concentrations of 12.5wt% Ru and 5.2wt% Ru used in this study have shown that, not only is higher ruthenium concentrations not economically viable, but they give limited enhancement on corrosion properties of AISI 316L stainless steel. The corrosion enhancements observed are not significantly higher to justify the amount of Ru used. It not possible to conclude from the results of this study, what the optimal Ru concentrations for maximum corrosion enhancement of AISI 316L is for various sulphuric acid concentrations and conditions. It will require further extensive

work on minor ruthenium additions to AISI 316L to establish optimal Ru concentration for maximum corrosion performance, and economical feasibility.

5.3. Cost Estimation: Economical feasibility

The correlation between the amount, hence cost, of ruthenium used in surface alloying, and the performance of the alloyed surface is essential in evaluating economical viability of surface alloying with ruthenium, particularly in the quest to replace Hastelloy© C-276 in sulphuric acid service. In order to discuss economic feasibility of surface alloyed AISI 316L stainless using the Nd:YAG laser, a simple mathematical function was developed to correlate cost as a function of depth of alloying and ruthenium content. The cost of the AISI 316 stainless steel sheet surface alloyed with ruthenium can be estimated as follows:

Total Alloy Cost = Cost of Ruthenium used + Cost of Alloying i.e. (Technology + labour) + Cost of Steel Sheet

$C_T = C_{Ru} + C_{Laser} + C_{316L}$ ……..1

C_{Ru} = Price per kg Ru x kg used in alloying

= P_{Ru} x M_{Ru} ----------1a

To calculate M_{Ru}, the depth and content of Ru in the alloyed zone should be determined.

Consider an alloyed layer:

If h represent the depth of alloyed zone, and A the alloyed area of the AISI 316 stainless steel sheet, then the volume of the alloyed layer, V_T can be represented as follows:

$V_T = A \times h$ ----------2

If X_{Ru} represent the weight fraction ruthenium in the alloyed layer, and M_T the total mass of the alloyed layer, then the mass of Ru in the alloyed layer, $M_{Ru,}$ can be calculated as follows:

$M_{Ru} = X_{Ru} \times M_T$ ----------3

$M_T = V_T \times \rho_T,$ ----------4

where ρ_T is the density of the alloyed layer.

Substituting equations 2 and 4 in equation 3 results in the following equation:

$M_{Ru} = X_{Ru} \times A \times h \times \rho_T$ ----------5

ρ_T can be calculated from the knowledge of composition of each alloying in the alloyed layer. Since the composition of AISI 316L stainless steel sample is known, a volume balance can be used to estimate the value of ρ_T with the following assumptions:

1. No porosity and cracks in the alloyed layer
2. Shrinkage due to alloying is insignificant

$V_T = V_{ss} + V_{Ru}$

Where V_{ss} is the volume occupied by stainless steel ingredients in the alloyed layer,

V_{Ru} is the volume in the alloyed layer occupied by Ru

$$\frac{M_T}{\rho_T} = \frac{M_{ss}}{\rho_{ss}} + \frac{M_{Ru}}{\rho_{Ru}}$$ ----------6

Divide equation 6 by $1/M_T$, and make ρ_T the subject of the formula. The following equation is obtained:

$$\rho_T = \left(\frac{X_{ss}}{\rho_{ss}} + \frac{X_{Ru}}{\rho_{Ru}}\right)^{-1}$$ ----------7

Where $X_{ss} = M_{ss}/M_T$ = mass fraction of AISI 316L stainless steel in the alloyed layer,

Substituting ρ_T in Equation 5 using equation 7 yield the following equation:

$$M_{Ru} = X_{Ru} \times A \times h \times \left(\frac{X_{ss}}{\rho_{ss}} + \frac{X_{Ru}}{\rho_{Ru}}\right)^{-1} \quad \ldots\ldots\ldots\ldots\ldots\ldots\ldots\ldots 8$$

X_{Ru} and X_{ss} are related by the following equation:

Assumption:

1. Ru is the only element added to the surface of the stainless steel

$$X_{Ru} + X_{ss} = 1 \qquad \text{----------9}$$

Therefore, substituting X_{ss} in equation 8 using equation 9 gives a simple mathematical model that relates the mass of ruthenium in the alloyed layer with the thickness of the layer, h, weight percentage ruthenium in the layer, X_{Ru}, density of Ru, ρ_{Ru}, density of AISI 316 stainless steel, ρ_{ss}, and the surface area of the alloyed steel sheet, A. The equation is given as:

$$M_{Ru} = X_{Ru} \times A \times h \times \left(\frac{1-X_{Ru}}{\rho_{ss}} + \frac{X_{Ru}}{\rho_{Ru}}\right)^{-1} \quad \ldots\ldots\ldots\ldots\ldots\ldots\ldots 10$$

For a given AISI 316 steel sheet of surface area, A, and alloyed layer of thickness, h, the mass of Ru used, M_{Ru}, can be calculated as a function of percentage ruthenium in the alloyed layer.

Consider a surface alloyed AISI 316L stainless steel sheet with the following parameters:

$A = 1\ m^2$, $h = 2\ mm = 0.002\ m$, $\rho_{ss} = 8000\ kg/m^3$, $\rho_{Ru} = 12410\ kg/m^3$

Using excel spreadsheet, values of M_{Ru} were calculated for each chosen value of X_{Ru} and a plot showing how the amount of Ru used varies with ruthenium content in the 2 mm alloyed layer, X_{Ru} was drawn as shown in Figure 4.18 below.

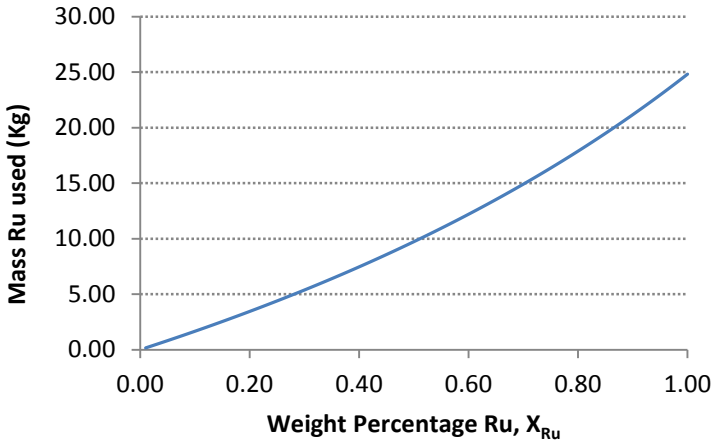


Figure 5.1: Mass of Ru used as a function of wt% Ru in the 2mm alloyed layer on AISI 316L stainless steel sheet with 1 m^2 surface area.

Furthermore, by substituting equation 10 in 1a, and the 1a in 1 will yield an equation that gives cost of the new alloy (AISI 316 stainless steel surface alloyed with Ru) as a function of other parameters as follows:

$$C_T = P_{Ru} \times X_{Ru} \times A \times h \times \left(\frac{X_{ss}}{\rho_{ss}} + \frac{X_{Ru}}{\rho_{Ru}}\right)^{-1} + C_{Laser} + C_{316L} \quad \text{.....10A}$$

P_{Ru}, C_{laser}, and C_{316L} are constants for a given sheet size. The actual values of these parameters are affected by economical conditions and do change with time. However at a given point in time they are treated as constants. Consider AISI 316L stainless steel sheet with surface area, A = 1 m^2, and thickness = 5 mm. According average price from manufacturers (average using alibaba.com website :):

Price of 5mm thick AISI 316 stainless steel sheet is = \$3000/ton

Ton of sheet (316L) = volume x density = 1 m^2 x 0.005 m x 8 ton/m^3 = 0.04 ton

$\therefore C_{316L}$ = \$3000/ton = \$3000/ton x R12.63/1\$ x 0.04 ton = R1515.6

C_{Laser} = Cost of laser operation to completely alloy AISI 316 stainless steel sheet of surface area, A= 1 m^2 to a depth, h.

The evarage ratings of Nd:YAG laser is R600 per hour

Since the scan speed used to treat the surface is 0.8 m/s, the time required to finish 1 m^2 surface area can be estimated as follows:

Number of laser tracks required to fully cover the 1 m x 1 m area is N_T

N_T = 1 m/0.004 m = 250

0.004 m is the width of each track, 250 of them will completely cover a sheet width of 1m.

The amount of time required to produce each track is t_T

t_T = distance/speed = 1 m/ 0.8 $m.s^{-1}$ = 1.25 s.

∴ Total time required to produce all 250 tracks = 1.25 s x 250 = 312.5 s

= 312.5 s x (1 min /60 s) x 1 h / 60 min = 0.087 h

Therefore total laser cost, C_{Laser} = 0.087 h x R600/h = R52.2

Once the values of C_{Laser} and C_{315L} are determined equation 10A can be update to the following:

$$C_T = P_{Ru} \times X_{Ru} \times A \times h \times \left(\frac{X_{ss}}{\rho_{ss}} + \frac{X_{Ru}}{\rho_{Ru}}\right)^{-1} + 52.2 + 1515.6 \quad \text{……..10A}$$

P_{Ru} is the price per kg of sponge ruthenium = $42/troy ounce

= $42/troy ounce x (1troy ounce/ 0.0311kg) x R12.63/1$ = R17056.59/kg

$$\therefore C_T = 17056.59 \times X_{Ru} \times A \times h \times \left(\frac{1-X_{Ru}}{\rho_{ss}} + \frac{X_{Ru}}{\rho_{Ru}}\right)^{-1} + 1567.8 \quad \text{……..10B}$$

As already discussed, A = 1 m^2, ρ_{ss} and ρ_{Ru} are known densities.

$$C_T = 17056.59 \times X_{Ru} \times h \times \left(\frac{1-X_{Ru}}{8000} + \frac{X_{Ru}}{12410}\right)^{-1} + 1567.8 \quad \text{……..10C}$$

Equation 10C can be used to estimate the cost of the new alloy as either a function of weight percentage ruthenium, X_{Ru}, in the alloyed layer of a fixed thickness h, or as a function of the thickness, h of the alloyed layer for fixed weight percentage ruthenium, X_{Ru}, in the alloyed layer. Using an excel spreadsheet, h was kept at a fixed value of 2 mm (0.002 m) and C_T as a function of X_{Ru} was plotted. Similarly, X_{Ru} was kept at a fixed value of 0.052 (5.2wt% Ru), and C_T was plotted as a function of h. The results are shown in Figures 5.2 and 5.3.

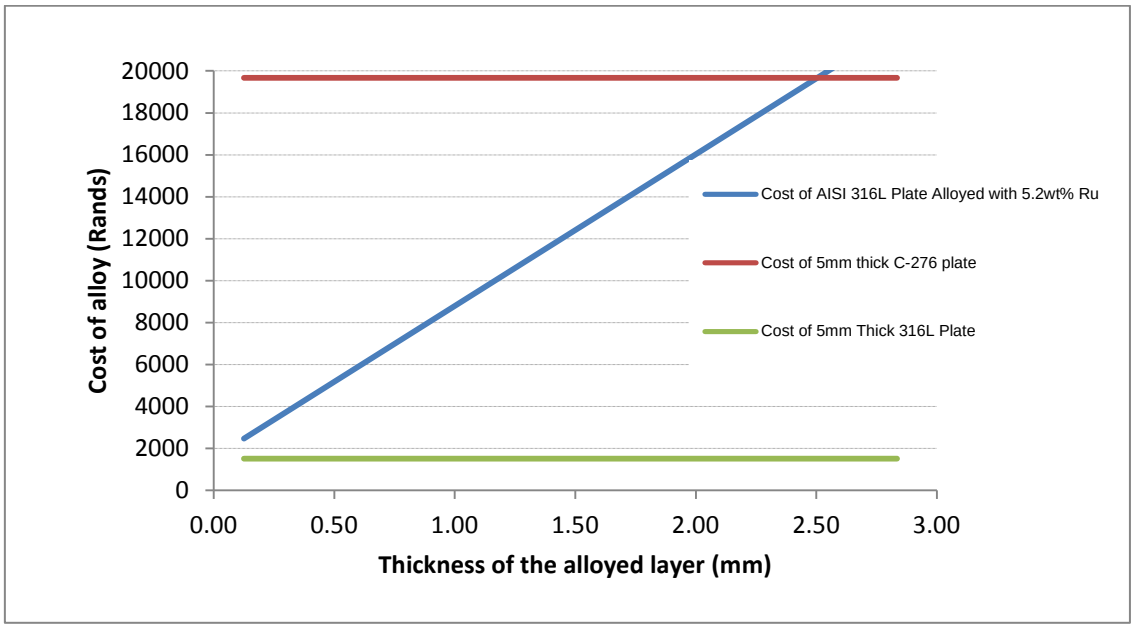


Figure 5.2: Cost, C_T, of AISI 316L plate surface alloyed with 5.2wt% Ru as a function of the thickness of the alloyed layer.

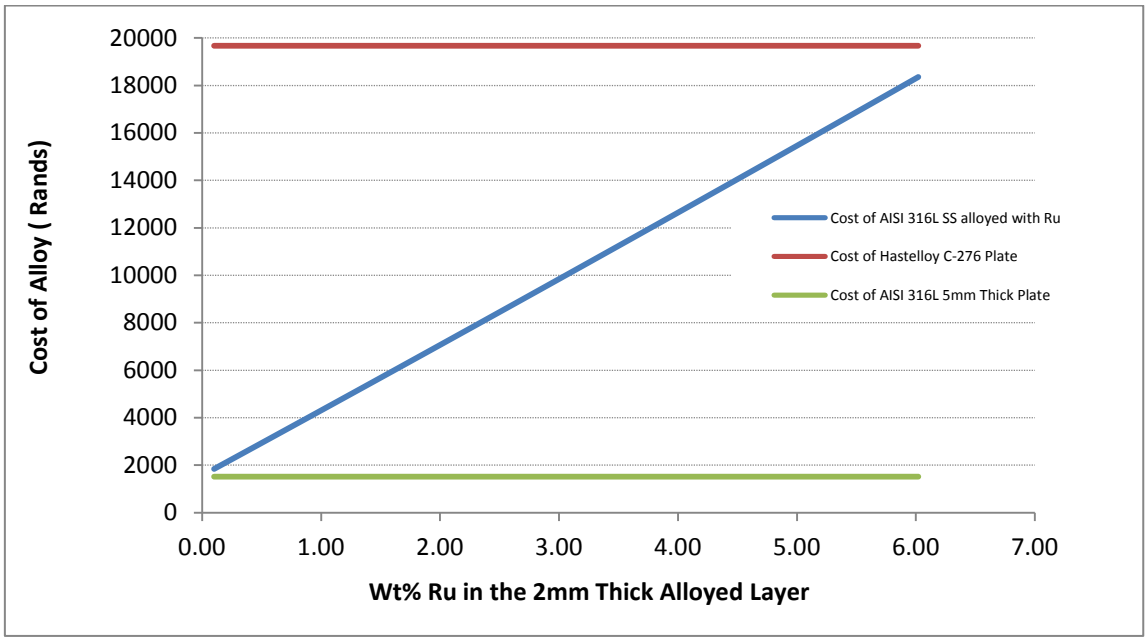


Figure 5.3: Cost, C_T, of AISI 316L plate surface alloyed to 2 mm depth as a function of the wt% Ru in the alloyed layer.

According to Figure 5.3, the cost of the AISI 316 stainless steel plate (1 m x 1 m x 0.05m) surface alloyed with 5.2wt% Ru is estimated as R15 989, and it is less than the cost of C276 plate of similar size which is estimated at R19 900. In light of the lower cost, it can therefore be concluded that surface alloying of AISI 316L stainless steel plate with Ru to content less than 5.2wt% Ru is economically feasible to replace Hastelloy© C-276. However, as it has already been seen from the potentiodynamic polarization results, the limit is its corrosion performance which is inferior to the corrosion performance of C-276. In order to replace C-276, the new alloy will need to be superior in resisting corrosion in acidic environment where C-276 is currently preferred.

The choice for the required thickness of the ruthenium alloyed layer is guided by the corrosion rate of the layer, which in turn dictates the life span of the layer. In comparison

with competing alloys i.e. Hastelloy© C-276, the layer must be thick enough to protect the substrate for a duration that surpasses that of the Hastelloy© C-276. The effect of the thickness on the cost of the alloy containing a specific amount of ruthenium is shown by Figure 5.2. As the thickness of the layer increases, the cost of the alloy increases linearly.

In short these improvements in corrosion resistance can be attributed to the fine and homogeneous dendritic structure, as well as the presence of ruthenium which was found throughout the melted zones [3-13]. There is a general observation that supplementary to adding optimal Ru levels it will take a combination of many factors such as microstructural development, manipulation of laser parameters, even distribution of Ru throughout the melted portion of the substrate, and microstructural homogeneity to produce a corrosion resistant surface to compete with alloy Hastelloy© C-276. The optimal Ru content in AISI 316L for maximum corrosion improvement is not known. It is difficult to conclude whether maximum improvements will come from Ru levels lower than 5.2wt%, but it is has been shown that even at levels around 0.5wt%, Ru modification effects can be dramatic.

CHAPTER VI: CONCLUSIONS

6.1. Conclusions

The aim of this project was to surface alloy AISI 316L substrate with mixtures of Ru and Ni powder using laser technology, and produce a surface layer with a higher ruthenium content to compete with Hastelloy© C-276 alloy in acidic environments at elevated temperatures. Although non-porous with no apparent micro-cracks, the surface layers consisted of inhomogenous microstructure and non-uniform distribution of Ru and Ni in the alloyed layer. Microstructural inhomogeneity and non-uniform distributions of the alloying elements makes the layers prone to localized corrosion attack in areas where the modifying elements are below optimal quantities. Therefore, it can be concluded that by applying laser surface alloying an ideal microstructure and element distribution was not achieved.

The results of the study have shown that as seen in literature addition of ruthenium to AISI 316L stainless steel improves corrosion properties although the improvements were not significant enough. It was realized that higher Ru content does not necessarily translate into better corrosion properties since 5.2wt% Ru gave better properties than 12.5wt% Ru. The inferior corrosion properties of the Ru alloyed layers in sulphuric acid environment as compared to Hastelloy© C-276 proved that the obtained layers are not competitive, and are therefore not candidate alloys to replace Hastelloy© C-276 and other Nickel alloys used in acidic conditions.

The estimated cost of 5.2wt% Ru alloyed AISI 316L stainless steel plate is less than the cost of C-276 plate of similar size, thus showing a possibility of cost effectiveness. Ruthenium containing layer applied using laser surface alloying does not make significant difference to the corrosion of 316L stainless steel in hot sulphuric acid solutions.

6.2. Suggestions for future work

There are several areas worthy of further investigation that were prompted by the results and observations from this work. Further investigations have a potential of making surface alloying of AISI 316L stainless steel with ruthenium a commercial breakthrough.

(1) Ruthenium concentration in AISI 316L stainless steel which give maximum corrosion resistance at economically feasible levels i.e. less than 5.2wt% Ru, has not been established. Investigations which focus on finding optimal ruthenium concentrations will be beneficial to the quest to find economical feasible ruthenium alloyed stainless steels.

(2) As only two Ru concentrations were studied, it was difficult to set a sense of relationship between concentrations beyond linear. Concentrations below 5.2wt% Ru and various Ru/Ni ratios need to be investigated to clarify relationships.

(3) Different microstructures such as columnar, CET, cellular, and equiaxed are known to have an effect on the corrosion resistance, and mode of corrosion of steels. The effect of microstructure on corrosion properties of AISI 316L stainless steel laser alloyed with ruthenium is not fully understood. A study in this area

might lead to valuable conclusion about the microstructures that give maximum benefit for a ruthenium alloyed AISI 316 stainless steel.

REFERENCES

[1] R. Javaherdashti, H. Nikraz. On the role of deterioration of structures in their performance; with a focus on mining industry equipment and structures, *Materials and Corrosion* 61, No. 10, 2010.

[2] Nickel Development Institute. Corrosion resistance of nickel-containing alloys in sulfuric acid and related compounds, *Publication no 1318*, 1990.

[3] N. D. Tomashov, Controlling factors in the protection of metals from corrosion, *Institute of Physical Chemistry, Academy of Sciences, USSR*, pp. 236-245, 1961

[4] N.D. Tomashov, *ibid.* 22, 1993.

[5] A. Higginson, The passivation of Fe-Cr-Ru alloys in acidic solutions, *Ph.D. thesis, University of Manchester*, 1987.

[6] J. H. Potgieter, A. M. Heyns, W. Skinner. Cathodic modification as a means of improving the corrosion resistance of alloys, *Journal of applied electrochemistry* 20 pp. 711-715, 1990.

[7] J. H. Potgieter, O. Barnard, G. Myburg, K. Varga, p. Baradlai, L. Tomcsanyi, Corrosion behaviour of duplex stainless steels containing minor ruthenium additions in reducing acid media, *Journal of applied electrochemistry 26* , pp. 1103-1110, 1996.

[8] P. A. Olubambi, J.H. Potgieter, L. Cornish, Corrosion behaviour of superferritic stainless steels cathodically modified with minor additions of ruthenium in sulphuric and hydrochloric acids, *Materials and Design* 30 pp. 1451–1457, 2009.

[9] El-Sayed M. Sherif, J.H. Potgieter, J.D. Comins, L. Cornish, P.A. Olubambi, C.N. Machio. The beneficial effect of ruthenium additions on the passivation of

duplex stainless steel corrosion in sodium chloride solutions, *Corrosion Science 51* pp. 1364–1371, 2009.

[10] K. Varga, P. Baradlai, W. O. Barnard, G. Myburg, T.P. Halmos and J. H. Potgieter, Comparative study of surface properties of austenitic stainless steels in sulfuric and hydrochloric acid solutions. *ElectrochimicaActa,* Vol. *42, No. 1,* pp. *25-35, 1997.*

[11] J.H. Potgieter, The effect of cathodic modifications on the corrosion behaviour of duplex stainless steels, PhD thesis, *University of the Witwatersrand*, June 1996.

[12] M.A. Streicher, *ibid.* 1997.

[13] S.C. Tjong, J.S. Ku, and N.J. Ho, Laser surface alloying of ferritic Fe-40Cr alloy with ruthenium, *Surface & Coatings Technology*, vol.90 pp. 203 – 209, 1997.

[14] E. Toyserkani, A. Khajepour, and S. Corbin, Laser Cladding, *CRC Press*, pp. 183 – 213, 2005.

[15] J.J. McEwan, Corrosion control in Southern Africa, 2nd edition, 2004

[16] P. Monnartz, Metallurgie 8 , pp.161, 1911.

[17] A. Alamr, D.F. Bahr, M. Jacroux, Effects of alloy and solution chemistry on the fracture of passive films on austenitic stainless steel, Corrosion Science 48 pp. 925–936, 2006.

[18] http://www.columbus.co.za/files/downloads/columbus_stainless_product_catalogue.pdf. Columbus technical Handbook.

[19] N.D. Tomashov, G. P. Sinelshchikova and M. A. Vedeeva, *Dokl. Akad. Nauk. USSR* 62 pp. 105-108, 1948.

[20] N.D. Greene, C. R. Bishop and M. Stern, *ibid.* 108 pp. 836-41, 1961.

[21] M. Stern and H. Wissenberg, *J. Electrochem. Soc.* 106 pp.759-64, 1959.

[22] J. H. Potgieter, W. Skinner, A.M. Heyns. The nature of the passive film on cathodically modified stainless steels, *Journal of applied electrochemistry* 23 pp. 11-18, 1993.

[23] E. van der Lingen, R.F. Sandenbergh. The cathodic modification behaviour of ruthenium additions to titanium in hydrochloric acid, *Corrosion Science 43*, pp. 577 – 590, 2001.

[24] G. Myburg, K. Varga, W.O. Barnard, P. Baradlai, L. Tomcs´anyi, J.H. Potgieter, C.W. Louw, M.J. Van Staden. Surface composition of Ru containing duplex stainless steel after passivation in non-oxidizing media, *Applied Surface Science* 136, pp. 29–35, 1998.

[25] R.W. Schutz. Ruthenium Enha.nced Titanium Alloys. *Platinum Metals Rev. vol.*40, *(2)*, pp.54-61, 1996.

[26] I.M. Wolff, L.E. Iorio, T. Rumpf, P.V.T. Scheers, J.H. Potgieter, Oxidation and corrosion behaviour of Fe–Cr and Fe–Cr–Al alloys with minor alloying additions, *Materials Science and Engineering* A241 pp. 264–276, 1998.

[27] R. W. Schutz, Ruthenium enhanced titanium alloys: Minor ruthenium additions produce cost effective corrosion resistant commercial titanium alloys. *Platinum metals rev.* 40, *(2)*, pp. 54-61, 1996.

[28] I. Olefjord, B. O. Elfstrom, *Corrosion* 38, (46), 1982.

[29] G.J. Biefer, *Can. Metall. Q* 9, pp. 537-50, 1970.

[30] H. Gerischer, W. Mindt, The mechanisms of the decomposition of semiconductors by electrochemical oxidation and reduction, *ElectrochimicaActa*, Vol. 13. pp. 1329 -1341, 1968.

[31] W. Porod, D.K. Ferry, An empirical approach to clustering based on atomic energies, *Solid State Communications*, Vol. 44, No. 11, pp. 1511-1514, 1982.

[32] N.D. Tomashov, G. P. Chernova, L. A. Chigirinskaya,E. A. Nasedkina, *Prot. Met.* 22, 704-10, 1986.

[33] R.F. Vines, E.M Wise, The platinum metals and their alloys, *New York International Nickel Company*, 1941.

[34] N. V. Ageev, V. G. Kuznetsov, *Izv. AkadNauk S.S.S.R. (Khim.)*, pp. 753-755, 1937.

[35] V. A. Nemilov, A. A. Rudnitskii. *Izv. AkadNauk S.S.S.R. (Khim.), pp.* 33 - 40, 1937.

[36] C.A. Hampel, *Rare metals handbook*, Reinhold Publishing Corporation, pp. 291 – 328, 1954.

[37] T.B. Massalski. *Binary alloys phase diagram*, *ASM International*. 1992

[38] E. Raub, Metals and Alloys of the Platinum Group, *Journal of the Less-Common Metals* Vol. 1, 1959.

[39] S.Hyun, O. Kraft, R.P. Vinci. Mechanical behaviour of Pt and Pt –Ru solid solution alloy thin films, *ActaMaterialia* 52, pp. 4199 – 4211, 2004.

[40] D.W. Rhys. The fabrication and properties of ruthenium, *Journal of the Less-Common Metals* Vol.1 1959.

[41] M. Riabkina, L. Gal-Or, Y. Fishman, G. Iram. Grain-Refined Recrystallised 14-carat gold alloy, effects of small additions of elements in an Au-Ag-Cu-Zn alloy. *Gold Bulletin*, 17 (2), 1984.

[42] D. Ott, C.J. Raub, Grain size of gold and gold alloys: A review of some recent developments, *gold bulletin*, 14 (2), 1981.

[43] Platinum Jewellery Alloys, *Platinum*. pp. 28 – 29, 2002.

[44] Noble Metals, Jewellery Alloys: *Platinum and Palladium.www.noble.matthey.com.*

[45] R. Gilchrist, The Platinum Metals, *National Bureau of Standards, U. S. Department of Commerce, Washington, D. C*, 1948.

[46] Nickel Company, *Ruthenium*, Pamphlets, 1960.

[47] Nickel Company, *Palladium*, Pamphlets, 1960.

[48] S. Hallstrom, D. Anderson, A. Ruban, J. Agren. Thermodynamic reassessment of the Ni-Ru system and assessment of the Al-Ni-Ru system at 1273 – 1523 using ab initio calculations, *ActaMaterialia* 56, pp. 4062 – 4069, 2008.

[49] Q. Feng, T.K. Nandy, S. Tin, T.M. Pollock. Solidification of high refractory ruthenium containing superalloys. *Actamaterialia* 51, pp. 269 – 284, 2003.

[50] A.S.D, Creep Tests on Platinum Alloys: A New Method of Assessing High-Temperature Properties, *Platinum Metals Rev.* 5, (4)1961.

[51] C. Xiao, Y. Han, S. Li, D. Wang, J. Song, Q. Li. Effect of Ru on the structural stability and mechanical properties of Ni – Al- Mo-B alloy IC6. *Materials letters* 57, pp. 3843 – 3846, 2003.

[52] F. Diologent, P. Caron, On the creep behaviour at 1033K of new generation single-crystal superalloys, *Materials Science and Engineering* A 385 pp. 245–257, 2004.

[53] L.J. Carroll, Q. Feng, J.F. Mansfield, T.M. Pollock, Elemental partitioning in Ru-containing nickel-base single crystal superalloys, *Materials Science and Engineering* A 457 pp. 292–299, 2007.

[54] M. Efendi ; S. Shingo ; M.Yoshinori ; K. Toshiyuki ; M. Masahiko, Diffusion and γ' Phase Coarsening Kinetics in Ruthenium Containing Nickel Based Alloys, *Materials transactions* 2008, vol. 49, no.4, pp. 792-799.

[55] Y. Koizumi, T. Kobayashi, Z. Jianxin, T. Yokokawa, H. Harada, Y. Aoki, M. Arai. Development of a Next-Generation Ni-base Single Crystal Superalloy. *Proceedings of the International Gas Turbine Congress*, Tokyo, 2003 .

[56] C. W. Corti, D. R. Coupland and G. L. Selman, Platinum-Enriched Superalloys: Enhanced Oxidation and Corrosion Resistance for Industrial and Aerospace Applications. *Platinum Metals Rev.* 24, (11) pp. 2-11, 1980.

[57] D. R. Coupland, C. W. Hall and I. R. McGill, Platinum-Enriched Superalloys: A Developmental Alloy for Use in Industrial and Marine Gas Turbine Environments, *Platinum Metals Rev.*, 26, (4), pp. 146-157, 1982.

[58] P.J. Hill, N. Adams, T. Biggs, P. Ellis, J. Hohls, S.S. Taylor, I.M. Wolff. Platinum alloys based on Pt-Pt_3Al for ultra-high temperature use. *Material science and engineering*, A Vol. 329 – 331, pp. 295 – 304, 2002.

[59] C.T. Kwok, F.T. Cheng, H.C. Man. Laser surface modification of UNS stainless steel. Part 1: Microstructure and corrosion characteristics, Materials Science & engineering, A290: pp. 55 – 73, 2000.

[60] W.T. Tsai, C.H. Shieh, J.T. Lee. Surface modification of ferritic stainless steel by laser alloying, Thin solid films, 247: pp. 79 – 84, 1994.

[61] E. Gemelli, A. Galerie, M. Caillet. Thermal oxidation resistant surface alloys processed by laser alloying on Z38CDV5 ferritic steel, solids state ionics, 95: pp. 81 -86, 1997.

[62] P.Peyre, X. Scherpereel, L. Berthe, C. Carboni, R. Fabbro, G. Beranger, C. Lamaitre. Surface modification induced in 316LL steel by laser peening and shot-peening. Influence on pitting corrosion resistance, *Materials Science and Engineering*, A280: pp. 294 – 302, 2000.

[63] S.C Tjong. Electrochemical and surface analysis of the Fe-Cr-Ru system in non-Oxidising acid solutions, *Applied Surface Science*, 44: 7 – 15, 1990.

[64] C.W. Draper. *Journal of Material Science* 34: 24-28,1982.

[65] M. L. Capp and J.M. Rigsbee: *Material Science and Engineering*, 62, pp. 49-56, 1984.

[66] Z. Brytan, M. Bonek, L.A. Dobrzański. Microstructure and properties of laser surface alloyed PM austenitic stainless steel, *Journal of Achievements in Materials and Manufacturing Engineering*, 40: 70- 78, 2010.

[67] C. Trepanier, A.R. Pelton. Effect of temperature and pH on the corrosion resistance of nitinol and stainless steel. *Proceedings of SMST*-2004: 361-366,

[68] S Katayama, *Handbook of Laser Welding Technologies*, 149 – 152. 2013.

[69] A.P.I. Popoola, T. Fedotoval, S.L. Pityana, O.M. Popoola. Quantitative study of the hardness property of laser surface 144 alloyed aluminium AA1200. The *Journal of the South African institute of Mining and Metallurgy*, 111:335-344, 2011.

[70] S.A. David, J.M. Vitek. International Materials Review, 34 (5) , 213, 1989.

[71] I.Y. Khalfallah, M.N. Rahoma, J.H. Abboud, K.Y. Benyounis. Microstructure and corrosion behaviour of austenitic stainless steel treated with laser, *Optics & Laser Technology*, Vol. 43, p.p. 806–813, 2011.

[72] Laudia Marcela Méndez, Mónica Mariela Covinich and Alicia Esther. Resistance to Corrosion and Passivity of 316L Stainless Steel Directionally Solidified Samples, *Developments in Corrosion Protection*, 2014.

[73] B.D. Craig, D.S. Anderson, *Handbook of Corrosion Data*, 2nd Edition. (849) 1997.

[74] O.A. Olaseinde, Comparative Study of the Effect of Temperature on the Corrosion Behaviour of 2205 Duplex Stainless Steel and 316 Austenitic Stainless Steel in Acidic Chloride Environment. *Advances in Materials Physics and Chemistry*, 5, 185-190, 2015.

[75] D.S. Gna na muthu, "Laser surface treatment", Applications of Lasers in Material Processing, Proceedings of Conference, Washington DC, Published: Metals Park, OH44073, American Society for Metals, pp. 177-21, 1979.

[76] C.Q. Jessen, Stainless steel and corrosion, Forlaget Møller & Nielsen, pp 77-79, 2011.

[77] M. Itagaki, H. Nakazawa, K. Watanabe, K. Noda, Study of Dissolution Mechanisms of Nickel in Sulfuric Acid Solution by Electrochemical Quartz Crystal Microbalance, *Corrosion Science*, Vol. 39, No. 5, pp. 90-911, 1997.

[78] K. Deo, S. G. Mehendale, S. Venkatachalam, Electrochemical Dissolution of Nickel in Sulphuric Acid by Alternating Current, *Journal Of Applied Electrochemistry* Vol. 6. pp. 37-43, 1976.

[79] J.R. Davis, Nickel, Cobalt, and their Alloys, *Technology & Engineering*, ASM International, pp. 129, 2000.

[80] J.K.L. Lai, Review of Precipitation Behaviour in AISI Type 316 Stainless Steel, *Materials Science and Engineering, 61* ,pp.101-109, 1983.

[81] C.O.A. Olsson , D. Landolt, Passive films on stainless steels: chemistry, structure and growth, *Electrochimica Acta*, 48, pp.1093- 1104, 2003.

[82] C.T. Sims, W.C. Hagel, The SuperalloysWiley, New York, 1972.

[83] A. Pardo, M.C. Merino, A.E. Coy, F. Viejo, R. Arrabal, E. Matykina, Effect of Mo and Mn additions on the corrosion behaviour of AISI 304 and 316 stainless steels in H2SO4, *Corrosion Science*, Vol. 50, pp. 780–794, 2008.

[84] I. Fedotov, T. Fedotova, S.L. Pityana, K. Labuschange, M. Shatalov, and J.H. Potgieter, A mathematical model of laser surface heat-cooling treatment for medium carbon steel, *The Journal of The Southern African Institute of Mining and Metallurgy*, Vol 111, pp. 379-384, 2011.

[85] D. Verdi, C.J. Múnez, F. Sevillano, P. Poza, Laser surface alloying of Gr22 ferritic steel with Ni(Al): Effect of processing parameters on the microstructure and high temperature performance, *Journal of Materials Processing Technology*, Vol.13. pp. 1825-1834, 2013.

[86] N.B. Dahotre, Lasers in Surface Engineering, *Surface Engineering Series*, Vol 1, pp. 121-131, 1998.

[87] Alan D. Hecht , Joseph Fiksel , Scott C. Fulton , Terry F. Yosie , Neil C. Hawkins , Heinz Leuenberger , Jay S. Golden , & Thomas E. Lovejoy ,Creating the future we want, *Sustainability: Science, Practice, & Policy* http://sspp.proquest.com.

[88] http://www.princetonappliedresearch.com/support-center/product-manuals/index.aspx.

[89] J. Tafel, K. Schmitz, B.B. K. Naremann, Emmert, *Zeitschrift fur Physikalische Chemie-International*, 50, pp. 713 – 752, 1905.

[90] J. Tafel, K. Schmitz, B.B. K. Naremann, Emmert, *Zeitschrift fur Physikalische Chemie-International*, 50, pp. 641 – 712, 1905.

[91] K. Lambrych, T. Johnson, and D. Kelley, Performance and Cost Comparison of Materials Used in Design and Fabrication of Hydrometallurgical Equipment, *Ashland Performance Materials*, Internal Study, 2013